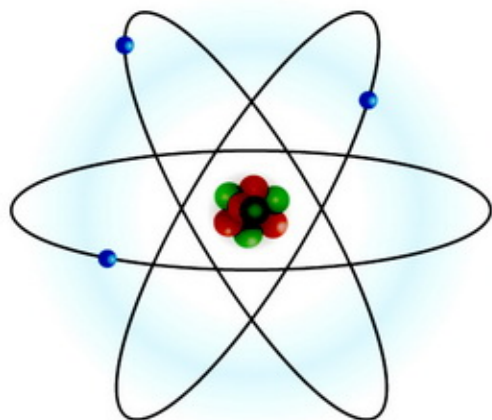
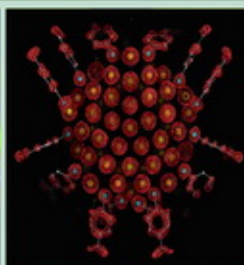
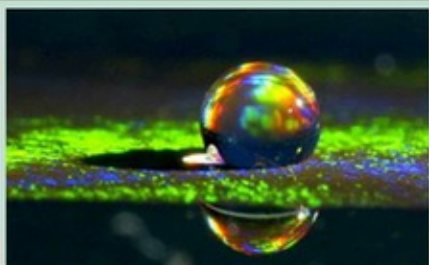
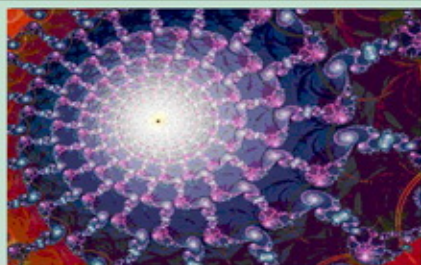




Valahia University of Targoviste  
FACULTY OF SCIENCES AND ARTS



# THE ANNALS OF "VALAHIA" UNIVERSITY



Year 7 • No. 1  
2007

[www.josa.ro](http://www.josa.ro)

**MINISTRY OF EDUCATION AND RESEARCH**

**“VALAHIA” UNIVERSITY OF TARGOVIȘTE**

**THE ANNALS  
OF “VALAHIA” UNIVERSITY**

**SECTION SCIENCES**

**Vol. 7  
2007**

## CONTENTS

### A. PHYSICS SECTION

PIXE APPLICATIONS IN ELEMENTAL ANALYSIS OF BIOLOGICAL AND METALLURGICAL SAMPLES ION V. POPESCU<sup>1</sup>, A. ENE<sup>2</sup>, CLAUDIA STIHI<sup>1</sup>, ANCA GHEBOIANU<sup>1</sup>, T. BADICA<sup>3</sup> / PAGE 7

SURFACE WATER POLLUTION MONITORING BY ICP AND TDS MEASUREMENTS CLAUDIA STIHI, ION V. POPESCU, VALERICĂ CIMPOCA, GHEORGHE VLAICU, CĂLIN OROS, SIMONA APOSTOL, D. STOIAN, GABRIEL D DIMA, SERGIU DINU / PAGE 13

FRACTAL DIMENSION OF BLOOD SERUM PIXE SPECTRA COLLECTED FROM ILL FARM ANIMALS GABRIEL D. DIMA, CĂLIN OROS, SERGIU DINU, CLAUDIA STIHI / PAGE 17

ATOMIC FORCE MICROSCOPY-ATOMIC INVESTIGATION METHOD OANA BUTE, VALERICĂ GH. CIMPOCA / PAGE 20

THE THEORETICAL AND EXPERIMENTAL STUDY OF SOME METALS HEATING AND MELTING UNDER THE ACTION OF LASER RADIATION CĂLIN OROS, SERGIU DINU, MARILENA VOICU / PAGE 26

### B. CHEMISTRY SECTION

EFFECTS OF CALCIUM CARBONATE NANOPHASE ON i-PP TRAIAN ZAHARESCU, SILVIU JIPA, LAURA MONICA GORGHIU, CRINELA DUMITRESCU, RADU LUCIAN OLTEANU / PAGE 33

THERMAL STABILITY OF POLY(URETHANE-LACTATE) SILVIU JIPA, TRAIAN ZAHARESCU, RADU SETNESECU, C. CIOBANU, C. N. CAȘCAVAL / PAGE 40

QUALITATIVE AND SEMIQUANTITATIVE TLC ANALYSIS OF VITAMIN D<sub>2</sub> ANA-MARIA HOSSU, CRISTIANA RĂDULESCU, IONICA IONITA, IRINA-ELENA MOATER, DUMITRA HOSSU / PAGE 48

THE PHOTOCHROMIC RESPONSE OF POLYMERS STRUCTURES MODIFIED WITH CLASSICAL AZO DYES IONICA IONIȚĂ, CRISTIANA RĂDULESCU, ANA-MARIA HOSSU / PAGE 52

DYEING ALTERNATIVES OF TEXTILE FIBRES WITH NEW DISPERSE AND CATIONIC DYES DERIVATIVES OF COMPACT CONDENSED SYSTEM 2-AMINOTHIAZOLO[4,5-f]INDAZOLE CRISTIANA RĂDULESCU, ANA-MARIA HOSSU, IONICA IONIȚĂ / PAGE 56

MELANA FIBRES PHOTOSTABILIZATION BY USING *UV* ABSORBER FROM  
BENZOTRIAZOLIC CLASS CRISTIANA RĂDULESCU, IONICA IONIȚĂ, ANA-MARIA HOSSU, ELENA VIRGINIA  
GRIGORESCU / PAGE 62

ANALYSES OF SOME PHISICOCHEMICAL PARAMETERS OF SURFACE  
WATERS FOR DETERMINATION OF POLLUTION GRADE ILEANA MARIN / PAGE 68

### **C. MATHEMATICS - INFORMATICS SECTION**

ABOUT SOME INTEGRALS ANDREI VERNESCU / PAGE 75

A SCHURER-POPOVICIU TYPE OPERATOR INGRID OANCEA / PAGE 79

ABOUT DIFFERENTIALSTOCHASTIC AND INTERGRAL CALCULATION  
ITÔ DOINA CONSTANȚA MIHAI / PAGE 82

USING FINITE DIFFERENCE METHOD TO PARALLEL ALGORITHMS  
DESIGN DUMITRU FANACHE / PAGE 85

A THEORETICAL CONSTRUCT FOR PARALLEL COMPUTATION DUMITRU  
FANACHE / PAGE 94

## **A. PHYSICS SECTION**

## PIXE APPLICATIONS IN ELEMENTAL ANALYSIS OF BIOLOGICAL AND METALLURGICAL SAMPLES

I.V. POPESCU<sup>1</sup>, A. ENE<sup>2</sup>, C. STIHI<sup>1</sup>, A. GHEBOIANU<sup>1</sup>, T. BADICA<sup>3</sup>

<sup>1</sup>"Valahia" University of Targoviste, Targoviste, Romania, e-mail: ivpopes@valahia.ro

<sup>2</sup>"Dunarea de Jos" University of Galati, Galati, Romania, e-mail: aene@ugal.ro

<sup>3</sup>"Horia Hulubei" National Institute of Physics and Nuclear Engineering (NIPNE),  
Măgurele, Bucharest, Romania, e-mail: badica@ifin.nipne.ro

**Abstract:** *In this paper a complex study of the capabilities of Particle-Induced X-ray Emission (PIXE) technique for the determination of major, minor and trace constituents of metallurgical, biological and environmental samples has been done. PIXE analyses have been carried out using a 3 MeV proton beam generated with the aid of the 7 MV FN tandem accelerator of the "Horia Hulubei" National Institute of Physics and Nuclear Engineering (NIPNE) Bucharest. The detection system included a GeHP detector with an energy resolution of 170 eV at 5.9 keV for the X rays. The targets were mounted in the irradiation chamber at 45° with respect to the beam and the detector's direction. A thin surface barrier silicon detector was also placed in the chamber, at 135° with respect to the beam direction, in order to detect the backscattered protons for spectra normalization. The X-ray and particle spectra were simultaneously collected and processed off-line. The elements identified in the metallurgical samples (steels) using PIXE were: K, Ca, V, Cr, Mn, Fe, Co, Cu, Ni, Zn, W, Ga, As, Pb, Mo, Rb, In, Rh, Zr, Pd, Nb, Sn and Sb. In the investigated biological and environmental samples (vegetables leaves, soil and mosses) PIXE analysis allowed determination of: S, Cl, K, Ca, Ti, Mn, Fe, Ni, Cu, Zn, As, Hg and Pb.*

**Keywords:** *PIXE, environmental samples, steel*

### 1. Introduction

The attractiveness of non-destructive methods and the ability to perform simultaneous multi-elemental determinations has led to an extensive application in different industrial and research laboratories of accurate, precise and sensitive atomic and nuclear analytical techniques such as neutron activation analysis (NAA) [1,2], particle-induced X-ray emission (PIXE) [3-5] and particle-induced gamma-ray emission (PIGE) [6-8]. In this work the capabilities of the PIXE technique for the determination of major, minor and trace constituents of metallurgical, biological and environmental samples have been investigated. In PIXE ions from low-energy accelerator are used for the irradiation of the samples. The characteristic X-ray radiation produced is measured by semiconductor detector. In analysis of measured X-ray spectra the concentrations of the elements present in the sample are deduced. In worldwide laboratories PIXE is routinely applied for several interdisciplinary problems: environmental studies [9,10], analysis of materials [4,5,11], biology and biomedicine [11, 12], archeometry and geology [4,11,13] etc. PIXE method is: multi-elemental, fast, sensitive (ppm), precise (< 5%), and non-destructive.

## 2. Experimental

### 2.1. Sampling

#### 2.1.1. Metallurgical samples

The steel samples and standards were obtained from the MITTAL STEEL Works of Galati (Romania). The used standards were British Chemical Standards BCS Nos. 320 (mild steel: Mo-0.22%; Ni-0.022%; Cr-0.131%; W-0.17%; Sn-0.085%; As-0.031%; Ti-0.021%; Al-0.013%;) and 402/1 (low alloy steel: C-1.2%; Si-0.13%; V-0.15%; Mn-0.16%; Cu-0.21%; Mo-0.17%; Ni-0.81%; Cr-0.77%; P-0.011%; S-0.032%), EURONORM CRM No. 085-1 (C-670 ppm; Si-80 ppm; P-620 ppm; S-3360 ppm; V-21 ppm; Mn-9770 ppm; Co-190 ppm; Cu-2910 ppm; Zn-25 ppm; Sb-73 ppm and Pb-10 ppm).

#### 2.1.2. Biological and environmental samples

Sampling of vegetables leaves (*Apium graveolens* –celery, *Brasica oleracea* cabbage) samples were made in phenological phase mature fruit of vegetables. The samples of fresh leaves were weighed, then were dried in drying stove at 105 °C for 1 hour. The soil samples were drew from different depths in soil: over surface, 10 cm in deep and 20 cm in deep. The soil samples were also dried in the same conditions as the biological samples.

Sampling of mosses (*Mnium undulatum*) was carried out in the investigated area - the transect from north to south of the Dambovită County, Romania in summer –autumn 2004. First, soil was washed off the samples in running water and then the samples were finely cut and dried at a room temperature in a clean box preventing further contamination. After that the dried mosses-with a constant weight have been grained.

The obtained powder of vegetal leaves, soil and mosses was mixed with 2 µg of Yttrium (internal standard) in 150 µl demineralised water and depicted on Mylar support.

### 2.2. Analysis

PIXE analyses have been carried out using a 3 MeV proton beam generated with the aid of the 7 MV FN tandem accelerator of the “Horia Hulubei” National Institute of Physics and Nuclear Engineering (NIPNE) Bucharest. A 3 nA proton beam current was employed and the exposure time was 30 min. The proton energy of 3 MeV has been chosen based on other authors’ studies [3] upon the dependence of the limit of detection on the atomic number of pure elements, this being minimum for almost all targets in the case of 3 MeV protons. The detection system included a 10 mm thick GeHp detector with an energy resolution of 170 eV at 5.9 keV for the X rays and with a 0.13 mm thick beryllium window. The steel plate targets (100-300 µm thick), previously polished and cleaned, and the biological and environmental samples were mounted in the irradiation chamber at 45° with respect to the beam and the detector’s direction. The target chamber had a beryllium window for X rays of 0.1 mm thickness. A thin surface barrier silicon detector was also placed in the chamber, at 135° with respect to the beam direction, in order to detect the backscattered protons for spectra normalization. The X-ray and particle spectra were simultaneously collected and processed off-line with the aid of LEONE computer program.

### **3. Results and disscusion**

#### **3.1 Metallurgical PIXE application**

Details of the PIXE spectrum obtained during the bombardment of a standard steel sample EURONORM CRM No. 085-1 with 3 MeV protons are presented in Fig. 1 a,b,c. Peaks in the spectrum occur at energies indicative of characteristic X rays and the qualitative analysis is an easy task in PIXE.

The minor and trace elements identified in the iron matrix of the steel samples were: K, Ca, Ti, V, Cr, Mn, Co, Ni, Cu, Zn, W, As, Mo, Rb, In, Rh, Pb, Sn, and Sb.

It is worth mentioning that the elements K, Ca, Ti, Cr, Ni, W, As, Mo, Rb, In, Rh, and Sn were not given by the manufacturer for the steel standard EURONORM CRM No. 085-1. Also, some of these elements were identified by NAA (Cr, Ni, W, As, Mo) or PIGE (Ti, Cr, As, Ni, Mo) methods and the results have been published in a previous paper [8].

The limitations of PIXE are the following: i) in the case of analysis of thick steel samples the main problem is the very strong X-ray emission from the iron matrix (Fig. 1 a), which tends to mask the small trace element peaks in the energy spectrum [3]; ii) in the case of the analysis of the elements with  $Z \leq 30$  an interference is frequently encountered between the  $K_{\alpha}(Z+1)$  X-ray and the  $K_{\beta}(Z)$  X-ray, which have virtually the same energy or between the X-K lines of medium elements and X-L lines of heavy elements (Fig. 1 b). Examples of such overlaps in the case of steel samples are: Co- $K_{\alpha}$  and Fe- $K_{\beta}$ ; Ni- $K_{\alpha}$  and Co- $K_{\beta}$ ; Fe- $K_{\alpha}$  and Mn- $K_{\beta}$ ; As- $K_{\alpha}$  and Pb- $L_{\alpha}$ ; Ni- $K_{\alpha}$  and W- $L_{\alpha}$  etc, and corrections have to be made for quantitative analysis of Co using known  $K_{\alpha}/K_{\beta}$  ratios.

In quantitative analysis considerable attention has to pay to matrix effects (non-spectral interferences), ranging from absorption to enhancement, which become important for concentrations bigger than 1% [13]. Matrix effects are well understood in thick target PIXE, and this is an advantage over the optical spectrometric techniques [4,14].

#### **3.2. Biological and environmental PIXE applications**

PIXE analysis allowed determination of S, Cl, K, Ca, Ti, Mn, Fe, Ni, Cu, Zn, Sr (table 1) in vegetable samples and of K, Ca, Mn, Fe, Cu, Zn, Cr, Sr, Mo (table 2) in soil samples. The uncertainties are of the order of 5-10%.

The elemental composition of soil obtained can be use to establish the optimal distances to plant the vegetables used in agroalimentary domain. The calcium, potassium and iron concentrations are higher at the surface soil and decrease inside the soil. A correlation between the elemental map of plants and the elemental map of soil samples can be made in the future.

Also, PIXE analysis allowed determination of Cl, K, Ca, Mn, Fe, Ni, Cu, Zn, As, Sr, Cd and Pb concentration in mosses samples along the Dambovită County with the uncertainties of the data point of the order of 10% (fig. 2) [10].

The obtained results demonstrate that the concentration of heavy and toxic metals in mosses depends on the industrial activity of studied area. The high concentration of Fe, Cl, Ca, Zn, and K in mosses from Fieni and Targoviste towns is explained by the existence of cement factory and steel industries. The present investigation is far from clearing up all aspects of environmental pollution in this region and so, these results will be the starting point of the next research project concerning the environmental monitoring using mosses as bioindicators and analytical methods.



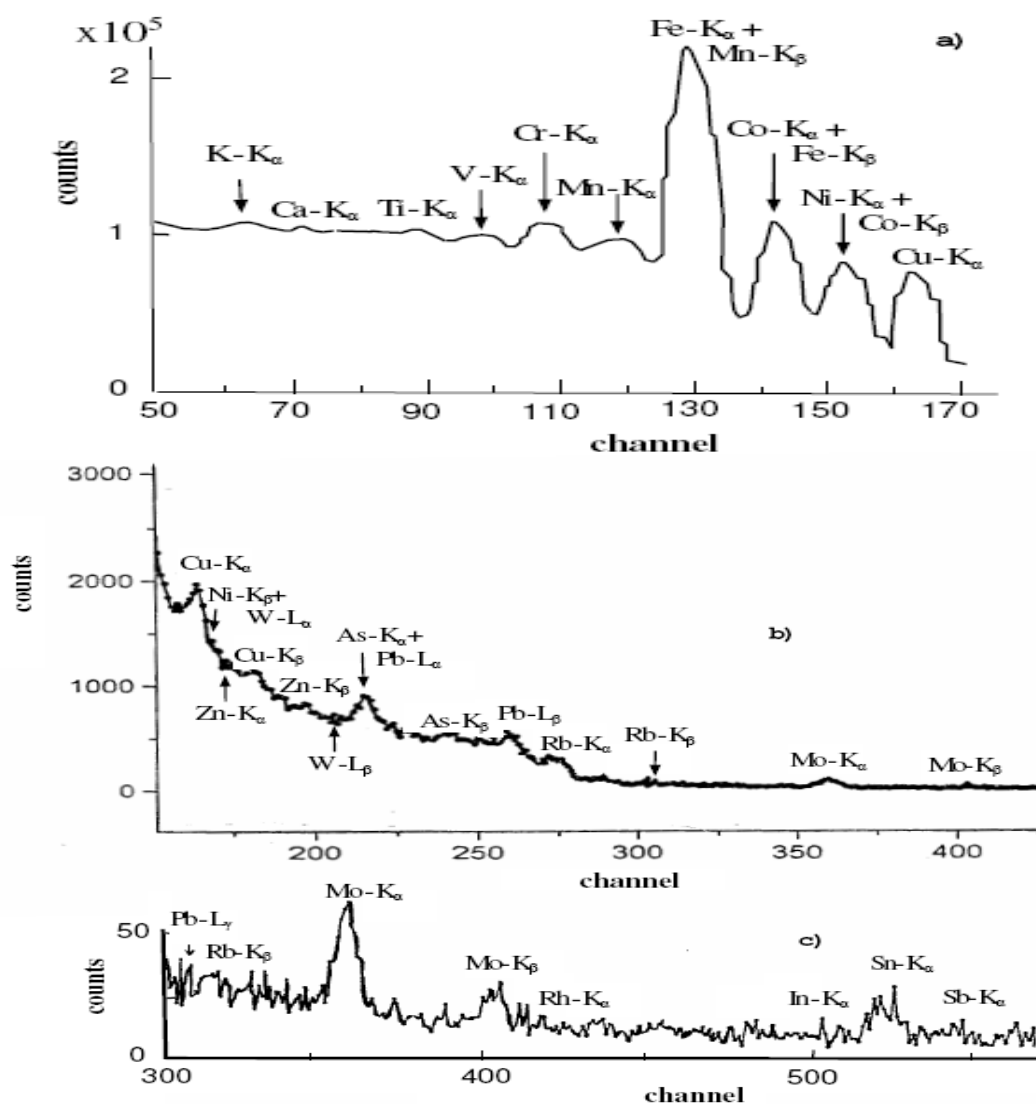


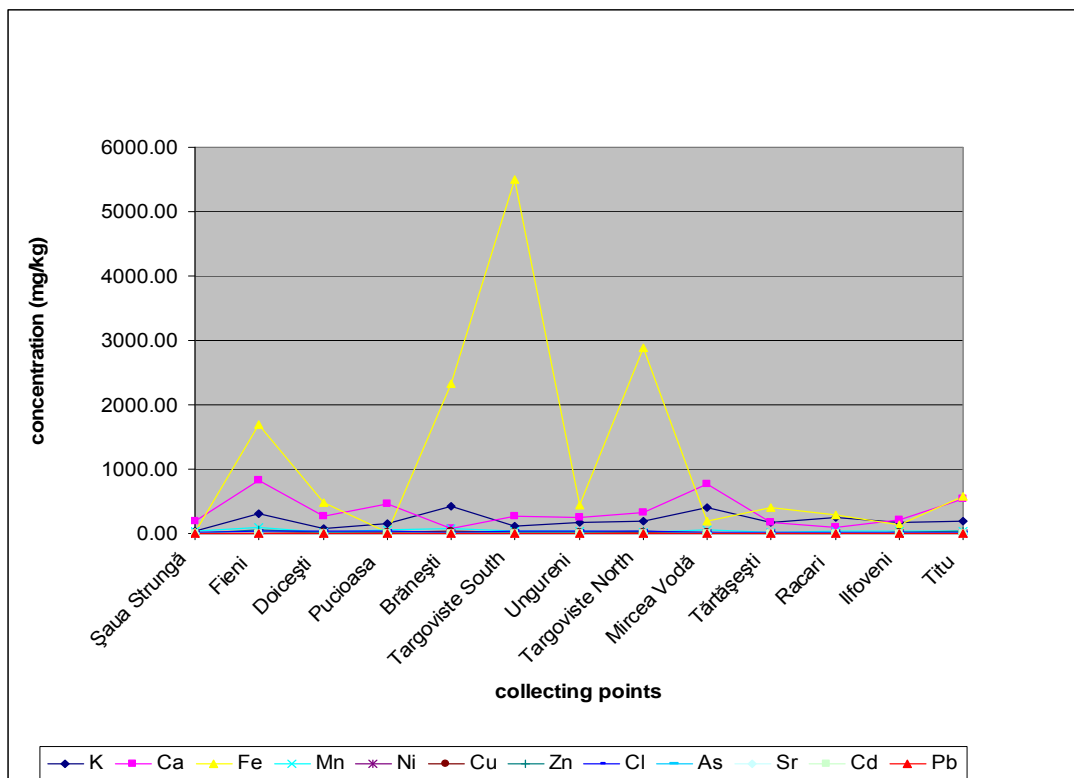
Fig. 1. Details of PIXE spectrum of a steel standard irradiated with 3 MeV protons.

Table 1. Concentration (mg/100g fresh sample ) of elements from vegetable leaves analyzed with PIXE method

Samples	S	Cl	K	Ca	Ti	Mn	Fe	Ni	Cu	Zn	Sr
<i>Apium graveolens</i> (celery) leaves	18	59	19.6	51	0.098	0.116	0.382	0.006	0.011	0.078	0.017
<i>Apium graveolens</i> (celery) leaves	14.3	51.5	15.78	66.6	0.111	0.172	0.346	Nd*	0.018	0.088	0.019
<i>Brasica oleracea</i> (cabbage) external leaves	45.6	89	12	7.84	Nd*	0.098	1.164	0.003	0.053	0.13	0.012
<i>Brasica oleracea</i> (cabbage) external leaves	49	88	10.7	6.7	Nd*	0.095	1.38	Nd*	0.061	0.138	0.014
<i>Brasica oleracea</i> (cabbage) inside leaves	21.84	5.99	36.3	11.9	Nd*	0.022	1.7	0.006	0.054	0.033	0.006
<i>Brasica oleracea</i> (cabbage) inside leaves	28.55	4.75	36	14.22	0.005	0.017	1.88	Nd*	0.045	0.031	0.008
* not detected											

**Table 2. Concentration (mg/100g ) of elements from soil samples analyzed with PIXE method**

Samples	K	Ca	Mn	Fe	Cu	Zn	Cr	Sr	Mo
Soil from surface	37	12	0.07	46	0.005	0.13	0.04	3.6	0.13
Soil from 10 cm deep	27.2	8.12	0.77	35.6	0.007	0.02	0.06	2.6	0.1
Soil from 20 cm deep	23.6	7,80	1.33	31	0.008	0.01	0.16	1.2	0.05



**Fig. 2 - Elements concentration in mosses (mg/kg) along from north to south Dambovită County**

#### 4. Conclusions

The presented PIXE technique is known for its sensitivity, accuracy, precision, simplicity of target preparation and the ability to perform non-destructive multielemental analysis of a large number of samples, sometimes quickly, requiring small amounts of material. Despite these merits, it does suffer from one drawback or another, which are discussed in this paper in the particular case of metallurgical, environmental and biological samples analysis. From this work it results that by applying PIXE method, a very good overall picture of the elemental composition of a complex target may be obtained. It could be a complement of PIGE when the determination of medium and heavy elements content with high sensitivity is necessary.

## References

- [1] Popescu, I.V., T. Badica, A. Olariu, C. Besliu, A. Ene, AL. Ivanescu, J. *Radioanal. Nucl. Chem., Letters*, 213, 369, 1996.
- [2] Ene, A., Besliu, C., Olariu, A., Popescu, I.V., Badica, T., *Rom. Rep. Phys.*, 52, 671, 2000.
- [3] Johansson, S.A.E., Johansson, T.B., *Nucl. Instr. and Meth.*, 137, 473, 1976.
- [4] Maenhaut, W., *Nucl. Instr. and Meth.*, B49, 518, 1990.
- [5] Wilson, D.K., Duggan, J.L., Weathers, D.L., McDaniel, F.D., Matteson, S., Thomson, T., Morgan, I.L., *Nucl. Instr. and Meth.* B56/57, 690, 1991.
- [6] Badica, T., Besliu, C., Ene, A., Olariu, A., Popescu, I., *Nucl. Instr. and Meth.*, B111, 321, 1996.
- [7] Ene, A., Badica, T., Olariu, A., Popescu, I.V., Besliu, C., *Nucl. Instr. and Meth.*, B179, 126, 2001.
- [8] ENE, A., *Nucl. Instr. and Meth.*, B222, 228, 2004.
- [9] Bancuta, A., Stihi, C., Popescu, I.V., Badica, T., Cimpoca, Gh.V., *Journal of Physics: Conference Series* 41,502, 2006.
- [10] Stihi, C., Bancuta, A., Popescu, I.V., Virgolici, M., Cimpoca, V., Gugiu, M., VLAICU, Gh., *Journal of Physics: Conference Series* 41, 565, 2006.
- [11] PILLA, A.E., *Radioanal. Nucl. Chem.*, 243(1), 191, 2000.
- [12] Stihi, C., Popescu, I.V., Busuioc, G., Badica, T., Olariu, A., Dima, G., *J. Radioanal. Nucl. Chem.*, 246(2), 445, 2000.
- [13] Raith, B., Stratmann, A., Wilde, H.R., Gonsior, B., Brüggerhoff, S., Jackwerth, E., *Nucl. Instr. and Meth.*, 181, 199, 1981.
- [14] Hill, S. J., Arowolo, T.A., Butler, O.T., Chenery, S. R. N., Cook, J.M., Cresser, M. S., and Miles, D. L., *J. Anal. At. Spectrom.*, 17, 284, 2002.

## SURFACE WATER POLLUTION MONITORING BY ICP AND TDS MEASUREMENTS

C. STIHI<sup>1</sup>, I.V. POPESCU<sup>1</sup>, V. CIMPOCA<sup>1</sup>, Gh. VLAICU<sup>1,2</sup>, C. OROS<sup>1</sup>, S. APOSTOL<sup>1</sup>,  
D. STOIAN<sup>3</sup>, G. DIMA<sup>1</sup>, S. DINU<sup>1</sup>

<sup>1</sup>*Valahia University of Targoviste, Faculty of Sciences, Physics Department, 2 Carol I street, 130024, Targoviste, Romania, e-mail: [stihi@valahia.ro](mailto:stihi@valahia.ro)*

<sup>2</sup>*Special Steel Complex, Physics laboratories, Targoviste, Romania*

<sup>3</sup>*“Dimitrie Gusti” High School, Bucharest, Romania*

**Abstract:** *In this paper the results of the heavy metals analysis and total dissolved solids (TDS) measurements of water from Ialomita River, Dambovita County are reported. Different samples of surface water, collected at points with industrial pollution sources, were measured using Inductively Coupled Plasma (ICP) spectrometry and conductometry.*

*The ICP measurements allowed determination of S, Cr, Fe, Pb, Cu, Zn, and Cd with a precision less then 6%. For this elements and TDS the migratory forms were determined.*

**Keywords:** *heavy metals, TDS, ICP spectrometry, conductometry, Ialomita River*

### 1. Introduction

Surface water is an important component of fresh water systems and surface water monitoring is essential to attaining a comprehensive understanding of the physical, chemical, and biological characteristics of aquatic systems.

Total Dissolved Solids (TDS) and heavy metals are used, together with another parameters, to classify the river water concerning their quality [1, 2]. The rapid increase in pollution in Dambovita county, due to the industrial processes, thermal power station and domestic sewage, modify the quality of Ialomita river along the county. So, it is necessary to determine the deviation from standard values of heavy metals concentration and TDS.

### 2. Experimental

Different samples of surface water, prelevated from Ialomita river, collected at points with industrial sources of pollution from Dambovita county (table 1), were subjected to two types of measurements: ICP measurements [3,4,5] with Baird ICP2070 spectrometer and conductometry by means of Hach CO150 conductometer.

The ICP measurements were carried out at the ICP Laboratory of the Special Steel Complex of Targoviste. Water samples were collected in 250-ml plastic bottles at one-half the total water depth. Water samples were dissolved in a mixture of 2 cm<sup>3</sup> of HNO<sub>3</sub> and 2 cm<sup>3</sup> of H<sub>2</sub>O<sub>2</sub>. The temperature of the solvent was kept at 120<sup>0</sup>C and the solving time was 20 min. The analysis was done by means of Baird ICP 2070 spectrometer with a plasma gas –Argon. The spectrometer was capable to a sequential determination of elements. For quantitative analysis, standard samples were used.

The TDS measurements [5] were performed at the sampling sites by means of Hach CO150 conductometer with a cell constant K=0.1.

**Table 1. Samples from Ialomita River**

Sample code	Collecting points/ polluting sources
P1	Dobresti – Bucegi Mountain area
P2	Moroieni-Mountain zone/Healthy sanatorium
P3	Pietroșița-Mountain zone
P4	Fieni – town –30 km north from Targoviste town/cement factory, light sources factory
P5	Pucioasa- town –20 km north from Targoviste town /textile factory
P6	Doicești –village area- 10 km north from Targoviste town/ energetic coal factory
P7	Târgoviște-input town/Steel Special Trust, Romlux – light sources factory, Victoria-chemicals factory, PETROM- oil extraction trust
P8	Târgoviște-output town /Steel Special Trust, Romlux – light sources factory, Victoria-chemicals factory, PETROM- oil extraction trust

### 3. Results and discussion

Experimental results obtained by ICP and conductometry are presented in table 2 and table 3.

Using ICP spectrometry we determined the concentration of heavy metals : Cr, Fe, Pb, Cu, Zn, Cd and S in surface water. The migratory forms of heavy metals were determined (figure 1). For S, we observed an increase of S concentration in collecting point corresponding to Pucioasa town, balneological station, where ground water is naturally enriched in S. The deviation from standard values of heavy metals concentration and can be used to establish if Ialomita river along the Dambovită county have degraded water, improper for the development of aquatic fauna or can be use for industry, pisciculture and for urban and recreational use.

Using conductivity measurements we observe a TDS variation presented in figure 2.

The total dissolved solids present a continuous increases starting from sources –Bucegi Mountains to the plains, excepting Fieni point, where we found a similar TDS to the source. The decrease of TDS in this point is in good agreement with the low values for salinity and conductivity. Another striking point is that between Targoviste input and an output point is a very small difference in the TDS. It can be the results of a very efficient system of domestic water depuration.

**Table 2. The concentration (mg/L) of elements in samples from Ialomita River obtained using ICP method**

Element	Concentration of elements (mg/L)							
	P1	P2	P3	P4	P5	P6	P7	P8
S	28.50	27.25	29.33	37.18	58.24	35.40	32.20	35.80
Cr	0.025	0.021	0.021	0.028	0.035	0.045	0.045	0.052
Fe	0.50	0.58	0.58	0.92	0.85	1.12	0.80	0.87
Pb	0.010	0.010	0.012	0.012	0.014	0.018	0.016	0.018
Cu	0.015	0.012	0.015	0.025	0.020	0.030	0.048	0.050
Zn	nd*	nd*	nd*	nd*	nd*	0.015	0.020	0.020
Cd	nd*	nd*	nd*	0.005	nd*	0.005	0.002	0.002
* not detected								

**Table 3. Experimental results of conductivity, salinity and TDS measurements**

Sample code	$\Sigma$ [ $\mu$ S]	Salinity [‰]	TDS [mg/l]
P1	266	0,1	128
P2	385	0,2	183
P3	404	0,2	191
P4	292	0,1	139
P5	416	0,2	199
P6	457	0,2	219
P7	533	0,3	255
P8	550	0,3	262

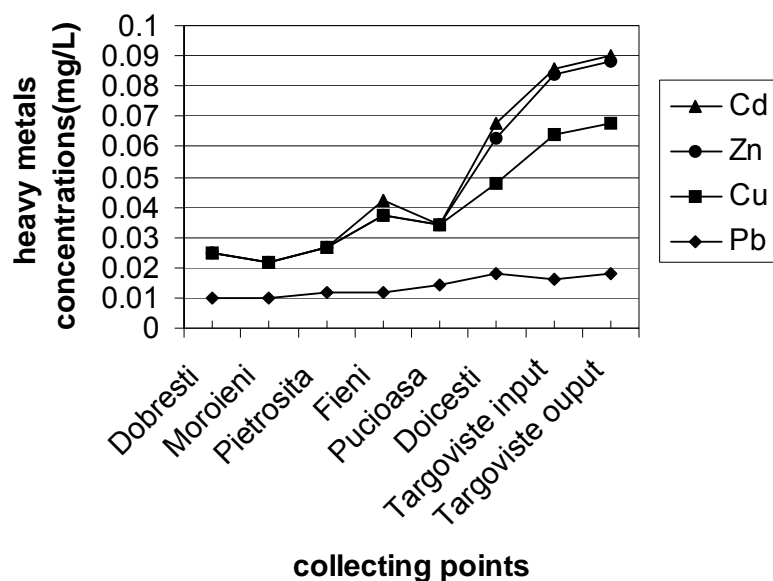


**Figure 1. Pb, Cu, Zn and Cd in the Ialomita River [mg/L]**

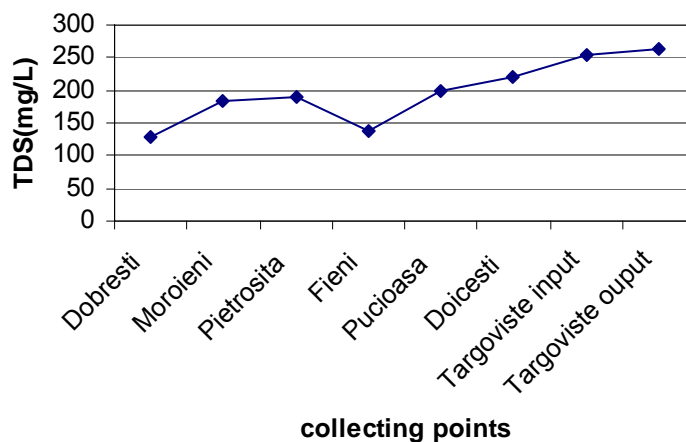


**Figure 2. TDS variation along the Ialomita river- Dambovită area**

#### **4. Conclusions**

Heavy metals were determined in different points of Ialomita River, Dambovita County, points with industrial pollution sources. Higher concentrations of heavy metals were found in samples from Targoviste town, due to the migration along the river. In all samples the heavy metals concentrations are lower than the Romanian maximum allowable limits for surface water which can be use for pisciculture, recreation and urban use. Also the TDS values are in the good agreements with the standards values of TDS surface water.

#### **References**

1. National standards STAS 4706 for surface waters, quality categories and conditions
2. Nguyen, H.L., Leermakers, M., Osan, J., Torok, S., Baeyens, W., *Science of the Total Environment* 340, 213, 2005
3. Boumans, R.W.J.M., *Inductively Coupled Plasma Emission Spectroscopy*, John Wiley and Sons, New York, 1987
4. Winge, R.K., Fassel, V.A. and al, *Spectrochim. Acta*, Part. B, 32-327, 1977
5. Wagner, R.E. (ed), *Guide to Environmental Analytical Methods*, 4<sup>th</sup> edition, Genium Publishing Corporation, Schenectady, NY, 1998
6. Wu, Koch, Hamer and Kay, *Review of Electrolytic Conductance Standards. J.Soln.Chem*, 16, 985, 1987

## FRACTAL DIMENSION OF BLOOD SERUM PIXE SPECTRA COLLECTED FROM ILL FARM ANIMALS

G. D. DIMA<sup>1</sup>, C. OROS<sup>1</sup>, S. DINU<sup>1</sup>, C. STIHI<sup>1</sup>

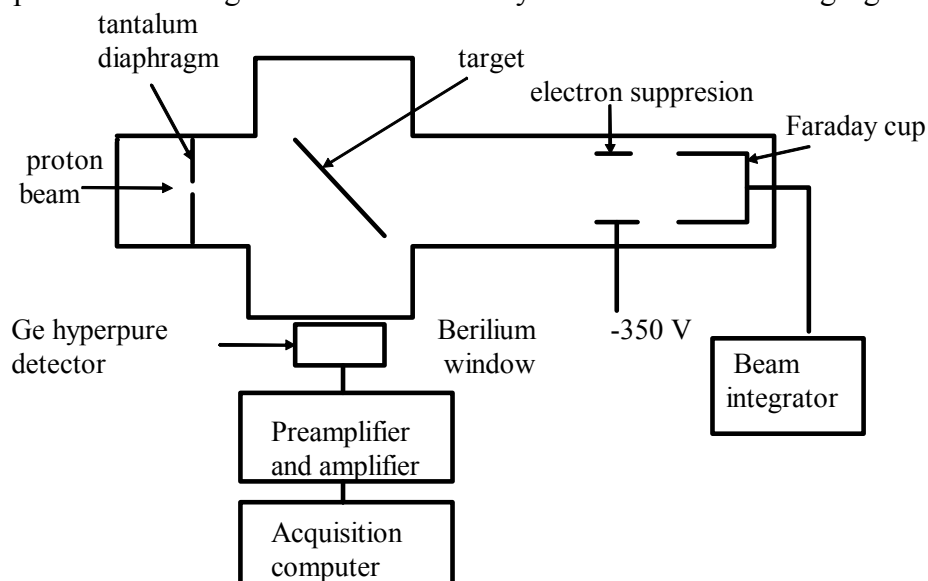
<sup>1</sup>“Valahia” University of Targoviste, Faculty of Sciences and Arts, Romania

**Abstract:** The aim of this work is the fractal dimension of Particle Induced X-Ray Emission (PIXE) spectra determination obtained from blood samples and correlation with various diseases. The blood samples were collected from normal and perturbed metabolism bovines witch lives in different media and doped with an internal standard (Yttrium) for a relative analysis. The samples were bombarded with a 3 MeV proton beam at the IFIN-HH Bucharest. The characteristic X-ray spectrum were detected by a hyperpure Ge detector with resolution of 160 eV at the  $K\alpha$  6.4 KeV X-ray Iron line and recorded using an acquisition computer. The fractal dimension of the obtained spectra was determined with Binary Encounter Theorem and Box Counting Theorem.

**Keywords:** PIXE, fractal dimension, anemia

Particle Induced X-Ray Emission (PIXE) method consists in producing holes in the deep electronic shells of the atoms, caused by accelerate charged particle impact, and in the immediate rearrangement of the electrons. The results of ionization are two types of de-excitation by means of X-ray emission and emission of low energy Auger electrons. Interesting is the X-ray emission, the energy of the emitted X-ray represents a smooth function of Z of elements contained in a sample target. To obtain the X- rays spectra, a beam of protons passes through an irradiation chamber. The intensity of the beam is made uniform by means of a diffuser foil and two pairs of electrostatic deflector plates sweeping the beam in two perpendicular directions. Then the beam is defined by a series of collimators. The target is a thin foil of carbon or plastic upon witch the sample to be analyzed has been deposited. The beam is dumped in a Faraday cup connected to a beam integrator. X- Rays emitted by the samples pass through a thin window in the chamber and are detected by a germanium detector. The pulses from the detector are analyzed in a multichannel analyzer.

The experimental arrangement is schematically shown in the following figure:



The irradiation chamber is made from aluminium and she can include 24 samples for analysis without breaking the vacuum needed for a background minimization [1]



### ***Sample preparation***

The target samples have been prepared in the following manner: we collected blood serum of bovines (in good health and with infections' diseases) that live in road about Targoviste town - Romania, and then the blood serum was doped with standard solution of Yttrium and deposited on hostaphan foils.

### ***Sample analysis***

Measurements were made using a 3.2 MeV protons beam extracted from the TANDEM accelerator from IFIN-HH Magurele, Bucharest. X-ray's spectra were measured with a spectrometric chain, with a CANBERRA Ge hyperpure detector with a 160 eV resolution at 6.4 KeV of XK $\alpha$  line of iron. Amplification, generation and analysis of electric signals were achieved by an adequate electronic device: a sensitive preamplifier with field effect cooled at the liquid nitrogen temperature, a linear amplifier and a multichannel analyzer with 4096 channels having an acquisition computer for data output - PDP11. For each sample target were recorded the characteristic X-ray spectra. The X-ray spectrum's analyses were made off-line using a computer fitting programme - ORIGIN. The calibrations of experimental set-up were made using standard targets witch are prepared by evaporating pure elements (Ni, Cu, Ge, Ag, Sn, Au, Pb) on hostaphan foil [2].

The sample analyses were made on two ways: a relative analysis's method - the internal standard method, which has the great advantage to eliminate the systematic errors [3], and a fractal analysis method of the obtained spectra. The fractal analysis method consists in fractal dimension determination of obtained spectra. There are various numbers associated with fractals' witch can be used to compare them. They are generally referred to as fractal dimensions. They are attempts to quantify a subjective feeling witch we have about how densely the fractal occupies the metric space in witch it lies. Fractal dimensions provide an objective means for comparing fractals. Fractal dimensions are important because they can be measured approximately by means of experiment. In our experiment we determine the fractal dimension of obtained spectra by means of a computer program witch using the Box Counting Theorem: cover the bidimensional space by closed just-touching square boxes of side length  $(1/2^n)$  for  $n$  an integer number. Let  $N_n$  connote the number of boxes of side length  $(1/2^n)$  witches intersect the obtained spectra. The fractal dimension associated

to the analyzing spectra is defined like: 
$$D = \lim_{n \rightarrow \infty} \left[ \frac{\ln(N_n)}{\ln(2^n)} \right].$$

### **Results and conclusions**

We have studying 15 blood serum samples grouped in two series: sample 1-5 containing blood serum from normal bovines and samples' 6-15 from ill bovines.

We identified elements with  $Z > 22$  in serum sample: Fe, Cu, Zn, Ni, Mn, Br, Cr, Ti and we make in evidence deviation from normal state in iron content of blood serum of bovine with infections' diseases. The pathological variations of iron concentration of blood serum are meet to: the feriprive anemia and acute morrhage diseases (sample 5-10, with decrease of iron concentration) and the pernicious anemia, hemolytic anemia and jaundice hepatitis (sample 11-16, with increase of iron concentration). With the aid of Box Counting Theorem we determine the fractal dimension of each spectrum and the results are presented in the following table:

Sample	Fractal dimension	Disease
1-5	0,77	normal
6-10	0,81	feriprive anemia
11-15	0,79	pernicious anemia

Because of the good reproducibility of the fractal dimension of the PIXE spectra we can make correlation between them and various diseases. The fractal dimension depends on the disease of the analyzing patient and her determination can be a diagnostic method.

### **References**

- [1.]T. Badica, C. Ciortea, A. Petrovici, I. Popescu,Rev. Roum. Phys. , Tome 26, No.7, P.635-671, Bucharest, 1981
- [2.]I. Popescu, et al. Proc.of National Conference of Physics, P. 152, Baia Mare, Romania,1996
- [3.]I. Popescu et al. Proc. of Balkan Biochemical Biophysical Days, Thessaloniki, Greece, 1997, No.153

## ATOMIC FORCE MICROSCOPY-ATOMIC INVESTIGATION METHOD

O. BUTE<sup>1</sup>, V. CIMPOCA<sup>1</sup>

<sup>1</sup>*“Valahia” University of Targoviste, Faculty of Sciences and Arts, Romania*

**Abstract:** *An AFM is a mechanical instrument that measures 3D-topography as well as physical properties of a surface. With an AFM is possible to view features on a surface having a few nanometersized dimensions including single atoms and molecules on a surface.*

*The goal of this paper is to briefly present the operation principle of AFM, the history of AFM and how this type of microscopy has opened a way to the nanotechnology.*

**Keywords:** *nanotechnology, AFM, Atomic Force Microscopy*

### 1. Introduction

Optical or electron microscopes belong to the traditional microscopes family creating a magnified image of an object by focusing electromagnetic radiation (photons or electrons) on its surface. These microscopes generate 2D (two-dimensional) magnified images of an object, the magnification being about 1000X for an optical microscope and about 100 000X for an electron microscope.

A disadvantage of these microscopes is the fact that we can obtain images only in the horizontal plane. Such microscopes don't supply the vertical dimensions on an object's surface. In order to exceed this disadvantage another microscopes family was created such as Scanning Probe Microscopy family (SPM).

Scanning Probe Microscopy consists of a family of microscopy forms in which a sharp probe is scanned across a surface and some probe-sample interaction are monitored. Primary forms of SPM are Scanning Tunneling Microscopy (STM) and Atomic Force Microscopy (AFM).

An AFM is a mechanical imaging instrument that measures 3D-topography as well as physical properties of a surface. With an AFM is possible to view features on a surface having a few nanometer-sized dimensions including single atoms and molecules on a surface.

The goal of this paper is to briefly present the operation principle of AFM, the history of AFM and how this type of microscopy has opened a way to the nanotechnology.

### *The operation principle of AFM*

A. The primary components of an AFM are the control system and microscope system (figure 1)

#### **A.1 Control System**

The control system includes:

- Computer;
- Control monitor;
- Display monitor;
- AFM control electronics;
- Software

#### **A.2 Microscope System**

The microscope system includes:

- Sample stage;
- Piezo-electric scanner;
- AFM detection electronics

## Basic SPM Components

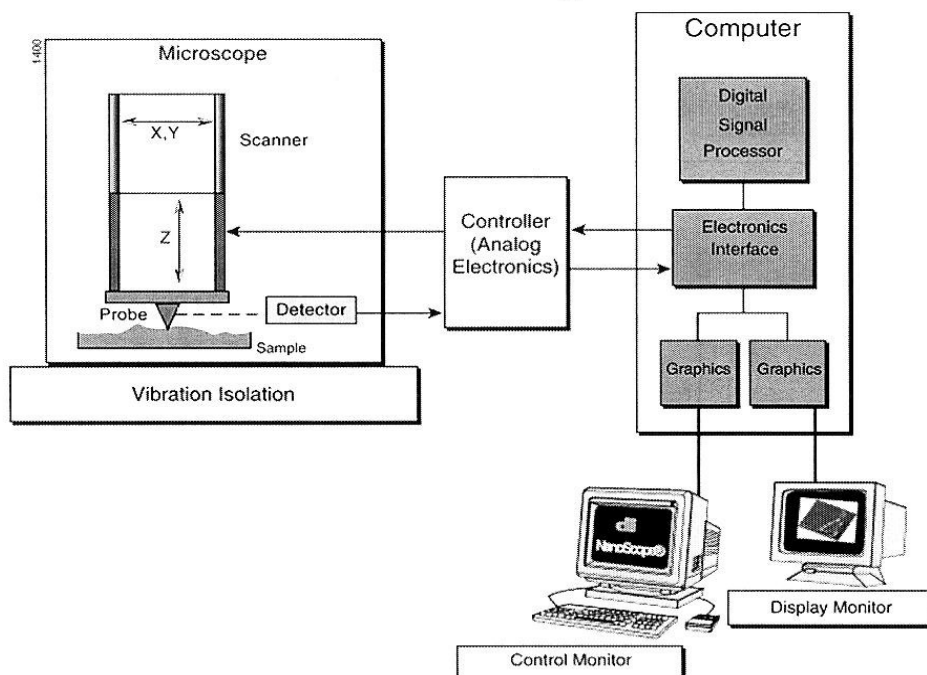


**Figure 1. The primary components of an AFM**

- B.** The primary modes of AFM are: contact mode AFM; non-contact mode AFM and tapping mode AFM.

### **B.1 Contact mode AFM**

This mode operates by scanning a tip attached to the end of a cantilever across the sample surface while monitoring the change in cantilever deflection with a split photodiode detector. The tip contacts the surface through the adsorbed fluid layer on the sample surface. A feedback loop maintains a constant deflection between the cantilever and the sample by vertically moving the scanner at each (X, Y) data point to maintain a set deflection. By maintaining a constant cantilever deflection, the force between the tip and the sample remains constant. The computer stores the distances the scanner moves vertically at each (x, y) data point to form the topographic image of the sample surface.

Operation can take place in ambient and liquid environments.

### **B.2 Tapping mode AFM**

This mode operates by scanning a tip attached to the end of an oscillating cantilever across the sample surface. The cantilever oscillates at or near its resonance frequency with amplitude ranging typically from 20nm to 100 nm. The tip lightly taps the sample surface during scanning, contacting the surface at the bottom of its swing (see figure 2). A feedback loop maintains a constant cantilever oscillation by vertically moving the scanner until a set amplitude is achieved. The computer stores the vertical position of the scanner at each (x, y) data point in order to form the topographic image of the sample surface.

Operation can take place in ambient and liquid environments.

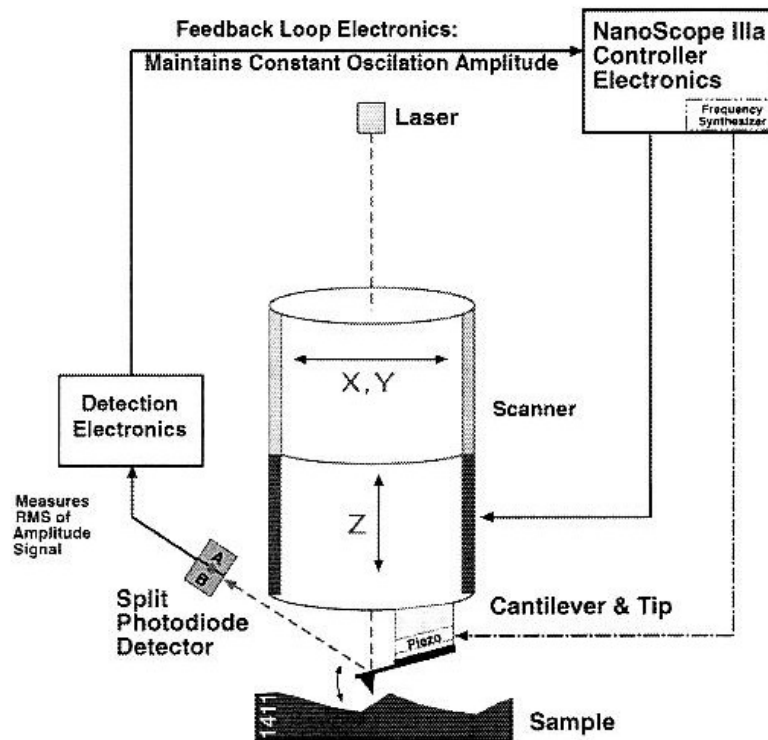


Figure 2.

C. Advantages and disadvantages of contact mode AFM and tapping mode AFM

Contact Mode AFM		Tapping Mode AFM	
Advantages	Disadvantages	Advantages	Disadvantages
<ul style="list-style-type: none"> <li>• High scan speeds;</li> <li>• Contact mode AFM is the only AFM technique which can obtain atomic resolution images;</li> <li>• Rough samples with extreme changes in vertical topography can sometimes be scanned more easily in contact mode.</li> </ul>	<ul style="list-style-type: none"> <li>• Lateral forces can distort features in the image;</li> <li>• The forces normal to the tip-sample interaction can be high in air due to capillary forces from the adsorbed fluid layer on the sample surface;</li> <li>• The combination of lateral forces and high normal forces can result in reduced spatial resolution and may damage soft samples (biological samples, polymers, silicon) due to scraping between the tip and sample.</li> </ul>	<ul style="list-style-type: none"> <li>• Higher lateral resolution on most samples (1nm to 5nm)</li> <li>• Lower forces and less damage to soft samples imaged in air;</li> <li>• Lateral forces are virtually eliminated, so there is no scraping.</li> </ul>	<ul style="list-style-type: none"> <li>• Slightly slower scan speed than contact mode AFM.</li> </ul>

#### D. AFM detection optics

The AFM detection optics includes:

- Laser light from a solid state diode;
- Split photodiode detector;
- Differential amplifier.

Laser light from a solid state diode is reflected off the back of the cantilever and collected by a split photodiode detector which consists of two closely spaced photodiodes whose output signal is collected by a differential amplifier. Angular displacement of cantilever results in one photodiode collecting more light than the other photodiode, producing an output signal (the difference between the photodiodes signals normalized by their sum), which is proportional to the deflection of the cantilever (see figure 3).

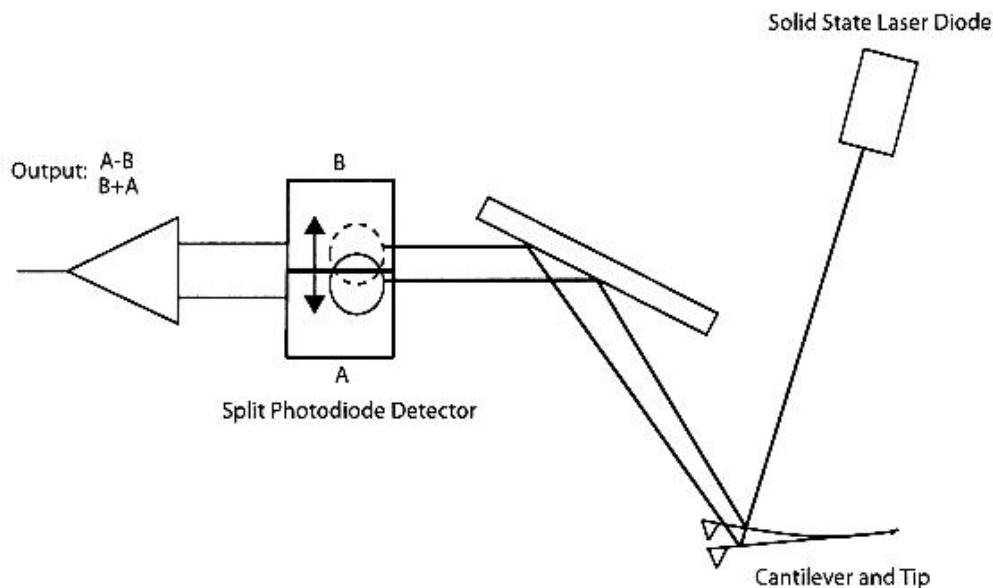


**Figure 3.**

#### E. AFM Probe

There are three major components of an AFM probe: a substrate, a cantilever and a tip.

- **Substrate**-the portion of the probe handled by the tweezers during installation into the cantilever holder.
- **Cantilever**-the portion of the probe that projects off of the end of the substrate. The tip mounts on the end of the cantilever.
- **Tip**-the portion of the probe that comes in proximity to the sample surface. The point of the tip has a radius of curvature from 5nm to 50nm depending on the type. If the tip is manufactured from silicon nitride then the radius of curvature is 20-50 nm while for the silicon tip the radius of curvature is 5-10 nm.

There are two primary features of the tip that affect the AFM image:

- Radius of curvature;
- Tip sidewall angles.

A sharper tip will be able to laterally resolve smaller features than a dull tip with a larger radius of curvature (see figure 4).

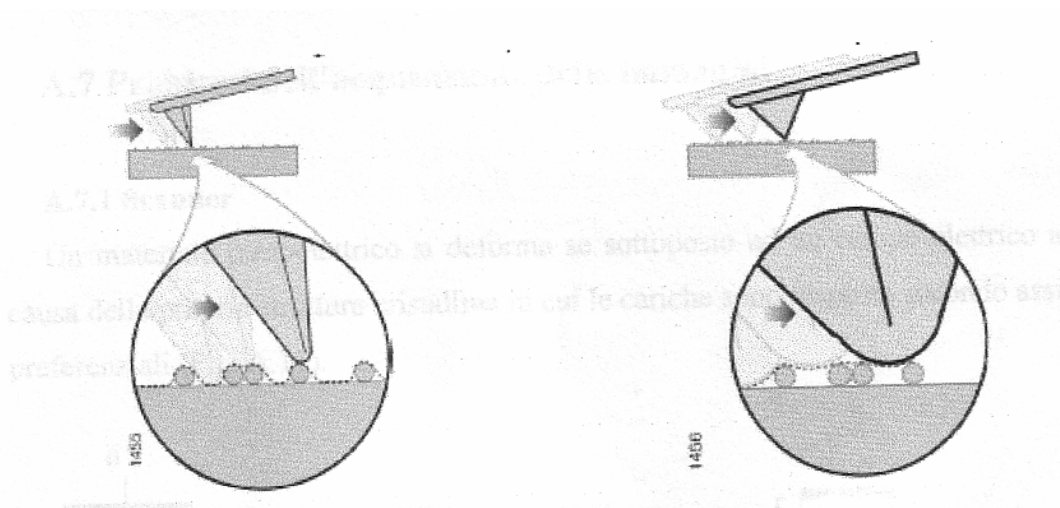


**Figure 4.**

The sidewall angles of the tip determine the ability to image steep sidewalls on a sample surface. The tip cannot profile sides of surfaces steeper than the sidewall angle of the tip.

### History of AFM

- **1929-Schmalz** invented the first profiler. A magnified profile of the surface was generated by recording the motion of a stylus on photographic paper. A disadvantage of this profiler was the bending of the probe from collisions with surface features.
- **1950-Becker and Lee** have resolved the bending probe problem. They suggested oscillating the probe from a null position above the surface to contact with the surface. In this case the detail of the images depends on the sharpness of the probe.
- **1971-Russell Young** demonstrated a non-contact type of stylus profiler. In this profiler, Young used the fact that electron field emission current between a sharp metal probe and a surface is very dependent on the probe sample distance for electrically conductive samples.
- **1981-Binning and Rohrer** have created the scanning tunneling microscope (STM). They demonstrated that by controlling the vibrations of an instrument very similar to Young's profiler, it was possible to monitor the electron tunneling current between a sharp probe and a sample. It was possible to scan very close to the surface because electron tunneling is much more sensitive than field emission. Binning and Rohrer were able to see individual silicon atoms on a surface. A problem of this microscope is related of the fact that this microscope works only on electrically conductive samples.
- **1986-Binning and Quate** exceeded this problem creating the Atomic Force Microscope (AFM).

### 3. Conclusions

#### *Atomic Force Microscope Contribution to the Nanotechnology*

With an AFM it is possible to directly view features on a surface having a few nanometer-sized dimensions including single atoms and molecules on a surface. This gives to scientists and engineers the possibility to directly visualize nanometer-sized objects and to measure the dimensions of the surface features.

On the other hand it is possible to write on a surface with an AFM. This new type of lithography results in a completely new method for making surface modifications at the nanometer

scale. It is already possible to modify surfaces by physically scratching the surface, by directly depositing molecules on a surface and by using electric fields to modify surfaces.

Furthermore, with an AFM it is possible to directly move objects across a surface. The objects may be pushed, rolled around or even picked up by the probe. We can say that such methods can create nanometer -sized objects.

An AFM has opened the door towards the nanotechnology, more exactly towards the future.

## **References**

- [1] Giessibl, F.J., *Rev. Mod. Phys.*, 75(3), 2003
- [2] \*\*\* *Basic SPM Training Course*, Digital instruments Veeco Inc., 2000
- [3] Young, R., Ward, J., Scire, F., *Rev. Sci. Inst.*, 43(7), 999, 2001
- [4] Binning, G., Rohrer, H., Geber, Ch., *Surface Studies by Scanning Tunneling Microscopy*, 49(1), 57, 1982
- [5] Binning, G., Quate, C.F., Geber, Ch., *Phys. Rev. Letters*, 56(9), 930, 1986



## THE THEORETICAL AND EXPERIMENTAL STUDY OF SOME METALS HEATING AND MEALTING UNDER THE ACTION OF LASER RADIATION

C. OROS<sup>1</sup>, S. DINU<sup>1</sup>, M. VOICU<sup>1</sup>

<sup>1</sup>“Valahia” University of Targoviste, Faculty of Sciences and Arts, Romania

**Abstract:** The study presents the theoretical and experimental results regarding at laser irradiation of some metals (steel, aluminum, titanium), using a Nd:YAG laser. The theoretical studies contain the solving of heat equation for half-infinite targets in case that, between the thickness of target ( $h$ ), the diameter of laser spot ( $D_s$ ) and the length of thermic diffusion ( $l_{th}$ ), exists the relation  $h \gg D_s > l_{th}$ . The determination of the temperature at the surface of the irradiated material allows quantitative estimations regarding the induced thermo-deformation and also the involved phase transition, in our case, the mealting. The confrontation with experience is achieved through the comparison of the thermo-deformation sizes and obtained craters and also of the others related parameters with the direct microscopically measurements. The calculated values are in proper correlation with the experimental ones, the observed differences having as major cause the insufficiently precise knowledge of the involved physical sizes values, at high reached temperatures on the irradiated surfaces.

**Keywords:** metal, Nd:YAG laser, thermo-deformation, laser mealting.

### Experimental

The samples of steel, aluminum and titanium have cylindrical shape, with height  $h \approx 5\text{mm}$  and base diameter  $d \approx 20\text{mm}$ .

The characteristics of emitted radiation by Nd:YAG laser are: the wavelength  $\lambda = 1,06\mu\text{m}$  (IR); the diameter of laser spot  $D_s = 0,4\text{ mm}$  (steel and titanium), respectively  $0,6\text{mm}$  in aluminium case; the length of laser pulse  $\tau_p = 3\text{ms}$  (irradiation regime is monopuls).

The analysis of irradiated surfaces has been done with an optical microscop whose accuracy in the estimate of the created drops (dilatations and craters) is  $2\mu\text{m}$ .

### Results and discussion

The samples have been irradiated differently trhough the modification of pulse energy. The adequate intensities have been established with the following relation:

$$I_i = \frac{E_i}{S \cdot \tau_p}, \quad i = \overline{1,10}, \quad (1)$$

with  $S = \pi \frac{D_s^2}{4}$  representing the area of irradiated surface and  $\tau_p$  representing the length of laser pulse.

The measured dimenssions of formatted thermodilatations (+) or craters (-), matched to the intensities given by the relation (1), are presented in the next table (tab 1):

Tabel 1

The sample	1	2	3	4	5	6	7	8	9	10
$E_i$ (unit)	450	500	550	600	650	700	750	800	850	900
$\Delta z_{i Al}$ (div) 1 div=2 $\mu$ m	-	-	0	0	0	-10	-20	-15	-15	-12
$\Delta z_{i Ti}$ (div) 1 div=2 $\mu$ m	-	-	+10	+5	+10	+13	-65	-50	-60	-140
$\Delta z_{i otel}$ (div) 1 div=2 $\mu$ m	0	0	+25	+20	+20	+40	-15	-10	-15	-100

These results will be interpreted on the bases of a thermic model of interaction between the laser radiation and metallic samples.

Thus, the spatial – temporal dependence of the reached temperature in the target,  $T(z,t)$ , can be established using the unidimensional equation of heat propagation in a solid medium whose forme is:

$$\rho c \frac{\partial T}{\partial t} = K_T \frac{\partial^2 T}{\partial z^2} + \alpha A I_0 e^{-\alpha z}, \quad (2)$$

where  $z$  is the depth in the target and  $t$  is the irradiated time. Because the laser radiation is, for the metallic sample, a superficial heat source, the solution of equation (2) has the forme:

$$T(z,t) = \frac{2AI_0}{K_T} \sqrt{\chi_T \cdot t} \cdot ierfc \frac{z}{2\sqrt{\chi_T \cdot t}}. \quad (3)$$

For  $z=0$  (at the sample surface) and  $t=\tau_p$ , the relation (3) became:

$$T(0, \tau_p) = \frac{2AI_0}{K_T} \sqrt{\chi_T \cdot \tau_p}. \quad (4)$$

This solution is valid in the mentioned conditions at the beginning of the article, that is:  $h \gg D_s \gg l_{th}$  ( $h=5mm$ ,  $D_s=0,4mm$ ,  $l_{th} = \sqrt{\pi \chi_T \tau_p} / 2 = 0,12mm$  for steel;  $h=5mm$ ,  $D_s= 0,6 mm$ ,  $l_{th}= 0,47 mm$  for aluminium;  $h=5mm$ ;  $D_s= 0,4 mm$ ;  $l_{th}= 0,14 mm$  for titanium).

For ALUMINUM,  $A=6 \%$ ,  $K_T=236 J/msK$ ,  $\chi_T = \frac{K_T}{\rho c} = 0,96 \cdot 10^{-4} m^2/s$  ( $\rho=2.71 \cdot 10^3 kg/m^3$ ,  $c$

$=902 J/kgK$ ),  $\tau_p = 3 \cdot 10^{-3} s$ ,  $I_{0i} \cong 0,7 I_i$  cu  $I_i = \frac{E_i}{S \tau_p}$  and the relation (4) get the forme:

$$T_i(0, \tau_p) = 225 E_i (K), \quad (5)$$

with the energies  $E_i$  expressed in Joule.

Now, because the used laser is calibrated in energy units and not in Joule, it can be achieved a correspondence from the knowledge of the aluminium mealting temperature, of the energy value (in units) that it was observed the mealting beginning and of the formula (5) thus:

$$E_{top}(J) = \frac{T_{top}(K)}{225} \cong 4,13J. \quad (6)$$

A first verification of the used model is achieved calculating the superficial density of electromagnetic energy needed for the beginning of aluminium sample mealting:

$$w_{em teor} = \sqrt{\pi \rho c K_T \tau_p} (T_{top} - T_0) / 2A, \quad (7)$$

$$\cong 12,7 \cdot 10^6 J / m^2,$$

$$w_{em teor} = \sqrt{\pi \rho c K_T \tau_p} (T_{top} - T_0) / 2A. \quad (8)$$

$$\cong 12,7 \cdot 10^6 J / m^2$$

An additional element, that is the time needed to the laser radiation for initiate the mealting process, can be calculated from:

$$t_{top} = \frac{K_T^2 \cdot T_{top}^2}{4A^2 I_{top \exp}^2} = 0,14 \mu s. \quad (9)$$

$$(I_{top \exp} = \frac{E_{top}}{S \tau_p} = 4,87 \cdot 10^9 \text{ W/m}^2)$$

It may be done as well a theoretical estimation of length of the craters formed in the Al sample based on the approximate formula:

$$\Delta z_{crater} \cong \frac{D_s}{4} \left( \frac{T_{vap}}{T_{top}} - \frac{T_{top}}{T_{vap}} \right). \quad (10)$$

Considering that  $T_{melting} = 930 \text{ K}$ ,  $T_{vap} = 2543 \text{ K}$  and  $D_s = 0,6 \text{ mm}$ , it is obtained the value:

$$\Delta z_{crater} \cong 350 \mu m \quad (11)$$

(thermodilatations of the Al surface were not observed at intensities lower then the mealting limit).

For STEEL,  $A=27 \%$ ,  $K_T=26 \text{ J/msK}$ ,  $\chi_T = \frac{K_T}{\rho c} = 6,9 \cdot 10^{-6} \text{ m}^2/\text{s}$  ( $\rho=8 \cdot 10^3 \text{ kg/m}^3$ ,  $c=470$

$\text{J/kgK}$ ) and, following a judgement similar to the one from the Al case, it can be obtained:

$$w_{emteor} = 2,73 \cdot 10^6 \text{ J/m}^2, \quad (12)$$

$$w_{emexp} = 1,89 \cdot 10^6 \text{ J/m}^2, \quad (13)$$

with  $T_{melting} = 1808 \text{ K}$ .

$$t_{top} = 1,1 \mu s, \quad (14)$$

$$\Delta z_{crater} = 72 \mu m, \quad (15)$$

with  $T_{vap} = 2573 \text{ K}$ .

Calculating the intensity of laser radiation needed for the mealting induction with the formula:

$$I_{melting} = 0,7 \frac{E_{top}}{S \tau} = 4,2 \cdot 10^4 \text{ W/cm}^2, \quad (16)$$

it can be observed an approached value, as dimension order, to the one from the tables,  $I_{melting} = 1,5 \cdot 10^4 \text{ W/cm}^2$ .

For TITANIUM,  $A=7\%$ ,  $K_T=22 \text{ J/msK}$ ,  $\chi_T = \frac{K_T}{\rho c} = 0,09 \cdot 10^{-4} \text{ m}^2/\text{s}$  ( $\rho=4500 \text{ kg/m}^3$ ,  $c=520$

$\text{J/kgK}$ ),  $T_{melting} = 2073 \text{ K}$ ,  $T_{vap} = 3523 \text{ K}$ .

It results:

$$w_{emteor} = 8,95 \cdot 10^6 \text{ J/m}^2, \quad (17)$$

$$w_{emexp} = 5,89 \cdot 10^6 \text{ J/m}^2, \quad (18)$$

$$t_{top} = 0,027 \mu s, \quad (19)$$

$$\Delta z_{crater} = 110 \mu m. \quad (20)$$

Another confrontation with the experience is possible, in the case of steel and Ti, from the estimation of the linear dimensions of the thermodilatation, based on the linear dilatation and the comparison of these with the measurements realised using optical microscop (table 1, values with “+”). Thus, considering the length dilatation of the cylinder with  $l_{th}$  high and  $S = \pi \frac{D_s^2}{4}$  base area, it may be written:

$$\Delta z_{i \text{ teor}} = \alpha z_0 \Delta T_i, \quad (21)$$

in which  $z_0 \approx l_{th} = 0,12 \text{ mm}$  and  $\alpha = 1,2 \cdot 10^{-5} \text{ K}^{-1}$  for steel and for Ti, the values are  $z_0 = 0,14 \text{ mm}$  and

$\alpha = 1,08 \cdot 10^{-5} K^{-1}$  ( $\Delta T_i \cong T_i - T_0$ , with  $T_0 = 273 K$ , and  $T_i$  is obtained considering the fact that the energies  $E_i$  values are proportional to the number of units on the adjustment rosette of laser,  $N_i$ , as following:

$$E_i = E_{\text{melting}} \frac{N_i}{750},$$

750 units correspond to the limit of the melting initiation).

The results are mentioned in the next tables (table 2 and table 3):

Table 2:

Proba (otel)	1	2	3	4	5	6
$E_i$ (J)	0,138	0,153	0,168	0,184	0,199	0,214
$T_i$ (K)	1090	1208	1327	1453	1572	1690
$\Delta z_{i\text{teor}}$ ( $\mu\text{m}$ )	1,17	1,34	1,51	1,69	1,87	2,04
$\Delta z_{i\text{exp}}$ ( $\mu\text{m}$ )	0	0	50	40	40	80

Table 3:

Proba (titan)	1	2	3	4
$T_i$ (K)	1515	1650	1805	1940
$\Delta z_{i\text{teor}}$ ( $\mu\text{m}$ )	1,87	2,08	2,31	2,52
$\Delta z_{i\text{exp}}$ ( $\mu\text{m}$ )	+20	+10	+20	+25

An interesting element is related to the comparison, using microscop, of the thermodilatation forme with that of the intensity distribution in the laser beam (fig. 1). This suggests the fact that in the central zone of the beam, because of the higher values, the reached temperature in the spot center is higher, therefore the dilatation extend will be higher too.

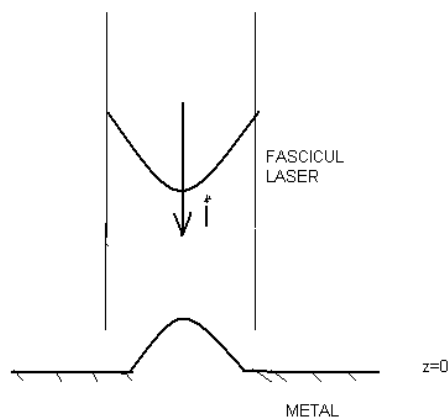


**Fig. 1. The thermodilatation forme with that of intensity distribution in the laser beam**

### Conclusions

It has been possible to observe an approach close enough to the theoretical results with the experimental ones, specially in the determination of the superficial density of the needed energy for induction of the each metal mealting, of the fusion depth (better concordances has been observed at steel and Ti) and even of the critical laser intensity in order to reach of the mealting limit (at steel). This suggests that, although the values of the involved physical parameters, in calculations, are insufficiently known, specially at high temperature reached at the samples surfaces, the used thermic model for estimating the shown up thermodilatation after the irradiation was not to suitable, but the explanation is simple enough: the dilatated and warmed volume is much more higher then the considered one in the application of the thermic dilatation law, fact that appreciably minimises the theoretical values of the dilatation at the samples surfaces. Finally, it is obtained that the necessity of the continuation of this type of experiences even in other metals case for more precise estimations regarding the used theoretical model.

## **B. CHEMISTRY SECTION**

## EFFECTS OF CALCIUM CARBONATE NANOPHASE ON i-PP

T. ZAHARESCU<sup>1</sup>, S. JIPA<sup>2</sup>, L. M. GORGHIU<sup>2</sup>, C. DUMITRESCU<sup>2</sup>, R. L. OLTEANU<sup>2</sup>

<sup>1</sup> INC DIE-ICPE CA, 313 Splaiul Unirii, P. O. Box 149, Bucharest 030138, Romania

<sup>2</sup> Faculty of Sciences, “Valahia” University of Targoviste,, 18-22 Unirii Av. Târgoviște 130082, Romania

**Abstract:** Thermal and  $\gamma$  radiation stability of i-PP containing  $\text{CaCO}_3$  nanoparticles were investigated by oxygen uptake procedure at 190 °C. The loading of i-PP matrix was maximum 25 % (w/w). The behavior on thermal oxidation was investigated for two formulations of i-PP compounds differing by the surface characteristics of nanoparticles (i.e. uncoated and stearic acid-coated filler). Three irradiation doses (5, 15 and 25 kGy) were applied. The efficient protection of stabilizers that are present in the as-prepared formulations was emphasized by proper values of the kinetic parameters obtained for oxidation. The contribution of  $\text{CaCO}_3$  nanoparticles to the oxidative process of i-PP is discussed.

**Keywords:** i-PP,  $\text{CaCO}_3$  nanoparticles, irradiation,  $\gamma$  radiation

### 1. Introduction

A large number of studies on the preparation and characterization of polymer/nanoparticles matrix were reported [1-10], because of their excellent functional properties. The presence of nanoscale inorganic fillers improves mechanical, thermal and gas barrier characteristics [1-15]. Several promising formulations of polymer hybrids were proposed for satisfying various requirements for a large number of applications. However, the problem of thermal stability of polymer composites is of a great interest being directly related to the material durability. The topic of thermal degradation has received a special attention due to the strong influence of the service conditions on the behavior of composites. The characterization of material depreciation by heat provides useful information for storage, processing and long-term use, namely the life of products. Ever using well-elaborated technologies of preparation, the stress factors act on any time. Recent papers [16, 17] have emphasized the phenomenological analysis of degradation in connection with various testing methods. The most applied procedures for depicting the thermal behavior of polymer composites were DSC and TGA. [4, 18-20] These papers have reported the difference between unloaded and polymer composites, which is caused by the modification in surface energy between the microphases, which would exist in the tested material.

For obtaining a high rate and advanced degradation, ionizing radiation may be used. Data obtained from accelerated ageing testing prove the capacity of material to resist for a certain period to the action of vigorous energetic agents. The durability of any material under high energy-radiation exposure depends on many features through which the chemical nature of basic material and the sample formulation determine the kinetic behavior during degradation. [21-23]

Effects of irradiation on polypropylene have been extensively studied. The most of them have emphasized the degradation of this polyolefin under radiochemical processing [21, 24-30] or its crosslinking in the presence of suitable additional monomer. [23, 31, 32] Other assays on radiation resistance of polypropylene have investigated the effects of stabilization additives (antioxidants), which delay the start of oxidation and mitigate the rate of destruction. [33, 34] The radiolysis of polymer substrate causes the free radical formation, which is followed by oxidation reactions. [35] The rate of oxygen consumption and the absorbent properties of calcium carbonate nanoparticles seem to influence the state of degradation of irradiated polypropylene [36].

This paper describes the stability of irradiated polypropylene containing calcium carbonate nanoparticles. The main goal of this investigation is the characterization of additive effect on the polymer matrix, which is degraded in two different environments (air and water).

## **2. Experimental**

Isotactic polypropylene, a commercial grade material, was supplied by HMC Polymers Co., Ltd (Rayong, Thailand) as Moplen CS-42 HEXP type. Its initial characteristics were presented in a previous paper [37]. The compounding had concerned two types of CaCO<sub>3</sub> nanoparticles (average size: 40 nm). The samples containing uncoated filler received mark A, while i-PP samples having carbonate particles superficially modified with stearic acid were placed in category B. The process of sample preparation was described earlier [37]. The reference (pristine material) and five different i-PP/carbonate filler formulations (5, 10, 15, 25 and 25% w/w) were prepared as thin sheets.

The exposure to  $\gamma$ -rays for control and modified i-PP sheets was performed in an irradiator GAMMATOR M-38-2 (USA) provided with a <sup>137</sup>Cs source. This step was carried out in air at room temperature. Two radiolysis surroundings (air and distilled water) were used in order to describe the oxidation resistance of material under these two common circumstances. For this investigation, a low value of dose rate (0.4 kGy/h) was used, which ensures an accelerated degradation. Three total doses, namely 5, 15 and 25 kGy were applied; higher irradiation doses were avoided due to the brittleness of polypropylene sheets accompanying high energy treatment in oxidizing medium.

The oxygen uptake measurements were accomplished with laboratory equipment, which was previously described [38]. The experimental conditions were chosen in order to obtain convenient values for kinetic parameters: 190<sup>0</sup>C for thermal degradation, normal pressure of oxidation environment, air as testing medium. The selected temperature seems to be somewhat higher, but the supplied polypropylene (control and modified polymer) presented high thermal stability due to the presence of antioxidants. Thin films were cut in small pieces having around 20 mg each. They were placed in round aluminum trays to be thermally oxidized in an electrically heated oven at constant temperature. Irradiated specimens were investigated for their thermal oxidability soon as they were withdrawn from exposure room.

The main kinetic parameters of oxidation: oxidation induction time and oxidation rates were determined from the dependencies of consumed oxygen on thermal degradation time. From these curves (sigmoidal type) induction period was assessed by the crossing point of drawing the tangent from the propagation part with OX axis; the rate of oxidation was determined on the propagation step, where it attends the maximum value.

## **3. Results and discussion**

Radiation processing of polymers is a useful tool for the check of material resistance under hard service conditions and provides a conclusive picture on the manner through which the material follows standard recommendations. For composite, the accelerated tests offer suitable conclusions concerning the effects of additives and fillers on the long term usage. Ionizing radiation causes the split of weaker bonds. Polypropylene is subjected to radiation degradation due to the presence of tertiary carbons in macromolecule backbone. Oxygen which preexists in virgin material or is diffused into polymer bulk during irradiation promotes oxidation by the reactions with free radicals. Final radiolysis products will be spread in the polymer mass in correlation with material crystallinity and the size of molecules. In the case of nanocomposites, the filler particles can influence the progress of oxidation.

Calcium carbonate nanoparticles modify the behavior of basic material because of their large specific surface and the homogenous dispersion in polymer. The decrease in mechanical properties was reported earlier [36], but it would be accompanied by the change in thermal stability.

In the case of coated particles, it would be expected that the covering film will influence the progress of oxidation.

Isotactic polypropylene filled with calcium carbonate nanoparticles presents slight differences in the values of oxidation induction time, while the propagation of oxidation looks somewhat unlike (Figure 1). The initial amount of dissolved oxygen is about the same for all samples, but, the  $O_2$  diffusion into polymer during uptake measurements depends on the filler consistency. The higher the concentration of nanoparticles, the faster the oxidation degradation (Tables 1 and 2), namely, the thermal stability is determined by the homogeneity spreading of carbonate particle in polymer.

The exposure of i-PP samples to  $\gamma$ -radiation brings about the decrease in the both kinetic parameters: oxidation induction time and oxidation rate. The nature of degradation environment determines different values of kinetic parameters for the advance in oxidation. In Figure 2 the dependencies of consumed oxygen on time is presented for samples containing coated  $CaCO_3$  nanoparticles, which were irradiated at 25 kGy in the both oxidative media.

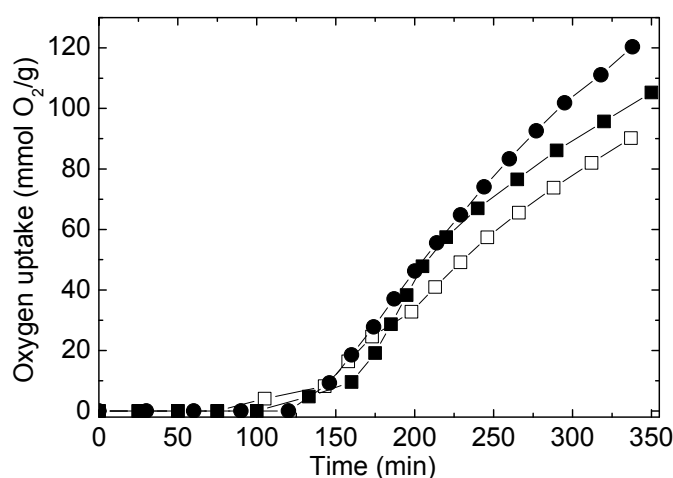


**Figure 1. The dependencies of oxygen uptake on degradation time for unirradiated samples consisting of i-PP and  $CaCO_3$  nanoparticles coated with stearic acid.**  
(□) control; (■) 5 % loading; (●) 25 % loading.

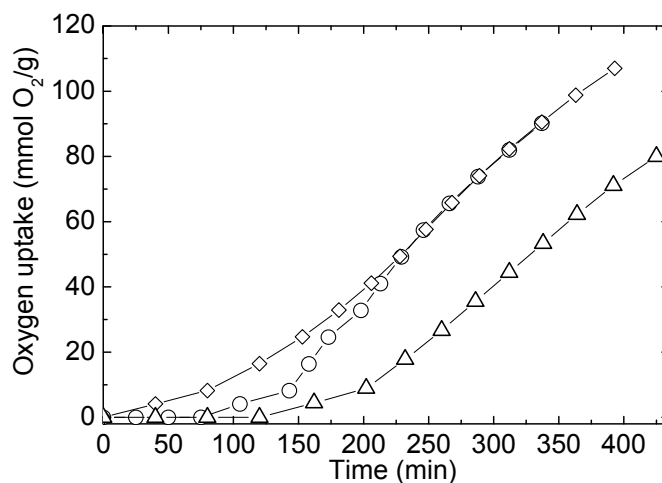


**Figure 2. Time dependencies of oxygen uptake for irradiated at 25 kGy i-PP samples/25%  $CaCO_3$  coated nanoparticles.**  
(○) control; (□) 10 % loading; (◇) 25 % loading.



**Table 1. The values of kinetic parameters of oxidation for radiolyzed nanostructured i-PP (environment: air)**

Experimental conditions		i-PP/uncoated CaCO <sub>3</sub> particles		i-PP/stearic acid coated CaCO <sub>3</sub> particles	
CaCO <sub>3</sub> load [%]	Dose [kGy]	Induction period [min]	Oxidation rate.10 <sup>4</sup> [mol O <sub>2</sub> .g <sup>-1</sup> .s <sup>-1</sup> ]	Induction period (min)	Oxidation rate.10 <sup>4</sup> [mol O <sub>2</sub> .g <sup>-1</sup> .s <sup>-1</sup> ]
0	0	52	6.33	110	5.63
	5	60	7.06	118	5.84
	15	61	7.41	96	5.99
	25	48	8.77	78	6.53
5	0	62	6.53	168	5.46
	5	71	6.84	170	5.82
	15	75	7.11	154	6.61
	25	70	7.93	131	7.00
10	0	85	7.23	199	6.48
	5	96	7.58	161	6.82
	15	113	7.84	125	7.09
	25	148	8.03	112	7.22
15	0	172	7.22	160	6.61
	5	155	7.51	148	6.84
	15	149	7.85	133	7.27
	25	137	8.09	129	7.17
20	0	160	7.61	183	7.38
	5	145	7.90	146	7.55
	15	120	8.37	119	7.93
	25	90	8.72	89	8.14
25	0	163	8.47	153	8.43
	5	143	9.04	133	8.70
	15	117	10.06	106	9.55
	25	102	11.88	86	10.03

**Table 2. The values of kinetic parameters of oxidation for radiolyzed nanostructured i-PP (environment: water)**

Experimental conditions		i-PP/uncoated CaCO <sub>3</sub> particles		i-PP/stearic acid coated CaCO <sub>3</sub> particles	
CaCO <sub>3</sub> load [%]	Dose [kGy]	Induction period [min]	Oxidation rate.104 [mol O <sub>2</sub> .g <sup>-1</sup> .s <sup>-1</sup> ]	Induction period [min]	Oxidation rate.104 [mol O <sub>2</sub> .g <sup>-1</sup> .s <sup>-1</sup> ]
0	0	52	6.33	110	5.63
	5	65	7.06	78	5.95
	15	70	7.72	70	6.41
	25	59	7.97	58	6.88
5	0	62	6.53	168	5.46
	5	86	7.24	157	6.34
	15	84	8.15	132	6.92
	25	80	8.43	109	7.70
10	0	85	7.23	122	6.48
	5	96	7.68	104	7.26
	15	101	8.44	90	7.65
	25	88	9.23	81	8.14
15	0	172	7.22	160	6.61
	5	148	7.91	140	7.43
	15	130	8.45	128	7.68
	25	120	9.49	119	8.93
20	0	160	7.61	183	7.38
	5	139	8.30	130	7.69
	15	132	8.96	109	8.34
	25	114	9.82	71	8.61
25	0	163	8.47	148	8.43
	5	121	9.14	103	9.86
	15	100	11.16	77	11.90
	25	87	12.73	63	13.29

During radiochemical ageing of studied systems, the formed intermediates are spread in the bulk of polymer, closer of further from carbonate nanoparticles. Hear that was transferred to samples increases the rate of diffusion of radicals through the polypropylene molecules attending filler particles on which they would be adsorbed. On the first step of thermal oxidation (oxygen uptake measurements), the oxygen consumption decrease with carbonate loading. It means that the precursors of oxygenated final products are efficiently scavenged by particles. On the propagation step of oxidation, when the rate of oxidative degradation increases with carbonate concentration, the desorption of radiolysis products increases the oxygen uptake and the oxidation occurs fast.

The radiolysis of water generates various intermediated, especially radicals (H., HO., HO<sub>2</sub>.), which initiate the superficial degradation of samples. The higher concentration of carbonate nanoparticles brings about an increase in oxidation induction time. The difference between the coated and pristine filler consists of the presumable penetration of organic shell by water intermediates, followed by their remove from stearic acid covering. This behavior was exhibited by all formulations of i-PP/nanocarbonate specimens.

The advanced exposure of materials to the action of  $\gamma$ -rays promotes a larger degradation, due to the greater abundance of radical intermediates. Their depletion will require higher oxygen amount starting from the beginning of thermal measurements. However, the longer induction times are presented by the polymer samples containing carbonate loading higher than 15 %.

The radiation ageing accelerates at higher rates the pristine polypropylene in comparison with the same material loaded with calcium carbonate nanoparticles; the coating shell ameliorates the thermal resistance of host material.

#### 4. Conclusion

The polypropylene compounds with calcium carbonate nanoparticles exhibits favorable kinetic parameters (induction time and process rate) during accelerated oxidation. The presence of these small particles modifies the interphase diffusion of radiolysis intermediates, which would react with molecular oxygen. The thermal strength of polypropylene is improved

The efficiency of carbonate nanoparticles in isotactic polypropylene on retardation of oxidation is a great advantage for prolongation of the product life, which are subjected to the action of various hazards.

The technological applications of i-PP/carbonate nanoparticles requires the decision on the temperature regime in connection with filler loading to satisfy simultaneously the manufacture conditions and the improved life of products.

#### References

- [1] Andrievski, R. A., *J. Mater. Sci.*, 38, 1367, 2003
- [2] Ellis, T. S., D'Angelo, J. S., *J. Appl. Polym. Sci.*, 90, 1639, 2003.
- [3] Jie, W., Yubao, L., Weiqun, C., Z. Yi, *J. Mater. Sci.*, 38, 3303, 2003.
- [4] Zanetti, M., Bracco, P., Costa, L., *Polym. Degrad. Stabil.*, 85, 657, 2004.
- [5] Ruan, W. H., Zhang, M. Q., Rong, M. Z., Friedrich, K., *J. Mater. Sci.*, 39, 3475, 2004.
- [6] Mallikarjuna, N. M., Venkataraman, A., Aminabavi, T. M., *J. Appl. Polym. Sci.*, 94, 2551, 2004.
- [7] Rocha, M. C. G., Silva, A. H. M. F. T., Coutinho, F. M. B., Silva, A. L. N., *Polym. Testing*, 24, 1049, 2005.
- [8] Diagni, M., Guèye, M., Vidal, L., Tadjani, A., *Polym. Degrad. Stabil.*, 89, 418, 2005.
- [9] Morlat-Therias, S., Mailhot, B., Gardette, J-L., C. da Silva, Haidar, B., Vidal, A., *Polym. Degrad. Stabil.*, 90, 78, 2005
- [10] Wan, T., Feng, F., Wang, Y-C., *Polym. Bull.*, 56, 413, 2006.
- [11] Gilman, J. W., *Appl. Clay Sci.*, 15, 31, 1999.
- [12] Haegawa, N., Okamoto, H., Kato, M., Usuki, A., *Appl. Polym. Sci.*, 78, 1918, 2000.
- [13] Sinha, R. S., Okamoto, M., *Prog. Polym. Sci.*, 28, 1, 2003
- [14] Patel, M., Morrel, P. R., Murphy, J. J., Maxwell, A. S., *Polym. Degrad. Stabil.*, 91, 406, 2006.
- [15] Zhang, J., Jiang, D. D., Wilkie, C. A., *Polym. Degrad. Stabil.*, 91, 298, 2006.
- [16] Pospíšil, J., Horák, Z., Pilař, J., Billingham, N. C., Zweifel, H., Nešpůrek, S., *Polym. Degrad. Stabil.*, 82, 145, 2003.
- [17] Pospíšil, J., Pilař, J., Billingham, N. C., Marek, A., Horák, Z., Nešpůrek, S., *Polym. Degrad. Stabil.*, 91, 417, 2006.
- [18] Bertini, F., Canetti, M., Audisio, G., Costa, G., Falqui, L., *Polym. Degrad. Stabil.*, 91, 600, 2006
- [19] Filho, F. G. R., Mélo, T. J. A., Rabello, M. S., Silva, S. M. L., *Polym. Degrad. Stabil.*, 89, 383, 2005.
- [20] Dobkowski, Z., *Polym. Degrad. Stabil.*, 89, 488, 2006.
- [21] Czvikovszki, T., Hargitai, H., *Radiat. Phys. Chem.*, 55, 727, 1999.
- [22] Dahlan, H. N., Khairul Zaman, M. D., Ibrahim, A., *Radiat. Phys. Chem.*, 64, 429, 2002.
- [23] Gao, J., Lu, Y., Wei, G., Zhang, X., Liu, Y., Qian, J., *J. Appl. Polym. Sci.*, 85, 1758, 2002.
- [24] Carlsson, D. J., Lacoste, J., *Polym. Degrad. Stabil.*, 32, 377, 1991.
- [25] Gijsman, P., Hennekens, J., *Polym. Degrad. Stabil.*, 42, 95, 1993.
- [26] Gorelik, B. A., Kolganova, I. V., Matisova-Rychlá, L., Listvojb, G. I., Drabkina, A. M., Gorelik, G. A., *Polym. Degrad. Stabil.*, 42, 263, 1993.

- [27] Szadkowska-Nicze, Mayer, M.J., Szreder, T., Faucinato A., *Radiat. Phys. Chem.* 54, 193, 1999
- [28] Denac, M., Musil, V., Šmit, I., Ranogajec, F., *Polym. Degrad. Stabil.*, 82, 263, 2003
- [29] Naguib, H. F., Aly, R. O., Sabaa, M. W., Mokhtar, S. M., *Polym. Testing*, 22, 825, 2003
- [30] Savasaki T. et al, *Radiat. Phys. Chem.*, 31, 877, 1998
- [31] Jones, R. A., Cail, J. I., Stepto, R. F. T., Ward, I. M., *Macromolecules*, 33, 7337, 2000
- [32] Stojanović, Z., Kačarević-Popović, Z., Galović, S., Miličević, D., Suljovrujić, E., *Polym. Degrad. Stabil.*, 87, 279, 2005
- [33] Shamshad, A., Basfar, A. A., *Radiat. Phys. Chem.*, 57, 447, 2002
- [34] Zaharescu, T., Jipa, S., Setnescu, R., Santos, C., Gigante, B., Gorghiu, L. M., Mihalcea, I., Podină, C., *Polym. Bull.*, 49, 289, 2002
- [35] Stags, J. S. J., *Polym. Degrad. Stabil.*, 85, 759, 2004.
- [36] Zaharescu, T., Kaci, M., Setnescu, R., Jipa, S., Touati, N., *Polym. Bull.*, 56, 405, 2006
- [37] Zaharescu, T., *Polym. Testing*, 20, 3, 2001
- [38] Dangtungee, R., Yun, J., Supaphol, P., *Polym. Testing*, 24, 2, 2005

## THERMAL STABILITY OF POLY(URETHANE-LACTATE)

S. JIPA<sup>1</sup>, T. ZAHARESCU<sup>2</sup>, R. SETNESCU<sup>1</sup>, C. CIOBANU<sup>3</sup>, C. N. CAȘCAVAL<sup>3</sup>

<sup>1</sup>*"Valachia" University of Târgoviște, 18-22 Unirii Av., Târgoviște 130082, Romania*

<sup>2</sup>*INCDIE, ICPE CA, 313 Splaiul Unirii, Bucharest 030138, Romania*

<sup>3</sup>*"Petru Poni" Institute of Macromolecular Chemistry, Iași 700487, Romania*

**Abstract:** *The thermal resistance of polyurethane lactate (PUL) doped with different concentrations of Er<sup>3+</sup> was investigated by chemiluminescence by isothermal and nonisothermal conditions. The modifications in thermal strength of these formulations are discussed in relation to erbium concentration. Several onset oxidation times of other polymers (polyolefins, EVA, polyamide 6, polyacrylates) are presented. The thermal degradation mechanism of polyurethane lactate based on model compounds containing the same functional units is reported in order to identify the scission sites.*

**Keywords:** *polyurethane lactate, chemiluminescence, erbium*

### 1. Introduction

The essential characteristics of polymers are related to their thermal resistance in the presence of oxygen. Several papers dealing with this essential and practical aspect have been reported [1-4]. Polyurethanes (PUs) are one of the most important engineering polymers because of their technical and scientific applications. They are the basic materials for manufacturing of foams, thermoplastic compounds, which can be processed by injection and extrusion, elastomeric products, sealants, adhesives, protective coatings especially for automotives, fibers [5], blood-contacting devices including vascular prosthesis [6], heart valve [7], electro-optic devices [8], etc. Their long-term usage requires detailed investigations on the effect of thermal degradation. Thermogravimetric analysis on the thermal stability of polyurethane [9, 10] reveals the complex aspect of this process. Kinetic results on thermooxidative stability of different PUs may depend on the ageing procedure and on the structure of polymers [11].

The thermal degradation of PUs takes place in two stages: first one, depolycondensation, starts at 2500C; the second process is attributed to the oxidation of the residual material, which starts from 3700C. However, before attending the end of structural cleavage, the new intermediates are oxidized and the chemiluminescence signal can be recorded [12].

The degradation of PU structures, poly(ester-urethane) and poly(acryl-urethane) previously studied by chemiluminescence [13] has demonstrated that this process occurs via peroxy intermediates. Two modes of explanation for the early stage of oxidation may be use for the delimitation of this conservative period: oxidation induction time (OIT) and onset oxidation temperature (OOT). These two kinetic characteristics depict properly the thermal strength of polyurethanes on the first term of oxidation, when insignificant modification of polymer matrix may be noticed. The assay on the effect of hard operation conditions for polyurethanes was preformed in sea water [14].

The molecular structure plays an important role in the defining of the degradation progress. The wearability of polyurethanes, which work in wet environments, depends on the chemical nature of elastomers. Polyurethane coatings are extensively used due to the remarkable resistance to UV light. The photolysis, the accelerated process of degradation, generates a broad hydroxyl absorption band in the IR spectrum, which is accompanied by carbonyl band made up of several overlapped maxima [15]. The FT-IR investigations on the weathering of polyurethane coatings have revealed the large abundance of ketonic structures through the final degradation products [15-17]. The diversity of modified polyurethane structures is now available [18, 19] for electronic engineering

due to their excellent mechanical properties and water resistance. The degradation mechanism of these organic configurations is based on the molecular splitting, where the molar ratio isocyanate/hydroxyl (NCO/OH) plays an important role in the rate of thermal oxidation [20].

This paper presents the investigation on thermooxidation resistance of polyurethane-lactate (PUL) doped with  $\text{Er}^{3+}$  on the medium temperature range by chemiluminescence knowing that the oxidation stability is one of the most severe problems both in processing and in long term application of polymeric materials, chiefly at polymeric biomaterials.

## 2. Experimental

### 2.1. Materials

#### 2.1.1. Synthesis of poly(urethane-lactate) and poly(diethylene adipate)diol

Both polyurethane-lactate (PUL) and poly(diethylene adipate)diol (PDEA) was prepared according to [21]. The erbium content in PUL is listed in table 1 for each studied formulation.

**Table 1. Erbiu content in polyurethane-lactate studied by isothermal chemiluminescence**

Sample mark	Erbium concentration [ $\mu\text{g}\cdot\text{g}^{-1}$ ]
Control	0
1	38.25
2	119.48
3	207.84

#### 2.1.2. Synthesis of poly(ethylene adipate)diol (PEA)

Poly(ethylene adipate)diol (PEA) was synthesized by fusion condensation of adipic acid with ethylene glycol (EG) (1:1.2 molar ratio). The reaction of esterification was carried out at temperature of 220 °C, for 4h, accompanied by the continuous moving off the water from the reaction system. After the water elimination was finished, the excess of ethylene glycol was removed by distillation at 220°C and pressure of 2 mm Hg for 2h. The synthesized PEA had a number-average molecular weight of 2000, which was determined by gel permeation chromatography (GPC). The prepared PEA is characterized by the hydroxyl number of 56 mg KOH/g polymer, and the acidity index of 0.08 mg KOH/g polymer.

#### 2.1.3. Synthesis of polyurethane models

Two PU models were obtained using 4,4'-methylene diphenyl diisocyanate (MDI) and ethylene glycol (EG) for PU-EG and MDI-diethylene glycol (DEG) for PU-DEG. MDI (purity 99.42%) was reacted separately with ethylene glycol and diethylene glycol in dimethylformamide (DMF) (purity 99.89%). The reactions, under stirring, were carried out at 42°C, for 8 h under  $\text{N}_2$  atmosphere. The reaction products were preserved at the room temperature for 48 h. The crude model PUs were precipitated and washed with distilled water and dried under vacuum.

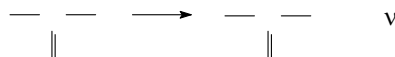
Elemental analysis was carried out using the Pregl's method. The following results were obtained for polyurethane ethylene glycol, PU-EG,  $\text{C}_{17}\text{H}_{16}\text{N}_2\text{O}_4$ ; calculated C% 65.38, H% 5.16, N% 8.97; found C% 65.26, H% 6.64, N% 8.66, 8.34; for polyurethane diethylene glycol, PU-DEG ( $\text{C}_{19}\text{H}_{20}\text{N}_2\text{O}_5$ ): calculated C% 64.04, H% 5.66, N% 7.86; found C% 64.77, H% 5.59, N% 7.27, 6.98.

Molecular weight was measured by gel-permeation chromatography PL-EMD-950 evaporation mass detector (Polymer Labs., Shropshire, UK). Calibration of the apparatus was performed using monodispersing polystyrene standard samples, with a narrow polydispersity (GmbH, Darmstadt, Germany). Number average molecular weight ( $\bar{M}_n$ ): for PU-EG was 56,766 and for PU-DEG was 50,667.

FTIR spectra of the synthesized samples were recorded on an M 80 Specord (Germany) spectrophotometer using KBr pellets. Wave number for PU-EG 3313s, 2948m, 2892m, 1705vs, 1600s, 1533vs, 1412s, 1313s, 1223vs, 1130s, 1064vs, 1016s, 939m, 816m, 768m cm<sup>-1</sup> and PU-DEG 3319s, 2954m, 2913m, 1709vs, 1600s, 1527vs, 1412s, 1311s, 1219vs, 1063s, 1016s, 914m, 816m, 766m cm<sup>-1</sup>, where: s-strong, m-medium, vs-very strong, w-weak.

## 2.2. Chemiluminescence measurements

Chemiluminescence (CL) of polymers is based on the triplet state phosphorescence of carbonyl during oxidation conformer reaction:



Several generally accepted mechanisms [22, 23] were proposed for the explanation of chemiluminescence emission during polymer oxidation.

For the determination of CL emission dependence on time Oxylumionograph OL 94 was used [24]. The equipment flow sheet and the typical CL diagram have been presented in an earlier paper [25].

Thin films were punched and identical area specimens were obtained. They were placed in aluminum round trays, which does not influence the degradation rate of polymer samples [26]. Isothermal and nonisothermal CL investigation was performed and time dependencies of chemiluminescence intensities were processed for the calculation of kinetic parameters.

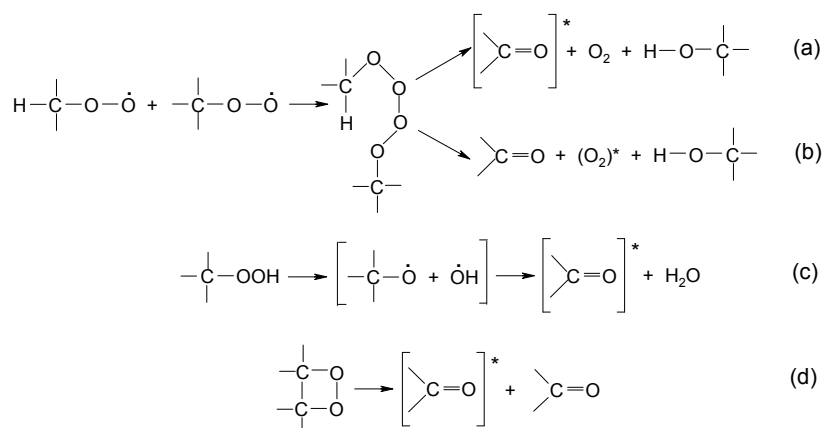


**Figure 1. Exothermal reactions for the formation of ketones in excited state**  
**(a) Russell's mechanism; (b) Stauff's mechanism; (c) Lloyd's mechanism; (d) McCapra mechanism**

For comparison, the thermal stability of other polymers (table 2) was investigated by unisothermal chemiluminescence.

**Table 2. Polymers investigated by nonisothermal chemiluminescence**

Polymer	Abreviation	Polymer	Abreviation
Isotactic polypropylene	i-PP	Ethylene-propylene diene monomer	EPDM
High density polyethylene	LDPE	Polyurethane-lactate	PUL
Ultra high molecular weight polyethylene	UHMWPE	Polymide 6	PA-6
Ethylene-vinylacetate copolymer	EVA	Poly(butylmethacrylate)	PMBA
Ethylene-propylene copolymer	EPR	Poly(methylmethacrylate)	PMMA

### 3. Results and discussion

#### 3.1. Isothermal measurements

In figure 2, the modification in the CL emission intensity of investigated  $\text{Er}^{3+}$  doped polyurethane-lactate samples is presented. Each graph represents the progress in the oxidative degradation of polymer, which shows a peak shifting toward longer degradation period, if the matrix is modified with erbium compound in higher concentration. The kinetic parameters depicting the thermal degradation of  $\text{Er}^{3+}$  doped-PUL are listed in Table 3, where it may be noticed the benefit of the presence of erbium. All kinetic characteristics decrease as the erbium content is enhanced, even though the maximum oxidation time (column 4) remains constant. The PUL samples free of erbium present significantly improved CL features (initial CL intensity, maximum emission intensity, the sum of intensity on the first 20 minutes), which explains the lack of additive contribution to the oxidative protection by the structuration of substrate. The values listed in the column of initial emission intensity prove the noticeable availability of compound to thermal oxidation, if the polyurethane substrate does not contain any additive. The kinetic parameters depicting the higher stability in the thermal oxidation of PUL- $\text{Er}^{3+}$  systems show the favourable effect of erbium that recommends it as a potential inhibitor of oxidation on the propagation stage.

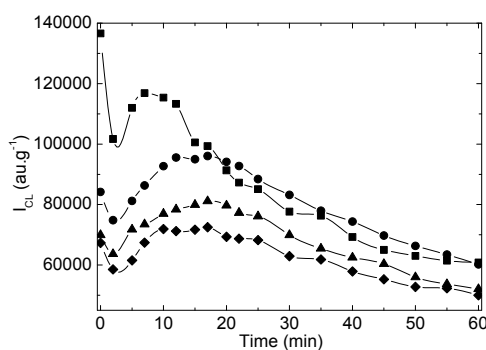


**Figure 2. Isothermal CL dependencies of emission intensity on time for several polyurethane samples; (■) control; (●) polyuterhane with 38.25 g/g  $\text{Er}^{3+}$ ; (▲) polyuterhane with 119.48 g/g  $\text{Er}^{3+}$ ; (◆) polyuterhane with 207.84 g/g  $\text{Er}^{3+}$ .**

**Table 3. The main kinetic parameters for thermal oxidation of polyurethane-lactate doped with  $\text{Er}^{3+}$  complex**

Sample	$\text{Er}^{3+}$ content [ $\mu\text{g/g}$ ]	Initial CL intensity [au/g]	Maximum CL intensity [au/g]	Maximum oxidation time [min]	$\sum_{t=0}^{t=20} I_{CL}$ [au/g]
0	0	136604	116887	7	987076
1	38.25	84188	96063	17	700041
2	119.48	69924	81136	17	674923
3	207.84	67328	71519	17	611450

In the polyurethane-lactate molecules, it is possible that urethane group ligand would play the selection role in controlling on the energetic absorption properties in the complexes PUL- $\text{Er}^{3+}$ . It may be assumed that  $\text{Er}^{3+}$  accepts energy from the  $-\text{NH}-\text{COO}-$  group ligand. The direct consequence would be the diminishing of CL emission intensity, which is demonstrated by the decrease in the value of total intensity (table 3, column 5).

On the other hand, the modification of the polyurethane-lactate with  $\text{Er}^{3+}$  led to formation and stabilization of supramolecular structure by increase in the crystallinity level and by improving mechanical and thermal stability [21]. The contribution of  $\text{Er}^{3+}$  compound could be pointed out by the analysis of nonlinear and continuous decrease in the kinetic parameters of oxidation evaluated



for selected additive concentrations (figure 3). This falling down in the CL intensities either for initial values, or for the sum on the first 20 minutes demonstrates the involvement of  $\text{Er}^{3+}$  in the thermal stability of polymer matrix, even at low concentration. The formulation containing 207.84

$\mu\text{g/g}$  of additive shows about half values for  $I_0$  and  $\sum_{t=0}^{t=20} I_{CL}$  in comparison to unmodified polyurethane-lactate. The sharp reduction in the initial CL intensity for the PUL sample containing only 38.25  $\mu\text{g.g}^{-1}$  confirms the inhibition on the formation of hydroperoxides.

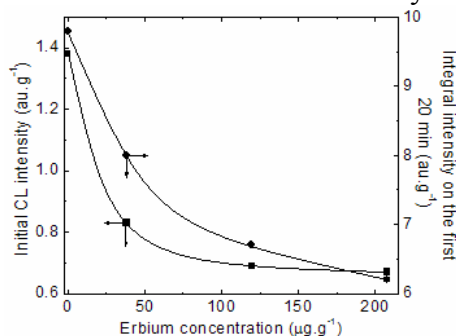


**Figure 3. Modifications in the main CL characteristics in the oxidation of PUL samples containing various amounts of erbium complex.**

The activation energy values (table 4) required for oxidation on different degradation stages demonstrate the concern of radical intermediates in the thermal oxidative degradation of polyurethanes. The withdrawing of intermediate content by their reaction with oxygen diminishes the energetic requirements of process.

**Table 4. Activation energy involved in the thermal degradation of unmodified polyurethane**

Parameter	Kinetic parameter involved in energy calculation		
	Maximul CL intensity $I_{\max}$	Maximum oxidation time $t_{\max}$	$\sum_{t=0}^{t=20} I_{CL}$
Ea [ $\text{kJ.mol}^{-1}$ ]	59.36	54.34	50.16
ln A	26.1	11.5	26.1
Correlation factor	0.980	0.986	0.986

These values are in a good agreement with other values previously reported ( $46.82 \text{ kJ.mol}^{-1}$ ) by Schard and Russell [27] or Wedlandt [28].

### 3.2. Nonisothermal measurements

The advance in the oxidation of polyurethane lactate (figure 4) occurs dissimilarly in relation with other types of polymers. It shows an intermediate maximum, which may split the temperature range into two regions. They may correspond to different oxidation sites on polyurethane-lactate molecules. Decrease CL intensity between  $175\text{--}210^\circ\text{C}$  can be the result of antioxidant activity provided by amino groups of PUL matrix, which is formed in the oxidation decomposition of PUL [29-31]. Beyond  $270^\circ\text{C}$  the antioxidant contribution of the amine is diminished due to decreases in reactive amino groups during oxidation. The CL intensity growths continuously as temperature increases that demonstrate the fast progress of oxidation.

The values obtained for onset oxidation time, OOT, (figure 5) are good indicators for the level of compound stability. It means that these temperatures represent the threshold, where oxidation effectively starts, depicting the peculiar resistance to thermal degradation.

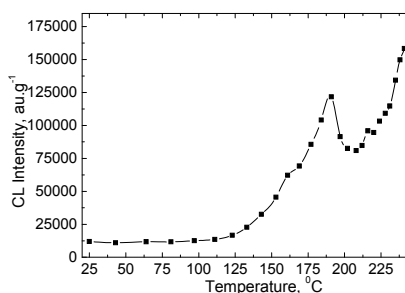


Figure 4. The dependence of chemiluminescence intensity on temperature for PUL.

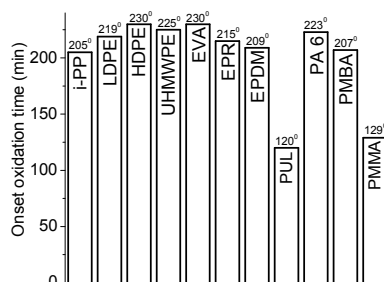


Figure 5. The values of onset oxidation time for various commercial polymers

### 3.3. Thermal decomposition of models

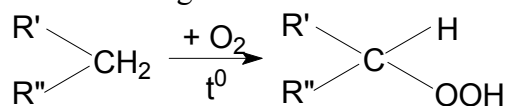
The question of bond splitting in the degradation of polyurethane lactate was solved by the investigation on similar structures. Poly(diethylene adipate)diol, poly(diethylene adipate)diol, poly(urethane ethylene)glycol and poly(urethane diethylene)glycol were subjected to thermal degradation. The main kinetic parameters: half oxidation time and maximum oxidation time, were evaluated at different temperatures. From Arrhenius diagrams, the activation energies and frequency factor were obtained (table 5).

Table 5. Activation energies and frequency factors for model structures

Kinetic parameter considered for evaluation	Activation energy [kJ.mol <sup>-1</sup> ]	ln A	Correlation factor
Poly(ethylene adipate)diol			
half oxidation time	102.09	22.97	0.997
maximum oxidation time	95.09	19.85	0.999
Poly(diethylene adipate)diol			
half oxidation time	93.14	24.86	0.999
maximum oxidation time	86.88	22.47	0.999
Poly(urethane ethylene)glycol			
half oxidation time	137.33	31.69	0.993
maximum oxidation time	76.72	14.79	0.980
Poly(urethane diethylene)glycol			
half oxidation time	102.59	27.42	0.915
maximum oxidation time	72.92	17.36	0.970

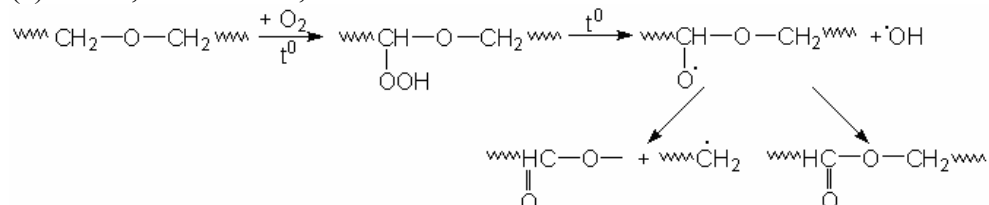
The large differences between the activation energy values for the compounds containing ethylene and diethylene units point out the higher susceptibility of the second configuration on faster oxidation. It means that the ether bond is stronger than the C-C that exists between the two –CH<sub>2</sub>– in diethylene fragments. Based on the model structures and on the results obtained for the thermal degradation of PUL, the most probable mechanisms that are applicable for the thermal oxidation of PUL involves several elementary reaction such fragmentation, rearrangement and electron transfer.

The basic stage of oxidation:

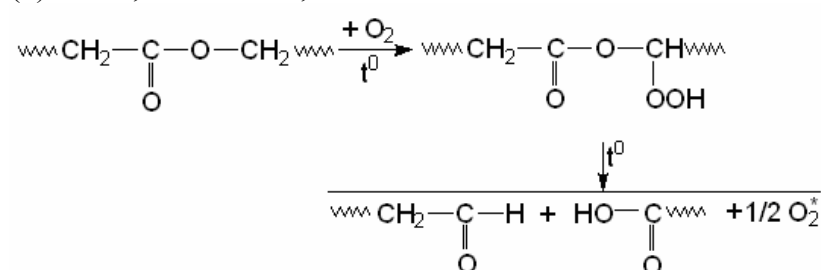


The subsequent reactions depend on the various moieties in the molecules:

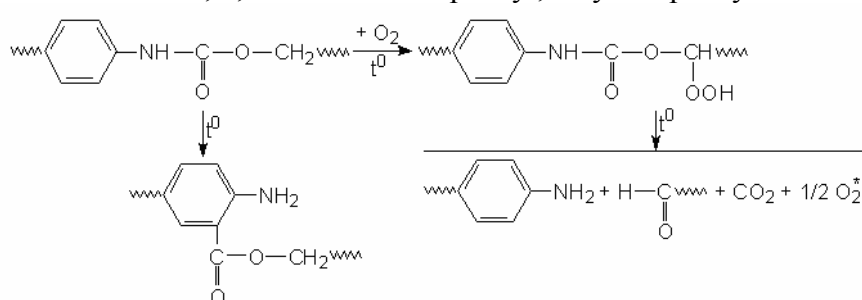
(a) for R', R'' = -CH<sub>2</sub>-, ether structure:



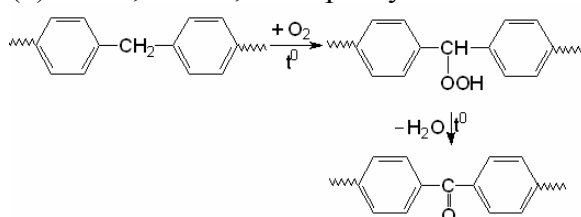
(b) for R', R'' = -CH<sub>2</sub>-, ester structure:



(c) for R' = -CH<sub>2</sub>-, 4,4' – substituted phenyl, ethylene phenyl urethane structure:



(d) for R', R'' = 4,4' – diphenyl methane structure



Analogue process occurs for R' = -CH<sub>2</sub>-, R'' = 4,4' – substituted phenyl, propylene phenyl urethane structure.

#### 4. Conclusion

The investigation on the thermal stability of PUL-Er<sup>3+</sup> allows emphasizing some relevant conclusions to the contribution of additive:

- poly(urethane lactate) presents a intensity maximum at 175<sup>0</sup>C, whose value decrease with Er<sup>3+</sup> concentration,
- Er<sup>3+</sup> compound improves the stability of polyurethane-lactate matrix on the whole duration of oxidation,
- the activation energy calculated from temporal parameters is in a good agreement with other reported values,

- the ester structure of polyurethane does not show a tendency to thermal oxidation, in spite of the certain sensitivity of neighbor alkyl moieties to the oxidative degradation,
- the ether unit is very sensitive to the oxygen attack, this molecular fragment being the source for the formation of hydroperoxides, the oxidation precursors of material,
- the thermal oxidation of PUL involving several elementary reaction such fragmentation, rearrangement and electron transfer.

### References

- [1] Wise J., Gillen K.T., Clough R.L., *Polym Degrad Stabil*, 49, 403, 1995
- [2] Zaharescu T., Jipa S., Setnescu R., Santos C., Gigante B., Podina C., Gorghiu L.M. *Polym Bull*, 49, 289, 2002
- [3] Pospíšil J., Horák Z., Pilař J., Billingham N.C., Zeifel H., Nešpůrek H., *Polym Degrad Stabil*, 82, 145, 2003
- [4] Andrievski RA (2003) *J Mater Sci* 38:1367
- [5] Wood G. *The ICI Polyurethans book*, 2nd ed., John Wiley & Sons, 1990, 1-6
- [6] Lelah D.M., Grasel T.G., Pierce A.J., Cooper L.S., *J. Biomed Mater Res*, 20, 433, 1986
- [7] Wisman B.C., Pierce S.W., Donachy H.J., Pae E.W., Myers L.J., Prophet A.G., *Trans. Amer Soc Artif Intern Organs*, 28, 164, 1982
- [8] Steier H., Chen A., Lee S-S., Garner S., Zhang H., Chuyanov V., Dalton R.L., Wang F., Ren A.S., Zhang C., Todorova G., Harper A., Fetterman R. H, Chen D, Udupa A., Bhattacharya D., Tsap B., *Chemical Physics*, 245, 487, 1999
- [9] Duquesne S., le Bras M., Boubigot S., Delobel R., Camino G., Eling B., Lindsay C., Roes T. *Polym Degrad Stabil*, 74:493, 2001
- [10] Coutinho F.M.B., Delpech M.C., Alves T.L., Ferreira, A.A. *Polym Degrad Stabil*, 81, 19, 2003
- [11] Fambri L., Pegoretti A., Gavazza C., Penati A., *J. Appl Polym Sci.*, 81, 1216, 2001
- [12] Matisová-Rychlá L., Rychlý J., Slovák J., *Polym Degrad Stabil*, 82, 173, 2003
- [13] Fratričová M., Šimon P., Schwarzer P., Wilde H.-F., *Polym Degrad Stabil*, 91, 94, 2006
- [14] Rutkowska M., Krasowska K., Heimowska A., Steinka I., Janik H., *Polym Degrad Stabil*, 76, 233, 2002
- [15] Singh R.P., Tomer N.S., Bhadraiah S.V., *Polym. Degrad Stabil*, 73, 443, 2001
- [16] Potter T., Schmelzer H., Baker R., (1984) *Prog Org Coat* 12:321
- [17] Yang X.F., Vang C., Tallman D.E., Bierwagen G.P., Croll S.G., Rohlik S., *Polym Degrad Stabil* 74, 341, 2001
- [18] Jia Q.M., Zheng M., Chen H.X., Shen R.J., *Polym Bull*, 54, 65, 2001
- [19] Lee J.Y., Park E.J., *Polym Bull*, 46, 159, 2005
- [20] Dominguez-Rosado E., Liggat J.J., Snape C.E., Eling B., Pichtel J., *Polym Degrad Stabil* 78, 91, 2002
- [21] Ciobanu C., Stoica E., Cașcaval N.C., Roșu D., Roșu L., State M., Emandi A., Nemeș E. Petrescu F., *J. Appl Polym Sci* 103, 659, 2007
- [22] George A.G. (1985) *Pure Appl Chem* 57:945
- [23] Kubera-Nowakowska L., Szychaj S., Kruk I., *Rev Adv Mater Sci.*, 12, 172, 2006
- [24] Jipa S., Constantinescu V., Setnescu R., Setnescu T., *RO Patent 110367*, 1996
- [25] Jipa S., Zaharescu T., Setnescu T., Setnescu R., Brites M.J.S., Silva A.M.G., Marcelo-Curto M.J., Gigante B., *Polym Int* 48, 414, 1999
- [26] Gorghiu L.M., Jipa S., Dumitrescu C., Zaharescu T., Setnescu T., *Mater Plast (Bucharest)*, 40:182, 2003
- [27] Schard M.P., Russell C.A., *J Appl Polym Sci.*, 8:997, 1964
- [28] Wedlandt W.W., *Thermochim Acta*, 72, 129, 363, 1984
- [29] Wilhelm C., Rivaton A., Gardette L.-J., *Polymer* 39, 1213, 1998
- [30] Rosu D., Ciobanu C., Cascaval N.C., *J Appl Polym Sci.*, 80, 1802, 2001
- [31] Newman R.C., Forciniti D., *Ind Eng Chem Res*, 40, 3346, 2001

## QUALITATIVE AND SEMIQUANTITATIVE TLC ANALYSIS OF VITAMIN D<sub>2</sub>

A.-M. HOSSU<sup>1</sup>, C. RADULESCU<sup>1</sup>, I. IONITA<sup>1</sup>, I.-E. MOATER<sup>1</sup>, D. HOSSU<sup>2</sup>

<sup>1</sup> University "Valahia" Targoviste, Department of Chemistry, 18-22 Unirii Blvd., Targoviste, Romania

<sup>2</sup> „Coresi" School, 2 Aleea Trandafirilor, Targoviste, Romania

Corresponding author – Ana-Maria Hossu, e-mail: anahossu@yahoo.co.uk

**Abstract:** This paper presents a TLC method for determination of vitamin D<sub>2</sub> from mixtures by using 60 F<sub>254</sub> TLC plates on plastic sheets and n-hexane/ether (9:1) and benzene/chloroform (1:1), as mobile phases for vitamin D<sub>2</sub>. The semi-quantitative assay of vitamin D<sub>2</sub> in the conditions given above resulted in a linear regression curve in the field 0.5-10.5 µg.

**Keywords:** vitamin D<sub>2</sub>, pharmaceutical, thin-layer chromatography.

### 1. Introduction

Vitamins are basic to human health and their determination gained increased significance in several areas of analytical chemistry such as pharmaceutical, clinical and food applications. A large number of methods have been developed for quantifying vitamins content in pharmaceuticals.

Most of the fat-soluble vitamins present in pharmaceutical preparations or in natural products are accompanied by a number of closely related compounds. This explains why the chromatographic methods are so frequently used in analysis of these compounds. Thin-layer chromatography (TLC) is almost ideally suited for these compounds because of its simplicity, speed, selectivity and sensitivity [1].

The paper presents results regarding the possibility to determine the fat-soluble vitamin D<sub>2</sub> in multivitamin products, by using the TLC method [2-9].

### 2. Experimental

#### *Materials and methods*

As standard vitamin D<sub>2</sub> purchased from Merck, chloroform stock solution of 5.2 mg/mL has been used.

The stationary phase was silica gel 60 F<sub>254</sub> on plastic sheets (from Merck) and as mobile phases: *system 1* - hexane/ether (9:1, v:v) and *system 2* - benzene/chloroform (1:1, v:v) have been used.

The examination of the plates was made in UV at 254 nm, by using a Vilber-Lourmat system, equi-PPed with a black-white video camera, BioCapt ver. 2.0 acquisitions and BioProfil ver. 2.0 analyzing software.

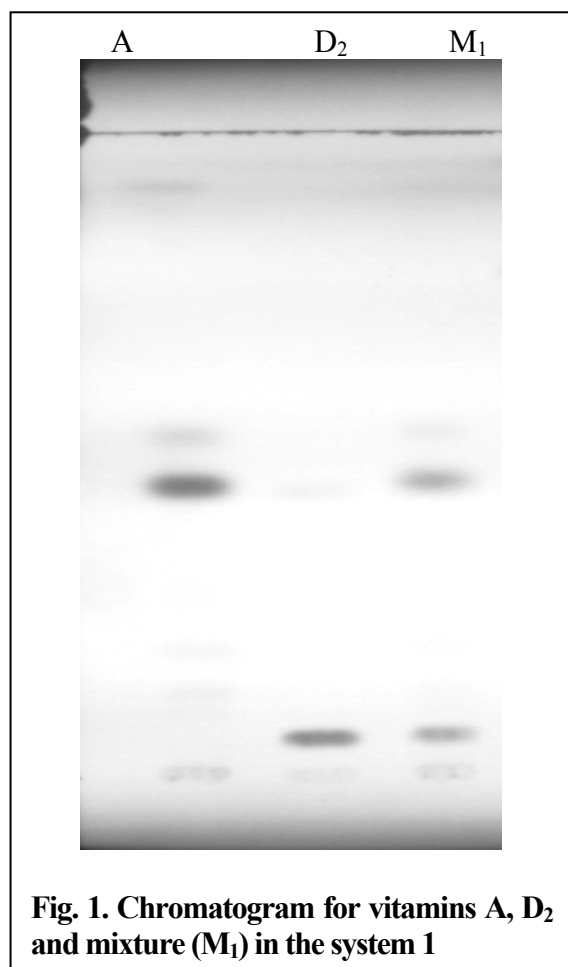
### 3. Results and discussions

Vitamin D<sub>2</sub> has been assayed in the system 1 (chromatogram presented in Fig. 1). For the purpose 2 µL of diluted solutions have been spotted and its 1:1 mixture with vitamin A (the concentration of the solutions were 10.27 mg/mL for vitamin A and 1.3 mg/mL for vitamin D<sub>2</sub>). The corresponding R<sub>f</sub>'s obtained are presented in Table 1.

**Table 1.  $R_f$  obtained for the vitamins**

	Vitamin A	Vitamin D <sub>2</sub>	Vitamin E
System 1	0.463	0.065	-
System 2	-	0.186	0.703

Then, vitamin D<sub>2</sub> has been assayed in the system 2 (Fig. 2). Aliquots of 2  $\mu$ L of diluted solutions have been spotted from each compound and its 1:1 mixture with vitamin E (the concentration of the solutions were 1.3 mg/mL for vitamin D<sub>2</sub> and 9.77 mg/mL for vitamin E). The corresponding  $R_f$ 's obtained are also presented in Table 1.



A semi quantitative assay of the vitamin was performed via the blacking-out curves obtained as function of the different amounts from vitamin D<sub>2</sub> spotted (Fig. 3).

The regression line obtained for the vitamin D<sub>2</sub> ( $R = 0.98994$ ) is plotted in Fig. 4. A grade I equation (1) was obtained:

$$Y = 41.49 + 9.2 \times m_{D_2} \quad (1),$$

where Y is the blacking-out (in relative units) and  $m_{D_2}$  represents the quantity spotted of vitamin D<sub>2</sub> (in  $\mu$ g).

As little as 0.5  $\mu$ g of vitamin D<sub>2</sub> could be assayed.

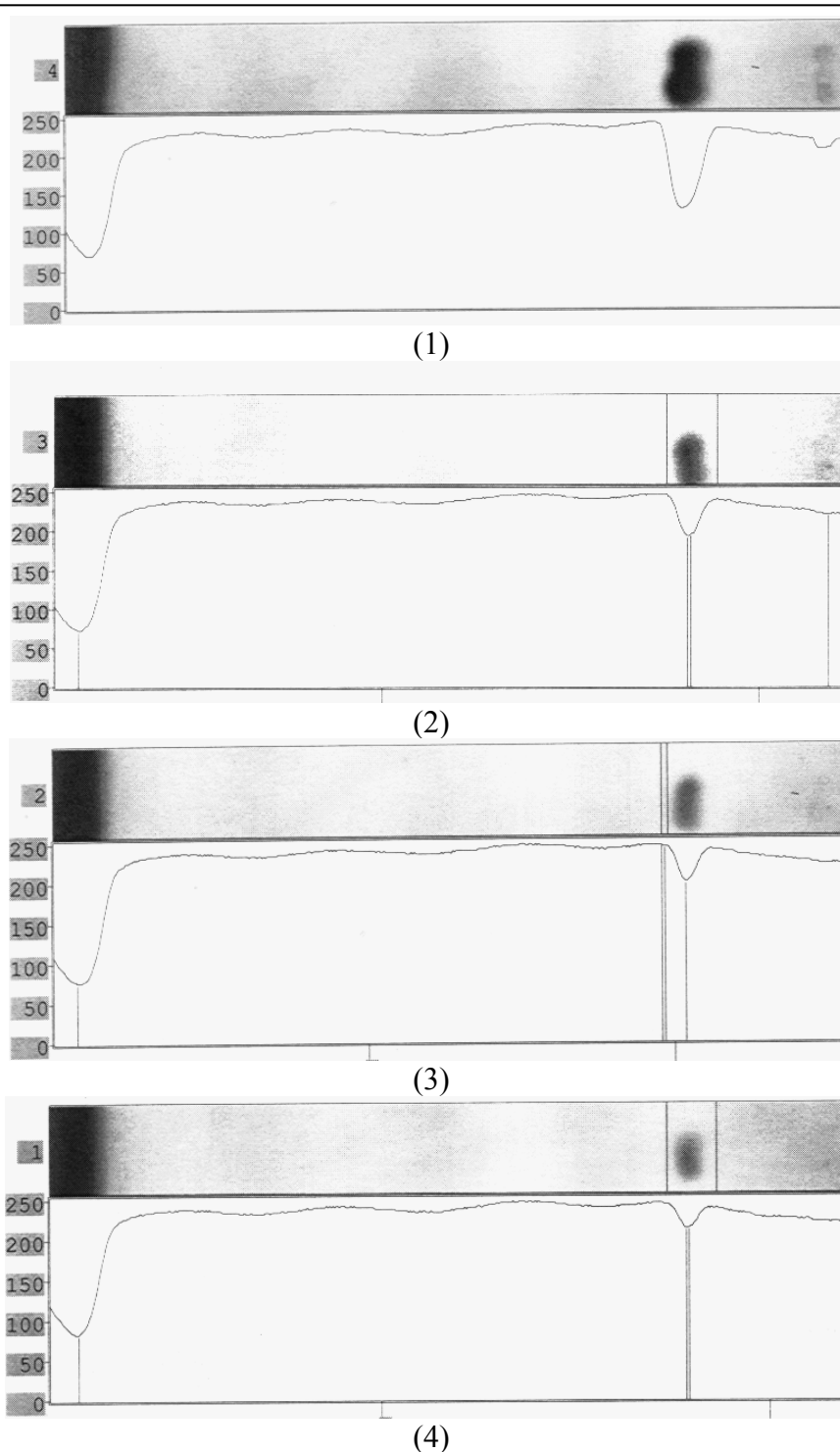
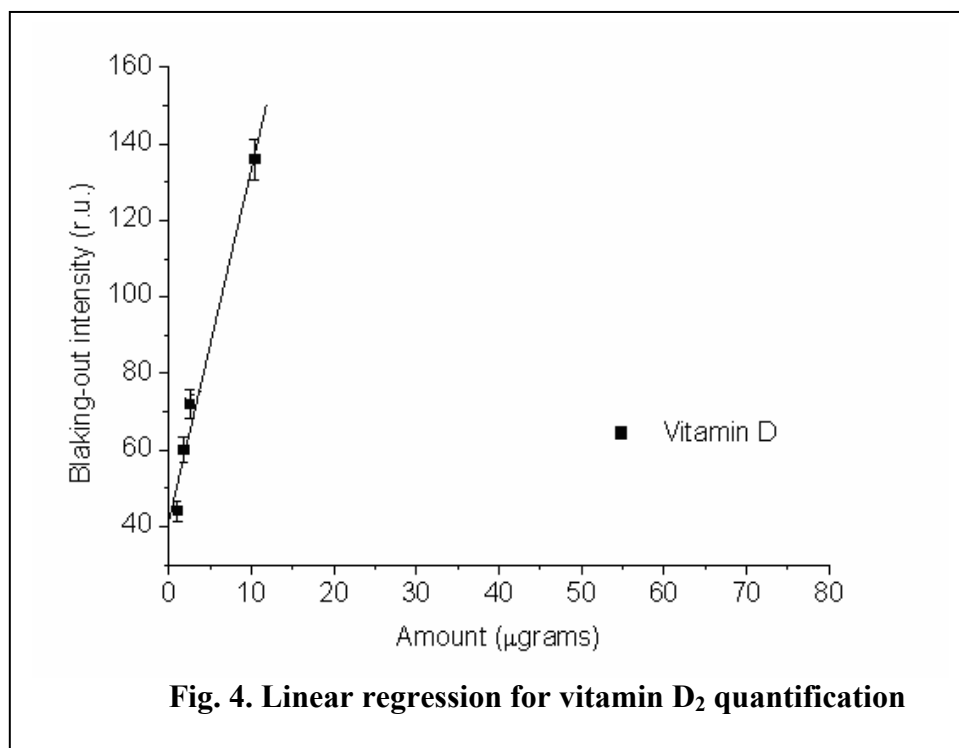


**Fig. 3. Blacking-out curves of the different amounts from vitamin D<sub>2</sub>**



#### 4. Conclusions

- TLC methods for qualitative and semi quantitative assay of vitamin D<sub>2</sub> have been developed (stationary phase: silica gel 60 F<sub>254</sub>, mobile phases: hexane/ether (9:1) and benzene/chloroform (1:1)).
- The semi quantitative assay of vitamin D<sub>2</sub> in the conditions given above resulted in a linear regression curves blacking-out vs. amount spotted in the field: 0.5-10.5 μg.

#### References

- [1] Funk, J., Fischer, W. – *Thin-Layer Chromatography. Reagents and Detection Methods* – VCH Verlagsgesellschaft mbH, Weinheim, 1990
- [2] Holasova, M., Parizkova, H., Blattna, J., *Proc. Of Euro Food Chem. III*, Vol. 2, 101-106, 1985, Antwerp, Belgium.
- [3] Chavan, J.D., Khatri, J.M., *J. Planar Chromatogr.*, 5, 280-282, 1992.
- [4] Li, G., Zhuang, Zh., Zhou, R., Shi, X., *Chinese J. Hosp. Pharm.*, 15, 162-162, 1995.
- [5] Sliwiok, J., Podgorny, A., Siwek, A., Witkowska, B., *J. Planar Chromatogr.*, 3, 429-430, 1990.
- [6] Bai, M., Lin, M., Bai, R., *Chinese J. Herb. Med.*, 24, 652-653, 1993.
- [7] Das, B., *J. Planar Chromatogr.*, 7, 162-164, 1994.
- [8] Zhong, W., Zhao, Y., *Chinese J. Hosp. Pharm.*, 21(3), 187-188, 2001.
- [9] Perisic-Janjic, N., Vujicic, B., *J. Planar Chromatogr.*, 10, 447-452, 1997.



## THE PHOTOCHROMIC RESPONSE OF POLYMERS STRUCTURES MODIFIED WITH CLASSICAL AZO DYES

I. IONIȚĂ<sup>1</sup>, C. RĂDULESCU<sup>1</sup>, A.-M. HOSSU<sup>1</sup>

<sup>1</sup>Valahia University Târgoviște, Faculty of Sciences and Arts, Department of Chemistry,  
18-22 Unirii Bdv., Târgoviște, Romania

**Abstract:** Photochromic compounds are able to change their absorption spectra when exposed to light or dark condition. This process is reversible when the photochromic moieties exist, as usually occurs, in two different forms, whose relative concentration depends on the wavelength of incident light. Polymers white side-chain photochromic groups have recently attracted a great deal of interest because the photoisomerisation of the chromophores can induce reversible variation of the macromolecular structure and hence their physical properties.

**Keywords:** photochromic compound, polymeric material.

### 1. Introduction

This work presents the preliminary results concerning synthesis, characterization of maleic anhydride(MA) copolymers with dicyclopentadiene (DCPD) and terpolymer with butyl-vinyl-ether (BVE)-DCPD, modified by condensative coupling reaction with commonly azoic photochrome (see figure 1) [1-9].

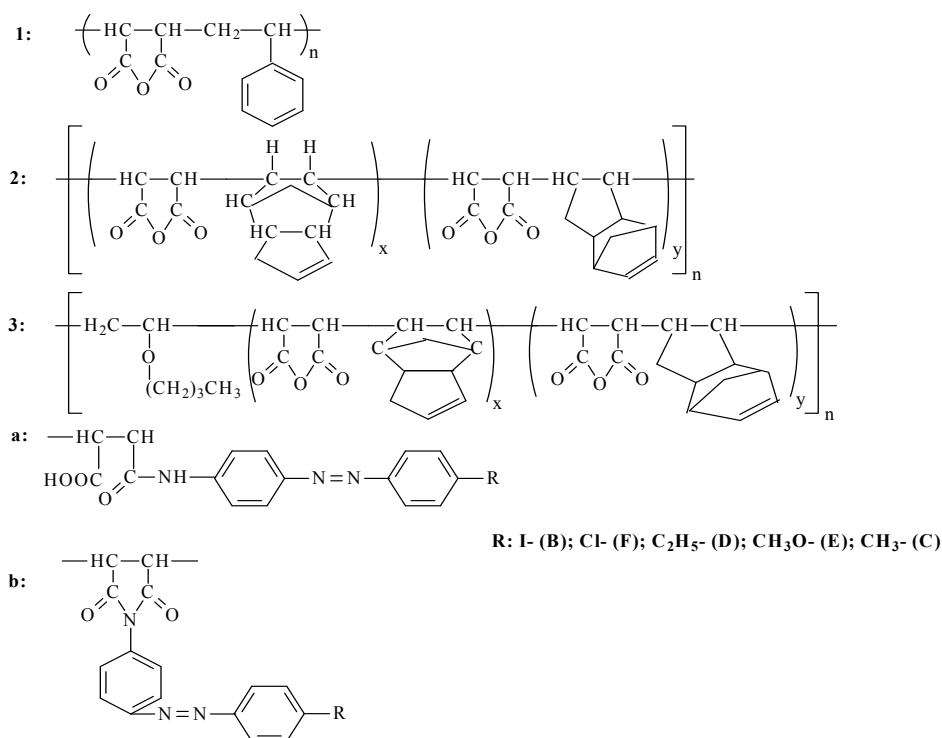


Figure 1. Chemical structures of the modified copolymers

### 2. Experimental section

#### 2.1. Synthesis

The synthesis method for obtaining modified polymers with azoderivate sequences [10], we applied the Patels and co-workers procedure, as for amic such as imidic structures [11]. The substances used for the synthesis are: Maleic Anhydride 99% from Fluka, purified by CH<sub>3</sub>Cl

recrystallization; dicyclopentadiene 99%, from Fluka, butyl-vinyl ether from Merck; styrene, purified by vacuum distillation; 2,2'-bis-azoizobutironitrile (AIBN) as initiator, purified by CH<sub>3</sub>Cl/CH<sub>3</sub>OH (1:1 vol) recrystallization.

The solvents utilized are 1,4-dioxane and N,N'-dimethyleformamide, were purified by anhydrazation procedure.

## 2.2. Measurement

**UV-Vis spectroscopy:** was SECOMAM S750 UV-Vis spectrophotometer for record the UV-Vis spectra of the dyes and polymeric materials. The synthetic results are presented in the table 1.

**Table 1. UV-Vis absorption for chromogen and modified copolymers**

R	$\lambda_1$ dye [nm]	$\lambda_2$ dye [nm]	$\varepsilon_1$ [l·cm/mol]	$\varepsilon_2$ [l·cm/mol]	$\lambda_1$ cop. [nm]	$\lambda_2$ cop. [nm]	Copolymer Cod
- H <sub>3</sub> C	261	403	3790	4327	269	411	<b>1Ca</b>
- C <sub>2</sub> H <sub>5</sub>	267	413	5407	3751	271	406	<b>1Da</b>
					271	349	<b>2Db</b>
-OCH <sub>3</sub>	269	440	3641	4366	269	379	<b>1Ea</b>
-Cl	261	406	4693	4337	269	419	<b>1Fa</b>
					272	419	<b>1Fb</b>
					270	397	<b>2Fb</b>
					272	411	<b>3Fa</b>
-I	267	406	6307	1141	272	355	<b>3Fb</b>
					270	381	<b>1Ba</b>
					270	379	<b>1Bb</b>
					269	397	<b>3Ba</b>
					269	380	<b>3Bb</b>
					269	380	<b>2Bb</b>

The intensity of absorption before and after irradiation was measured with the same UV-VIS spectrophotometer. The irradiated polymer samples were transported in the dark. The solutions were exposed to UV light to increase the rate of Z(sin)-E(anti) isomerization.

## 3. Results and discussion

All experiments and measurements are realized at room temperature. We are determined the isomerization rate constant,  $k$ , by performing UV measurements, as a function of time, applying equation 1:

$$k_t = \ln \left( \frac{A_{E(trans)} - A_{Z(cis)}}{A_{E(trans)} - A_t} \right) \quad (1)$$

where:  $A_{E(anti)}$  is the absorbance after storage in the dark before irradiation with UV light;  $A_{Z(sin)}$  is the absorbance measured after irradiation;  $A_t$  is the absorbance at time  $t$  after irradiation.

The values for the absorbance were evaluated at  $\lambda_{max}$  ( $t$ ). The half-time,  $t_{1/2}$ , of the Z(sin) form were derived from:

$$A_{t_{1/2}} = A_{Z(cis)} + (A_{E(trans)} - A_{Z(cis)}) \quad (2)$$

$$t_{1/2} = \frac{\ln 2}{k} \quad (3)$$

As indicated in figure 4,  $k$  versus  $t$  relation is not linear, as would be expected for first – order kinetics. This nonlinearity is thought to be caused by the difference in the environment of azobenzene groups. The rate of the thermal isomerization is enhanced by steric factors such as limited free volume in the polymer matrix or movements of chain segments.

**Table 2. Results for the investigated polymers**

Polymer Cod	Substituent	X*	$\lambda_{\max}$ (t) [nm]	$t_{1/2}$
1Ca	-CH <sub>3</sub>	0.5873	407	3322
1Fa	-Cl	0.6056	416	101
1Fb		0.6056	382	5950
2Fb		0.5925	360	1214
3Fa		0.4930	409	6189
3Fb		0.5870	366	1130
1Ba	-I	0.6385	379	97
1Bb		0.5802	383	1181
2Ba		0.4011	379	172
3Ba		0.6120	379	933
3Bb		0.4035	379	237
1Ea	CH <sub>3</sub> O-	0.6550	379	2077
1Da	-C <sub>2</sub> H <sub>5</sub>	0.4977	399	5713
1Db		0.4456	349	2923

\*fraction of photochromic sequences bonded from the total anhydride sequences. The evaluation was realized on specific absorption base of pure dye and modified

$$\text{polymer} \left[ x = \frac{A_{\text{dye}}}{A_{\text{polymer}} + A_{\text{dye}}} \right]$$

The variation curves,  $k$  versus time, are the results of incremental summarization of  $k$  values for each sequence. The isomerization process is strong affected by conformational modification at macromolecular chain.

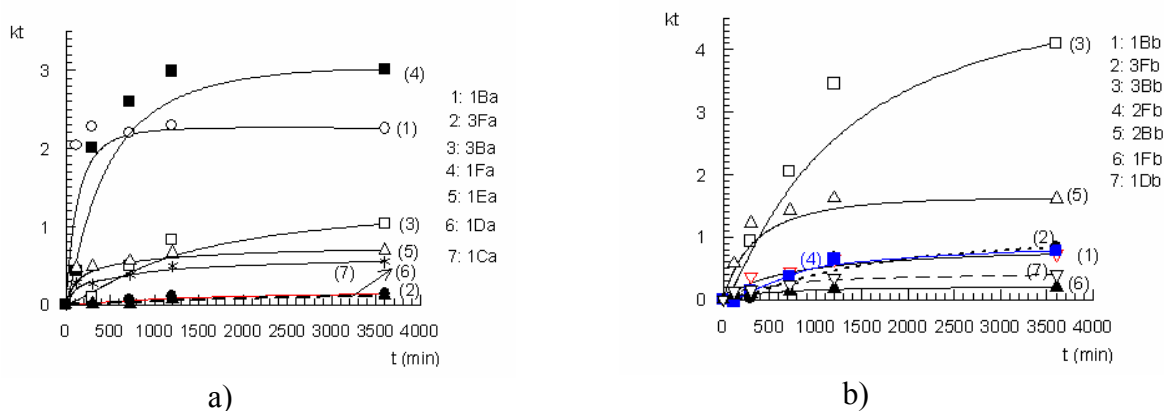


**Figure 2. Variation Curve K versus time for a) amic form of polymers and b) imidic form of polymers**

The most relevant interpretations are a comparison result at half times from Z(sin) state ( $t_{1/2}$ ), whose values are presented in the table 2. The first an ascertainment points out a fact as the stability of Z(sin) isomer can be enlargement through the polymeric structure modification (amic-imidic) or copolymer (MA-St  $\rightarrow$  MA-DCPD  $\rightarrow$  BVE- MA-DCPD) composition. For same structural polymeric support (see table 2; structure MA-St- all copolymers with index 1),  $t_{1/2}$  increasing whit decreasing of the substituents electronegativity. Therewith, on same type of copolymer, appears a variation of  $t_{1/2}$  at modification of bonding chromogen sequences at polymeric chain (amic or imidic). That last observation involve in fact the electric nature modification of the immediately neighbourhood of photochromic group corroborated with steric hindrance (rigidization of polymer - photochrom's bond). The relatively short half-times for Z(sin) isomer obtained for amic forms of MA-St copolymer, modify with photochroms substitute with Cl (101 min) respectively I (97 min),

as the copolymer case MA–St– imidic form, with azoic chromophore sequence with I substituent (172 min). The modification of  $t_{1/2}$  to the change of substituent at azoic group is owed the different activation energies of transaction  $\pi-\pi^*$  and  $n-\pi^*$ . That is due to the electronegativity differences between azobenzene group substituents. The large increase of  $t_{1/2}$  values at structural – conformational copolymer (MASt//MA-DCPD//BVE-MA-DCPD) modification owed exclusive physical property's support. Rigidity of the basic chain, through introduction of the units of DCPD, induces the neighbourhood of steric hindrance at photochromic group by the impossible of rotation around basic chain. Consequently the free internal useful volume for  $E(anti) \rightarrow Z(sin) \rightarrow E(anti)$  isomerization is reduced. Therefore,  $t_{1/2}$  grows in the case in which first transition sequence  $E(anti) \rightarrow Z(sin)$  is possible. Probably as introduction of spacer between the chromophore group and polymeric chain reduce from these orientation discommodities to the polymeric chain's level, just as point out and his study Challa and co-workers for acrylic copolymers [12]. Apparently not all azobenzene derivate side groups in the polymer matrix are available for photoisomerization, which is probably mainly due to steric hindrance.

#### 4. Conclusion

The preliminary studies at photochromic investigation of modify polymers with azobenzene developed into this work distinguished:

- The influence nature of chromophore – polymeric chain's bond:  $t_{1/2}$  of Z(sin)-isomer rise with that rigidity (amic  $\rightarrow$  imidic).
- To the same level of chain, the determinate factor for stability of Z(sin) -isomer becomes the nature of azoic group substituent.
- The type of polymeric chain has a decisive influence about the stability of Z(sin) -isomer. The big values  $t_{1/2}$  are obtained in the case of chains with free useful reduced volume, due steric hindrances, consequence of reducing the possibility of rotation around of basic chain.

These materials can be utilised as systems of photoinduce stabilization alignment nematic liquid crystals [13].

#### References

- [1] Detaire, J. A., Nakatani, K., *Chem. Rev.*, 100, 1817, 2000.
- [2] Natanshon, A., Rochon, P., *Chem. Rev.*, 102, 4139, 2002.
- [3] Natanshon, A., Rochon, P., Pezolet, M., Audet, P., Brown, D., To, S., *Macromolecules*, 27(9), 2580, 1994.
- [4] Rochon, P., Gosselin, J., *Appl. Phys. Lett.*, 60(1), 4-5, 1992.
- [5] Natanshon, A., Rochon, P., *Can. J. Chem.*, 79, 1093, 2001.
- [6] Hore, D., Natanshon, A.; Rochon, P., *Can. J. Chem.*, 76, 1648, 1998.
- [7] Meng, X., Natanshon, A., Rochon, P., Barrett, C., *Macromolecules*, 29(3), 946, 1994.
- [8] Meng, X., Natanshon, A.; Rochon, P.; Ho M Barrett C, *Macromolecules*, 28(12), 4179, 1995.
- [9] Durr, H., Bous-Laurent, H., "Photochromism. Molecules and systems", Elsevier, Amsterdam, 1999
- [10] Ioniță, I., Tărăbășanu–Mihăilă, C., Rădulescu, C., *Annals of University Ovidius Constanța*, vol. XIV, 118, 2003.
- [11] Parman, J. S., Patel, C. G., Patel, D. K., *High Performance Polym.*, 3(2), 89-97, 1991.
- [12] Haitjema, H. J, van Morgen, G. L, Tan, Y, Y, Challa, G, *Macromolecules*, 27(21), 6201, 1994.
- [13] Galstian, T. V., Zohrasian, L., Albu, A.-M., Rusen, E., Mărculescu, B., Vasilescu, D.S.V., *Nonlinear Optics, Quantum Optics*, 2004.

## DYEING ALTERNATIVES OF TEXTILE FIBRES WITH NEW DISPERSE AND CATIONIC DYES DERIVATIVES OF COMPACT CONDENSED SYSTEM 2-AMINOTHIAZOLO[4,5-f]INDAZOLE

C. RĂDULESCU<sup>1</sup>, A.-M. HOSSU<sup>1</sup>, I. IONIȚĂ<sup>1</sup>

<sup>1</sup> "Valahia" University of Târgoviste, Faculty of Sciences and Arts, 18-22 Unirii Bdv. Târgoviste

**Abstract:** *In this study some dyeing alternatives of textile fibres with new disperse and cationic dyes obtained by synthesis are presented. The results obtained by dyeing polyacrylic fibers and PAN/cotton texture (intense and brightness color, fastness to washing, fastness to perspiration, fastness to boiling and to bleaching, exposure to sunlight, ability to be absorbed and beginning from retained by the fiber) and also, the relationship between chemical structure of dyes and perspiration/light fastness were discussed.*

**Keywords:** *polyacrylic fibre, cotton, dye, tinctorial properties*

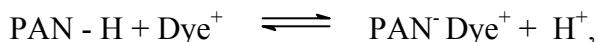
### 1. Introduction

At the same time with the extension utilization of polyacrylic fibres, it has begun a profound study of dyeing process. In this scope the classic dyes are utilised, but their tinctorial performances are very modest. The deficiencies of tinctorial properties of classic dyes refer to dyeing uniformity and the exhaustion of application fleet. In the last years the non-uniform dyeing in "dégradé" was considered a "fashion mode", but it rested only a technologic failure. In this context the studies [1-4] which refer at the synthesis and application of some new products for dyeing of synthetic fibres, rested an important problem as theoretic and practical interest.

It is known from specialty literature [5] the fact that the polyacrylic fibres can be dyed with disperse and cationic dyes, but some dyes have modest tinctorial performances, as standardization of dyeing and the exhaustion of application fleet.

Disperse dyes are used mainly for polyester, but also for cellulose (acetate and triacetate), polyamide and polyacrylic fibres. In generally, disperse dyes are characterized by some tinctorial properties: fastness to light is quite good, while fastness to washing is highly dependent on the fibre. In particular, in polyamides and acrylic fibres they are used mostly for pastel shades because in dark shades they have limited build-up properties and poor wash fastness. Also, it is known [6] that the disperse dyes are characterized by the absence of solubilising groups and low molecular weight. From a chemical point of view more than 50% of disperse dyes are simple azo compounds, about 25 % are anthraquinone dyestuffs and the rest are methine, nitro and naphthaquinone dyes [7].

Cationic dyes are the dyes which contain an auxochrome group beside chromophore, a quaternization nitrogen heteroatom or a quaternary group type  $-N(CH_3)_3$  tied an alchilic chain, always existed a guide anion. This anion doesn't influence the colour, but it has an important role because it has consequence about the solubility of product and the isolation possibility of him in pure state. The positive charge of colour cation conferred to him a sufficient solubility in water for having the capacity to dyeing of synthetic fibres (example polyacrylic fibres – PAN symbol) from acid aqueous fleets. The attractive electron cationic group has a batocrom effect and amelioration of resistances at light and industrial gases action, due the increase of electrons mobility from chromophore system. So, the affinity of cationic dyes for polyacrylic fibres is the result of anionic character of them. The fixation mechanism of cationic dyes on the polyacrylic fibre, in the first step, is ionic [8, 9]:



where PAN is polyacrylic fibre rest.

In the same time, the cationic dyes are dissolved in polyacrylic fibre; the fibre with terminal anionic groups can be considerate like an electrolyte. Also, the polyacrylic fibres obtained with same initiator, but witch are differing between them by medium polymerization grade, require different quantities of dyes. The used equivalent of dye has correlated very well with terminal anionic groups from fibre. So, a dyeing mechanism results by ionic change, because the sulpho or hydroxyl groups existed in fibre (resulted from initiators as persulphate or urea, thyourea) represented the fixing active centres. At this ionic change process participates and carboxyl groups resulted from accidental hydrolyze of nitrilic groups from polymer. In general, it is proportionality between the quantity of acid groups from polyacrylic fibre ( $3.2 - 4.5 \cdot 10^{-5}$  equivalent/g support) and saturation concentration of dye in textile support.

The polyacrylonitrilic fibres are a big molecular mass and high polymerization grade, a big number monomers are united top-tail, one after other, izotactic, without  $180^0$  turnings a one face to other. So, the asymmetrical alternation of the crystalline zones with the amorphous zones, from polyacrylic fibre, leads to non-uniform dyeing, because only the amorphous zones, is accessible to the dyestuff. The increasing of the percent through the finishing temperature increasing in the most cases it doesn't lead to the favorable results from two reasons [9-11]:

1. The reaching of the nitrification (or in the proximity) leads to the fixing processes of hidden motive associate of the substantial contribution of the hydrolysis reaction.
2. The extinguishing of the polyacrylic fibres using it owned to the fact that they mime the wool. Gradually the  $-\text{CN}$  groups hydrolyze to the  $-\text{COOH}$  ones under look “touch” and hydrolyze partial fibre to get near to the wool.

The dyeing process of polyacrylic fibres is realized only in amorphous places of fibres; the increase of them can be created by the increase of temperature at which is realized the fixation process, until in close proximity of vitrifying point of support.

In reality, the dyeing process has been taken place in four steps [11, 12]: the migration of dye from solution at external surface of fibre; the adsorption of cation of dye on external surface of fibre; the diffusion of dye inside of fibre; the formation of electrovalent bounds between cation of dye and anion of fibre.

The specialty literature [13] presents some dyeing methods of polyacrylic fibres, continuous and discontinuous procedures; in these alternatives can be used some organic and inorganic auxiliaries substances which are the role to lead at uniform dyeing on synthetic fibres.

Until now cationic dyes with a high degree of light fastness have been selected to solve the problems of dyeing process [14, 15].

In this study is presented some dyeing alternatives of polyacrylic fibres and PAN/cotton texture with disperse and cationic dyes derivatives from compact condensed systems acid 2-aminothiazolo[4,5-f]indazole and the tinctorial properties are analyzed.

## **2. Experimental**

### *Materials*

- Polyacrylonitrilic fibres type Melana, 2.5 den and PAN/cotton texture is treated with active superficial substances [16] for the increase of fibres quality. These fibres are washed with surfactants. A mixture of non-ionic (70% etoxilated fatty alcohol) and anionic surfactants (about

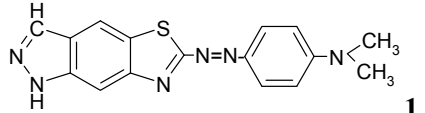
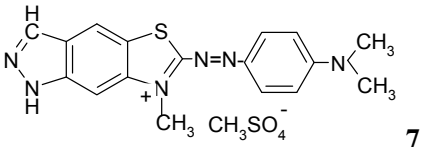
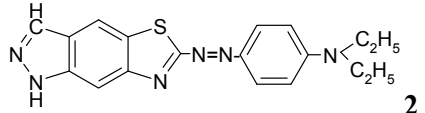
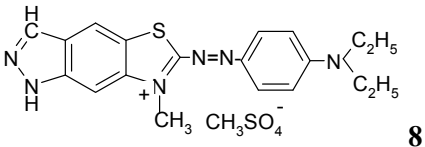
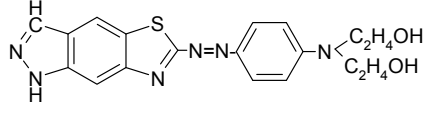
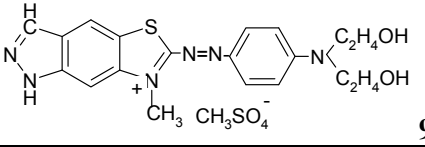
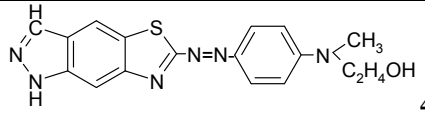
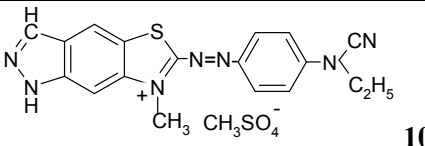
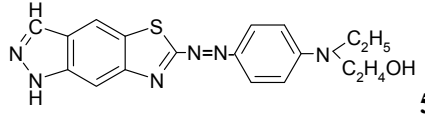
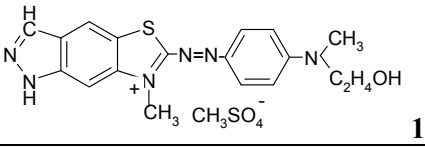
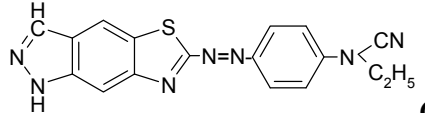
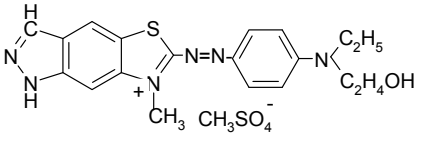
30% sodium alkylsulfonates as sodium dodecylbenzensulfonat, but also alkyl sulfate and linear alkyl benzensulfonates) are utilized for washing fibres before dyeing and after dyeing. After treating with surfactants mixture the fibres are washed with hot water (50-60°C), then with cold water and then the same operations are repeated; finally the fibres are dried in an oven at 60°C.

- Disperse and cationic dyes derivatives from compact condensed system 2-aminothiazolo[4,5-f]indazole [17] obtained by synthesis with structures are presented in Table 1.

- Auxiliaries substances for dyeing process: acetic acid (pH 4.0) solution 2%; sodium sulfate 10% solution; standardization agent for shade type ammonium quaternary salt with lateral chain at alkyl C<sub>12</sub>-C<sub>14</sub> (optional) agent retard.

The selection of dyes has been realized depending on the next criteria: the affinity face on the textile fibre; the colour of obtained compound; the stability in time of the chosen dyes.

**Table 1. Structure of some disperse and cationic dyes derivatives from compact condensed system 2-aminothiazolo[4,5-f]indazole**

Disperse dye	Colour $\lambda_{\max}$ [nm] $\epsilon_{\max}$	Cationic dye	Colour $\lambda_{\max}$ [nm] $\epsilon_{\max}$
 <b>1</b>	Light red 524.0 29800	 <b>7</b>	Blue 596 nm 22670
 <b>2</b>	Dark red 540.3 34200	 <b>8</b>	Violet-Blue 591 nm 21850
 <b>3</b>	Light red 531.1 31800	 <b>9</b>	Blue 598 nm 22600
 <b>4</b>	Red-orange 550.2 32100	 <b>10</b>	Dark-blue 603 nm 23000
 <b>5</b>	Red-orange 543.0 32900	 <b>11</b>	Dark-blue 600 nm 25900
 <b>6</b>	Dark-red 536.0 26200	 <b>12</b>	Dark-blue 604 nm 24200

#### *Dyeing process of textile fibres*

The polyacrylic fibres are hydrophobic and contain anionic groups in the molecule [18]. As a result, they can be dyed with disperse and cationic dyes.

Dyeing with cationic dyes can be performed at temperatures below 100°C without carriers [18, 19]. So, the dyebath was prepared at room temperature with cationic dye (2.0% and 3.0 aqueous solution) acetic acid 1% solution and sodium sulfate 10% solution for adjusted the pH at 3.8 – 4; the fleet rapport in dyebath was 1:40. The dyebath temperature was raised to 60°C, 70°C and 100°C and held constant during the whole dyeing process. The dyed polyacrylic fibre was rinsed first in cold water and then boiling water to remove unfixed dye, then again with cold water, and finally, it was dried at room temperature.

Dyeing PAN/cotton texture under atmospheric conditions (below 100°C) was also frequently done in the past with the aid of carriers [19]. Furthermore, due to the good migration properties of disperse dyes, leveling agents are not required. Because of environmental problems associated with the use of these substances, the PAN/cotton texture is preferably dyed under pressure at temperature > 100°C without carriers. Batch dyeing is commonly applied for cable. So, the dyeing technique for PAN/cotton texture with disperse dyes obtained by synthesis, used batch dyeing at 125-135°C, under pressure and pH = 4.5 by acetic acid. The fibres need only to be soaped after dyeing. Usually, the disperse dyes are used to produce light to medium-deep shades.

### **3. Results and discussion**

The solving of dyeing problems have been made up the object of many studies [18, 21, 21]; the resolving being possible then the dyestuff has manifested a great affinity for substrate, only: the affinity is doubled by the quick capability of desorption on the primary active centers. Just, in this case the ends chain ionization can contribute to the first step of the process to increasing the migration rate of the dyestuff from the solution to the external surface of the fibre.

A special importance is the interaction study between two partners, dye and fibre, knowing that each step from dyeing polyacrylic fibre can be rate controlling step, as [18]:

- The migration of dye from solution to the external surface of fibre (electrostatic attraction – ends of chain – dyestuff).
- The electrostatic interaction and producing of salts at the external surface of the fibre (the reversible process).
- The migration of the dyestuff to the internal surface of the fibre and anionic centres releasing from the substrate chain ends, fact that permits the tacking again of the process from the beggining.

So, through admitting these steps we can justify the possibility of obtaining some intense dyeing then when the number of equivalents of dyes is much more then the anions number which are presented at the fibre chain ends. So, the introducing in structure of cationic dyes a protonation supplementary centre of reduced relative basic capacity can be favorized the decoupled process then when the dye arrives on the external surface of the fibre. In this case the dye migrated easy to the internal surface of the fibre.

The affinity of cationic dyes for Melana fibres is the result of anionic character of them. The fixation mechanism of cationic dyes on the polyacrylic fibre, in the first step is categorical ionic.

Also, the dye-fibre affinity is a result of different types of interactions: hydrogen bonds, dipole-dipole interactions and van der Waals forces. Disperse dyes have hydrogen atoms in their molecule, which are capable of forming hydrogen bonds with oxygen and nitrogen atoms on the fibre. Dipole-dipole interactions result from the asymmetrical structure of the dye molecules, which makes possible electrostatic interactions between dipoles on the dye molecular and polarized bond on the fibre. Van der Waals forces take effect when the molecules of the fibre and dye are aligned



and close to each other. These forces are very important in textile fibre because they can take effect between the aromatic groups of the fibre and those of the dye.

If these problems which appeared always in the dyeing process are known, then can be synthesized a new disperse and cationic dyes class, non-toxic, which can be degradation from wastewaters resulted from dyeing process of polyacrylic fibres.

In general, the selection of dyes depending on criterion concerning the affinity of dyes on the fibres, because this is the principal which influences the dyeing procedure of textile fibres. Depending on structure/complexity of molecule, the dyes presented in table 1 must be intense coloured (the colour is gave by chromophore systems) thus the obtained shadows on synthetic fibres to be brightness and proof of light. If the fading phenomenon is produced by the exposure at light of dyed fibre then is possible destruction more or less advanced of dye. This degradation process of dye on fibre is depending of their structure and nature of used fibre.

The presence of donor groups of electrons in dye molecules can be lead at displacing of absorption maximum at greatest wavelength and also, at a decreasing of light resistance (red disperse dyes **3-5** and blue cationic dyes **9-11**). The dyes **1-12** (in function of steric configuration of molecule and a great molecular mass) are a good diffusion rate in polyacrylic fibre.

In conclusion, the affinity of new synthesized disperse and cationic dyes depends on the presence of the functional groups in dye molecule, also the dispersion degree of dye and the fibres nature dyeing submitted.

#### *Tinctorial tests*

Tinctorial tests were realized on the polyacrylic fibres and PAN/cotton texture. The fibres submitted the qualitative tests by estimation fastness shades with grey scale; the results were expressed by note from 1 at 5 (Table 2 and 3).

**Table 2. The fastness\* test of disperse dyes on polyacrylic fibers and PAN/cotton texture**

Disperse dyes (red shades)	Fastness to cold water	Fastness to light	Fastness to washing 40°C	Fastness to perspiration acid (pH=5.5)	Fastness to perspiration alkali (pH=8.0)	Fastness to ironing	Fastness to rubbing
<b>1</b>	4-5 (4)	4-5 (4-5)	4 (3-4)	4 (4)	4 (4)	5 (4-5)	4-5 (4)
<b>2</b>	4-5 (4)	4-5 (4-5)	4 (3-4)	4 (4)	4 (4)	5 (4-5)	4-5 (4)
<b>3</b>	4 (4)	4 (4)	4 (3)	4 (3-4)	4 (3-4)	4 (4)	4 (3)
<b>4</b>	4 (4)	4 (4)	4 (3)	4 (3-4)	4 (3-4)	4 (4)	4 (3-4)
<b>5</b>	4 (4)	4 (4)	4 (3)	4 (3-4)	4 (3-4)	4 (4)	4 (3-4)
<b>6</b>	4 (4)	4 (4-5)	4 (3)	4 (4)	4 (4)	4 (4)	4-5 (4)

\*These fastness measures were made in accordance with strength standards.

**Table 3. The fastness\* test of cationic dyes on polyacrylic fibers and PAN/cotton texture**

Cationic dyes (blue shades)	Fastness to cold water	Fastness to light	Fastness to washing 40°C	Fastness to perspiration acid (pH=5.5)	Fastness to perspiration alkali (pH=8.0)	Fastness to ironing	Fastness to rubbing
<b>7</b>	4-5 (4-5)	5 (4-5)	4 (3-4)	4-5 (4-5)	4-5 (4-5)	5 (4-5)	4-5 (4)
<b>8</b>	4-5 (4-5)	5 (4-5)	4 (3-4)	4-5 (4-5)	4-5 (4-5)	5 (4-5)	4-5 (4)
<b>9</b>	4 (4-5)	4 (4)	4 (3)	4-5 (4)	4-5 (4)	4-5 (4)	4 (3)
<b>10</b>	4-5 (4-5)	5 (4-5)	4 (3)	4-5 (4)	4-5 (4)	5 (4)	4 (3-4)
<b>11</b>	4-5 (4-5)	5 (4-5)	4 (3)	4-5 (4)	4-5 (4)	5 (4)	4 (3-4)
<b>12</b>	4-5 (4-5)	5 (4-5)	4 (3-4)	4-5 (4-5)	4-5 (4-5)	4-5 (4-5)	4-5 (4)

The perspiration/light fastness at disperse dyes increases if it used dye solution 2-3%. This aspect determines the improvement at the dyeing fastness with 1/2-1 tone.

The disperse dyes derivatives from 2-aminothiazolo[4,5-f]indazole (Table 1) are dyed polyacrylic and especially, PAN/cotton texture in red shades, with good fastness to perspiration/light, good fastness to ironing and rubbing, but it isn't so good the fastness to washing at 40°C (Table 2).

The cationic dyes (Table 1) are dyed the Melana Fibres and PAN/cotton texture in light blue – violet blue shades; the colours on fibre are brightness (the case of violet blue shades), with good fastness to light, ironing and perspiration and medium fastness to washing at 40°C (Table 3).

The relationship between color and perspiration/light fastness test was influenced by coupler colorant (Table 1). Also the number of electrons donating group in disperse dye molecule lead at displace of absorption maximum at greatest wavelengths and implicit at light fastness diminution.

#### **4. Conclusions**

In this article have been presented some dyeing alternatives of polyacrylic fibres type Melana and PAN/cotton texture. These alternatives are adapted from speciality literature for these fibres. The chosen dyeing procedures are discontinuous. For dyeing processes of textile fibres the new, non-toxic disperse and cationic dyes are used. The tinctorial properties of these dyes on the fibres are very good and they can be used with success in dyeing process from textile fabrics.

#### **References**

- [1] Okada, Y., Kato T. and Morita, Z., *J. Japan Res. Assoc Textile End Uses*, 32 , 171, 1991
- [2] Okano, S., *J. Japan Res. Assoc Textile End Uses*, 32, 194, 1991
- [3] Urahata, T., *Dyeing Ind.*, 35, 148, 1987
- [4] Kelemen, K., *Dyes Pigments*, 3, 27, 1982
- [5] Rosen, C. A., *Basic dyes for textile*, 2000, Unites States Patent, 4,985,258
- [6] Reinert, G., *Melliand Textilber*, 72, E, 151, 1994
- [7] Reinert, G., *Melliand Textilber*, 1, 58, 1998
- [8] Palacin, F., *Textilveredlung*, 11/12, 12, 1996
- [9] Tărăbășanu-Mihăilă, C., Floru, L., Urseanu, F., Sebe, I., *Chimia și tehnologia coloranților organici*, 1980, Editura Tehnică, București
- [10] Rădulescu, C., Tărăbășanu-Mihăilă, C., Hossu, A.-M., Ioniță, I., *Revista de Chimie*, 55(12), 1006, 2004
- [11] Rădulescu, C., Tărăbășanu-Mihăilă, C., *Revista de Chimie*, 55(1), 25, 2004
- [12] Rădulescu, C., Tărăbășanu-Mihăilă, C., *Revista de Chimie*, 55(2), 102, 2004
- [13] Reinert, G., Fuso, F., Hifiker, H., Schimdt, E., *Textile Chemist and Colorist*, 29(12), 34, 1997
- [14] Kuramoto, N., *J. Soc. Dyers and Col.*, 106, 181, 1990
- [15] Carrey, W.S., *Journal Textile Inst.*, 76, 415, 1985
- [16] Săndescu, F., *Surfactanți utilizați ca auxiliari textili în prelucrarea fibrelor*, 2001, Editura Matrix Rom, București
- [17] Rădulescu, C., *Sisteme Heterociclice Compact Condensate*, 2004, Ed. Bibliotheca, Târgoviște
- [18] Săndescu, F., *Polimeri și fibre acrilice*, 2001, Editura Matrix Rom, București
- [19] Grindea, M., Frost, T., Hanganu, A., *Tehnologia vopsirii și imprimării textilelor*, 1983, Editura Tehnică, București
- [20] Rădulescu, C., Hossu, A.M., Ioniță, I., *Dyes and Pigments*, 65(2), 175, 2005
- [21] Rădulescu, C., Hossu, A.M., Ioniță, I., *Dyes and Pigments*, 71(2), 123, 2006

## MELANA FIBRES PHOTOSTABILIZATION BY USING UV ABSORBER FROM BENZOTRIAZOLIC CLASS

C. RĂDULESCU<sup>1</sup>, I. IONIȚĂ<sup>1</sup>, A.-M. HOSSU<sup>1</sup>, E. V. GRIGORESCU<sup>2</sup>

<sup>1</sup>"Valahia" University of Târgoviste, Faculty of Sciences and Arts, 18-22 Unirii Bdv. Târgoviste

<sup>2</sup>"I.H. Radulescu" Secondary School, 18-22 Unirii Bdv. Târgoviste

**Abstract:** In this article is presented a photostabilization alternative of polyacrylonitrilic fibres undyed and dyed with cationic dyes. For the increase of fastness to light of dyes and for the photostabilization of undyed and dyed fibres, UV absorber 2-(2'-hidroxi-5'-metilfenil)-benzotriazole were used.

**Keywords:** Melana fibre, dye, UV absorber, 2-(2'-hidroxi-5'-metilfenil)-benzotriazole

### 1. Introduction

The many types of radiation emitted by sun, mainly visible (light) and infrared (heat) reach the earth's surface. Ultraviolet radiation (UVR) is also presented but we cannot see it or feel it. Ozone in the atmosphere absorbs much of the dangerous UVR before it reaches the ground but we can still receive enough sunburn and more serious health problems [1, 2]. Exposure to UVR can cause not only sunburn but also lasting skin damage. This may result in premature skin ageing and skin cancer. UVR can also cause eye disorders such as cataracts [3-7].

To define UVR protection properties of textile the UPF value of particular textile can be measured. UPF is the abbreviation of the Ultraviolet Protection Factor and is calculated on the base of transmitted UVR through the textile support (similar to SPF of cosmetics). It shows how much longer a person wearing the textile can stay out in the sun before the onset of skin reddening as compared to an unprotected person. According to following classification system UPF range 15 to 24 (effective UVR transmission 6.7 to 4.2%) gives good protection, UPF 25 – 39 very good protection and UPF 40 – 50 and more – excellent protection (Table 1 and 2) [8, 9].

**Table 1. Ultraviolet Protection Factor (UPF) for the amount of effective UVR transmitted and absorbed**

%UVR Transmitted	%UVR Absorbed	UPF	Protection Category
10	90.0	10	Moderate Protection
5	95.0	20	High Protection
3.3	96.7	30	Very High Protection
2.5	97.5	40	Excellent Protection
2.0	98.0	50+	Excellent Protection

**Table 2. UPF Ratings and protection categories**

UPF Rating	Protection Category	%UVR Blocked
15 – 24	Good	93.3 – 95.9
25 – 39	Very good	96.0 – 97.4
40 and over	Excellent	97.5 or more

Textiles used in clothing are not necessarily complete absorbers of natural UVR and may give a false sense of security against sunburn and skin cancer [10].

The average white shirts worn by men may transmit 20% of the solar *UVR*, whereas lighter weaves favored by women may allow up to 50% to penetrate to the covered skin. Transmission of *UVR* through various samples of fabrics ranges from 64% for 100% nylon to 5% for black cotton, the values being reduced by thickness and dyes and increased with the intensity of *UVR*. The depths of penetration of *UVR* and visible light into the human skin are as follows: 0.01 – 0.1 mm for *UV-B* (280-320 nm), 0.1-1.0 mm for *UV-A* (320-400 nm) and 1.0-10.0 mm for the visible spectrum [11-14].

*UV* absorbers used for the protection of undyed and dyed textile must to carry the next conditions [15]: to absorber in near and far *UV*; to confer a high stability of white grade; to improve the resistance at light of dyes and to prevent or to delay the photo-degradation of textile support; to present a long effect; to be stable at light and heat; to be soluble in water; to not change the physico-chemical qualities of fibres; to be not toxic; to be compatible with chemical auxiliaries used in dyeing process; to have a uniform distribution on/or in textile material.

The studies [16-18] specify that the colour of dyes is very important, because the small resistance of light presents, to begin with, the textile supports dyed in pastel shadows. So, on these supports can't apply the coloured compounds because these can lead at modification of their shades.

For increasing the *UV* resistance of dyes on fibres is used frequently, some organic compounds special synthesized in this scope and marketing as Tinuvin P, Tinuvin 8 SPT from Ciba-Geigy, Rayosan C or CO from Clariant firm, Eastman antioxidants etc., named *UVR* absorbers or *UVR* protection agents [19-22].

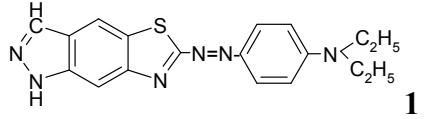
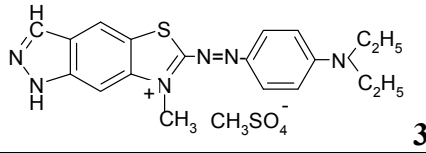
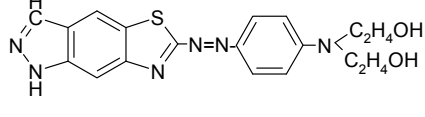
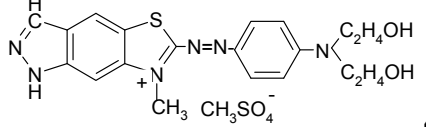
This study presents a photostabilization method of dyes and undyed and dyed fibres, using *UVR* absorber 2-(2'-hidroxi-5'-metilfenil)-benzotriazole.

## 2. Experimental

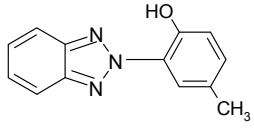
### 2.1. Materials

- Polyacrylonitrilic fibres type Melana, 2.5 den, undyed and dyed; the undyed fibres are washed with non-ionic and anionic surfactants mixture and then the fibres are washed again but with hot water (50-60°C), then with cold water and then the same operations are repeated; finally the fibres are dried in an oven at 60°C. The dyed fibres are washed with the same surfactants mixture, then with hot and cold water, alternative, and finally the fibres are dried at vacuum at the room temperature.
- Dyes obtained by synthesis [19, 23, 24] with structures and properties are presented in Table 3.
- *UVR* absorber 2-(2'-hidroxi-5'-metilfenil)-benzotriazole with structure and properties presented in Table 4.

**Table 3. The dyes obtained by original synthesis**

Disperse dye	Colour $\lambda_{\max}$ [nm] $\epsilon_{\max}$	Cationic dye	Colour $\lambda_{\max}$ [nm] $\epsilon_{\max}$
 <b>1</b>	Dark red 540.3 34200	 <b>3</b>	Violet-Blue 591 21850
 <b>2</b>	Light red 531.1 31800	 <b>4</b>	Blue 598 22600

**Table 4. The structure and properties of absorber 2-(2'-hidroxi-5'-metilfenil)-benzotriazole**

Structure	Chemical Name	Commercial Name	$\lambda_{\max}$ [nm]	$\lg[I_0/I]$	Melting point [ $^{\circ}\text{C}$ ]	Relative photostability
	2-(2'-hidroxi-5'-metilfenil)-benzotriazole	Tinuvin P	296 334 Strong absorption between 300-380 nm	2,822 1,952	128-130	10

### 2.2. Application of UV absorber for photostabilization of dyes and undyed and dyed fibres

An UV absorber, Tinuvin P (Table 4), from benzotriazole class, of Ciba-Geigy firm, was chosen for photostabilization of dyes (Table 3) and textile fibres. This absorber was chosen by next criteria: the colour of UV absorber; the variation of residual absorption depending on concentration of compound (the  $\lambda_{\max} = 220\text{-}340$  nm, in this area the degradation is maximum); the stability in time of UV absorber at UVR action.

Also, this absorber presents some advantages, such as: a good solubility in water; it can be applied in the time or after of dyeing process at  $\text{pH} < 3$  and temperature  $20\text{-}70^{\circ}\text{C}$ , in 30 minutes; it can be applied alone or in combination with other substances; it is very stabile at light and temperature in the dyebath; it has a good capacity of equalization and migration; it has good fastness to washing and ironing.

For the first time, the influence of 2-(2'-hidroxi-5'-metilfenil)-benzotriazole absorber on selected dyes is tested. Experimental: at 2% solution of 1-4 dyes was added 2% solution 2-(2'-hidroxi-5'-metilfenil)-benzotriazole absorber, the rapport = dye : absorber = 1:1. The solutions (10 mL volumes) have been photolysis in quartz cell, in exposure cavity with lamps with mercury steams, which emitted light with  $\lambda = 254$  nm. It was followed the exercised effect of absorber on selected dyes, by the determination of maximum absorbance's at certain time intervals after irradiation. The results are presented in table 5.

**Table 5. The results of dyes photolysis in presence of UV absorber**

Compound	Irradiation time [h]					
	0		124		248	
	$\lambda_{\max}$ [nm]	$\lg[I_0/I]$	$\lambda_{\max}$ [nm]	$\lg[I_0/I]$	$\lambda_{\max}$ [nm]	$\lg[I_0/I]$
2-(2'-hidroxi-5'-metilfenil)-benzotriazole	296 334	2,822 1,952	296 333	1,852 1,843	296 335	1,412 1,496
Red disperse dye <b>1</b> + 2-(2'-hidroxi-5'-metilfenil)-benzotriazole	296 332 540.3	2,412 2,296 1,299	299 328 539.5	2,287 2,232 1,143	298 327.5 538	1,995 1,988 0,987
Dark-red disperse dye <b>2</b> + 2-(2'-hidroxi-5'-metilfenil)-benzotriazole	295 333 531.1	2,269 2,224 1,247	294 332 531.5	2,243 2,203 1,009	293.5 331.5 530	1,982 1,981 0,974
Violet-blue cationic dye <b>3</b> + 2-(2'-hidroxi-5'-metilfenil)-benzotriazole	295 332.5 591	2,302 2,192 1,242	299.5 332 590	2,138 2,102 1,099	298.5 331.5 588	1,948 1,911 0,982
Blue cationic dye <b>4</b> + 2-(2'-hidroxi-5'-metilfenil)-benzotriazole	295.5 333.5 598	2,398 2,253 1,350	297.5 328.5 697.5	2,162 2,102 1,174	295.5 328 596	1,949 1,895 0,991

The application of 2-(2'-hidroxi-5'-metylfenil)-benzotriazole absorber on undyed Melana fibres was realized very easy: in treated bath at 25<sup>0</sup>C was added 60 g/L Na<sub>2</sub>SO<sub>4</sub> and 1% absorber solution; then 3% solution Na<sub>2</sub>CO<sub>3</sub> until pH= 9-9.5 was added; the mixture was stirred 30 minutes, then the fibres were washing with hot and cold water.

The application of 2-(2'-hidroxi-5'-metylfenil)-benzotriazole absorber on dyed Melana fibres can be realized by two procedures: a. absorber solution 2% was added in dye bath in the same time with dye solution, at fleet rapport 1:40, and then was introduced the other auxiliaries substances; b. after the dyeing process of Melana fibres was applied the absorber by boiling 30 minutes, at pH~3.5-4; then the fibres were washing with hot and cold water and then its dried at room temperature.

The undyed and dyed Melana fibres treated with UV absorber was irradiated by the same process presented at the photolysis of dyes. The photodegradation was evaluated by the measurement at certain time intervals of absorption capacity by the registration of spectra using a UV-VIS Specord 210 Analytik Jena; then it was analyzed the fastness to light face to the grey scale.

### **3. Results and discussion**

The photostabilization of dyes and undyed and dyed Melana fibres was realized by the using of 2-(2'-hidroxi-5'-metylfenil)-benzotriazole absorber. The absorption of UV radiation by this absorber is possible by free rotation of hydroxylic group and the existence of keto-enolic tautomerism. The absorber was chosen by theoretical considerations concerning the chemical structure of 2-(2'-hidroxi-5'-metylfenil)-benzotriazole, as: the presence of hydroxyl group in *ortho* position on benzenic cycle permit the formation of strong intramolecular hydrogen bond, between electronegative heteroatom and hydrogen atom from hydroxyl group; also, the presence of –OH group in *ortho* position lead to two maximum of absorption in UV for this absorber; therefore it presents an intense absorption between 300-340 nm, region with yellowish maximum. The absorber without –OH groups can't be used, because they haven't a good stability at irradiation due the fact they can't form the intramolecular hydrogen bonds. Also, the polarity of substrate is very important in the choice of absorber.

The efficiency of 2-(2'-hidroxi-5'-metylfenil)-benzotriazole absorber depends by stability in time of their at *UVR* action (Table 5). So, conform to obtained dates the stability in time of 2-(2'-hidroxi-5'-metylfenil)-benzotriazole absorber at *UVR* action is great, because is necessary more than 248 exposure hours for to register a considerable decreasing of the absorption.

The adding of 2-(2'-hidroxi-5'-metylfenil)-benzotriazole absorber at dye solutions prevent the degradation of dyes and assure the maintenance of absorption capacity at values of 2.5 great face to dye solution without absorber. This absorber didn't react with dyes **1-4** because the decreasing order is the same as in case of *UV* spectra registration only for the alone absorber. The degradation of dyes increases proportional with irradiation time, demonstrated by the decreasing of molar extinction coefficient (Table 5) and by moving of absorption maximums to small wavelength. Also, due the degradation of dyes, is possible to appear the supplementary absorption maximums which indicated some secondary compounds.

The advantages resulted by the introduction of 2-(2'-hidroxi-5'-metylfenil)-benzotriazole absorber in dye solutions are: the increasing of absorption capacity of dyes after exposure at *UV* radiations; in *UV* area the absorption intensity for *UV* absorber is the greatest as absorption intensity of dyes, therefore the energy of *UV* radiations is absorbed by 2-(2'-hidroxi-5'-metylfenil)-benzotriazole absorber; the presence of *UV* absorber moving the absorption maximum of dyes from visible to greatest wavelength (bathochromic shift).

**Table 6. The fastness to light values of Melana samples treated and un-treated with UV absorber**

The exposure time at irradiation of Melana fibres [h]	100	200	300
White Melana fibres, undyed, without UV absorber	4	3	2 - 3
Dyed Melana fibres with dark-red disperse dye <b>1</b> without UV absorber	4/5	4	3
Dyed Melana fibres with red disperse dye <b>2</b> without UV absorber	4	4/3	3
Dyed Melana fibres with violet-blue cationic dye <b>3</b> without UV absorber	4/5	4/5	4
Dyed Melana fibres with blue cationic dye <b>4</b> without UV absorber	4	4	3
Dyed Melana fibres with red disperse dye <b>1</b> with 2-(2'-hidroxi-5'-metylfenil)-benzotriazole absorber	5	5/4	4
Dyed Melana fibres with dark-red disperse dye <b>2</b> with 2-(2'-hidroxi-5'-metylfenil)-benzotriazole absorber	5	5	4
Dyed Melana fibres with violet-blue cationic dye <b>3</b> with 2-(2'-hidroxi-5'-metylfenil)-benzotriazole absorber	5	5	5/4
Dyed Melana fibres with blue cationic dye <b>4</b> with 2-(2'-hidroxi-5'-metylfenil)-benzotriazole absorber	5	4	4

The evaluation of undyed and dyed Melana fibres degradation, treated and untreated with UV absorber was realized by the analysis of samples exposed of radiation (Table 6), analyzing the dyeing colour, the fastness to light and discoloration grade.

The Melana fibres un-treated with UV absorber are degraded very fast face to dyed fibres, therefore is remarked a protection effect of dye contrary to light. For dyed samples, the introduction of 2-(2'-hidroxi-5'-metylfenil)-benzotriazole absorber lead to the modification of shade, maximum a tone on grey scale (4/5 only at 4). Also, the pH from dyebath is very important, because at acid pH the photostabilization of fibre is the best.

The Melana fibres tread with 2-(2'-hidroxi-5'-metylfenil)-benzotriazole absorber, in the time of exposing at UV radiations, didn't lead to significant discoloration of textile fibres.

#### 4. Conclusions

This paper presents a phostabilization alternative of polyacrylonitrilic fibres, type Melana, by the application of 2-(2'-hidroxi-5'-metylfenil)-benzotriazole absorber. The choice of this absorber has required an attend study from specialty literature. The effectuated tests have demonstrated the fact that the application on Melana fibres a proper dyes and UV absorber lead at remarkable increasing of dark shades fastness at the action of solar radiations.

#### References

- [1] CIE tehcnical raport: Sunscreen Testing, pub. No. CIE 90-1991
- [2] McKinley, A.F. and Diffey, B.L., CIE Journal, 17, 1987
- [3] Cunningham M.L., Johnson J.S., Giovanazzi S.M., Peak M.J., *Photochem.Photobiol.*, 42, 125, 1985
- [4] de Gruijl F.R., *Methods.Enzymol.* 319, 359, 2000
- [5] Huda A., *Health Phys.*,78 (5 Suppl): S75, 2000
- [6] Somosy Z., *Micron*, 31, 165, 2000
- [7] Shore R.E., *Med.Pediatr.Oncol.* 36, 549, 2001
- [8] Holton, J.R et al., *Rev. Geophys.*, 33, 403, 1995
- [9] Baldwin, M.P. and Dunkerton, J.T., *J. Geophys. Res.*, 104, 30937, 1999
- [10] Cole C., *Photodermatol.Photoimmunol.Photomed.* 17, 2, 2001

- [11] Thompson D.W. and Solomon, S., *Science*, 296, 895, 2002
- [12] Baldwin, M.P. et al. *Science*, 301, 317, 2003
- [13] Randel W. et al., *J. of Climate*, 17, 986, 2004
- [14] WHO, *Global Solar UV Index, A practical guide*. Fact Sheet 271, 2002
- [15] Applegate L.A., Frenk E., *Eur.J.Dermatol.* 5, 97, 1995
- [16] Koepke, P., *Photochem. Photobio.*, 67, 657, 1998
- [17] Rădulescu, C., Hossu, A.M., Ioniță, I., *Dyes and Pigments*, 65(2), 175, 2005
- [18] Rădulescu, C., Hossu, A.M., Ioniță, I., Moater, E.I., *Dyes and Pigments*, 67(7), 779, 2007
- [19] Rădulescu, C., Manea, L., Hossu, A.M., Tărăbășanu-Mihailă, C., *Revista de Chimie*, 58(6), 572, 2007
- [20] Koshyk, J.N. et al., *J. Geophys. Res.*, 104, 27177, 1999
- [21] Pewson, N.N. et al., *Bulletin of the American Meteorological Society*, 81(4), 781, 2000
- [22] Baldwin, M.P. et al., *Rev. Geophys.*, 39, 179, 2001
- [23] Rădulescu, C., Tărăbășanu-Mihailă, C., Hossu, A.M., Ioniță, I., *Revista de Chimie*, 55(12), 1006, 2004
- [24] Rădulescu, C., Ioniță, I., Hossu, A.M., Tărăbășanu-Mihailă, C., Moater E. I., *Ovidius University Annals of Chemistry*, vol. XVI, no. 2, 221, 2005



## **ANALYSES OF SOME PHISICOCHEMICAL PARAMETERS OF SURFACE WATERS FOR DETERMINATION OF POLLUTION GRADE**

ILEANA MARIN<sup>1</sup>

<sup>1</sup>*"Ienăchiță Văcărescu" Secondary School, Târgoviște*

**Abstract:** *This paper some physicochemical analyses for determinate the parameters of surface water, in order to define the degree of pollution. The experiments performed lead to the extract assessment of the water quality category.*

**Keywords:** *water quality, pollution, analysis*

### **1. Introduction**

The impact of human health of polluted emission from water is the subject of major interest and concern. Pollution is a generic term that covers the different releases into the environment of compounds having a negative and / or a toxic effect [1]. Pollutants from surface water can be generated both by natural ways and by human activities, as for example through mining, energy production, industrial activities, human domestic activities, transport etc. To limit their impact on the environment, clean air and water acts have been adopted in industrial countries. Consequently, environmental pollutants need to be identified and measured. The main difficulties of their measurements are: the complexity of the associated environmental matrices; their low amounts; the presence of different types of pollutants in the same environmental system [2].

There are many causes for water pollution but two general categories exist: direct and indirect contaminant sources. Direct sources include effluent outfalls from factories, refineries and waste treatment plants etc., which emit fluids of varying quality into urban water supplies. Indirect sources include contaminants that enter the water supply from soil/groundwater systems and from the atmosphere via rain water. Soils and groundwater contain the residue of human agricultural practices (fertilizers, pesticides etc.) and improperly disposed of industrial wastes. Atmospheric contaminants are also derived from human practices (such as gaseous emissions from automobiles, factories and even bakeries). It is generally accepted fact that the developed countries suffer from problems of chemical discharge into the water sources mainly groundwater, while developing countries face problems of agricultural run-off in water sources. Polluted water like chemical in drinking water causes problem to health and leads to water-borne diseases which can be prevented by taking measures can be taken even at the household level [3].

Contaminants can be broadly classified into organic, inorganic, radioactive and acid/base. Example for each class and their potential sources are too numerous to discuss here but some of their can be mentioned. So, the synthetic organics are mentioned the first. Many of the 100 000 synthetic compounds in use today are found in the aquatic environment and accumulate in the food chain. Persistent organic pollutants or POPs, represent the most harmful element for the ecosystem and for the human health, for example, industrial chemical and agricultural pesticides. These chemicals can accumulate in fish and cause serious damage to human health. Where pesticides are used on a large-scale, groundwater gets contaminated and this leads to the chemical contamination of drinking water [3, 4].

Run-off from farms, backyards and golf courses contain pesticides such as DDT that in turn contaminate the water. Leechate from landfill sites is another major contaminating source. Its effect on the ecosystems and health are endocrine and reproductive damage in wildlife. Groundwater is susceptible to contamination, as pesticides are mobile in the soil. It is a matter of concern as these chemicals are persistent in the soil and water [4].

Nutrients are founded in water sources. Domestic wastewater agricultural run-off and industrial effluents contain phosphorus and nitrogen, fertilizer run-off, manure from livestock operations, which increase the level of nutrients in water bodies and can cause eutrophication in the lakes and rivers and continue on the coastal areas. The nitrates come mainly from the fertilizer that is added to the fields. Excessive use of fertilizers cause nitrate contamination of groundwater, with the result that nitrate levels in drinking water is far above the safety levels recommended. Good agricultural practice can help in reducing the amount of nitrates in the soil and thereby lower its content in the water [4].

Untreated and inadequately treated municipal sewage is a major source of groundwater and surface water pollution in the developing countries. The organic material that is discharged with municipal water into the watercourses uses substantial oxygen for biological degradation thereby upsetting the ecological balance of river and lakes. Sewage also carries microbial pathogens that are cause of the spread of disease [5].

Acidification of surface water, mainly lakes and reservoirs, is one the major environmental impacts of transports over long distance of air pollutants such as sulphur dioxide from power plants, other heavy industry such as steel plants and motor vehicles [4].

Therefore all chemicals in water can be both naturally occurring or introduced by human interference and can have serious health effects.

Pollutants levels exceeding WHO or national standards have adverse health effects, ranging from a loss of IQ points in children due to airborne heavy metal particles; cardiovascular and respiratory disorders due to particulate matter and sulphur dioxide; cancers due to hydrocarbons [6]. Water pollution may affect marine life, transferring pollutants to humans. Human activities are not only accelerating local air pollution, but also contribute to long-term effects such as ozone depletion and climate change.

Normalized methodologies have been adopted to characterize numerous organic and inorganic pollutants. Internationally determined emissions standards (ISO, EPA, SR etc) have to be put into effect by national and local governments. Current emission levels in various countries indicate that additional efforts and initiatives are needed for the achievement of a less-polluted environment worldwide. Global Conventions to protect the environment its Kyoto protocol, as well as the Montreal protocol, also provide unique opportunities for nations and their cities to contribute to a global campaign for better air and water quality [7, 8].

In this paper some indicators concerning the surface water quality are analyzed. It was chosen, as surface water, the Ialomita River, near Targoviste city, the most important river from Dambovita County. The analyzed samples were collected from upstream and downstream of the mentioned river, in consecutive 7 day from May.

## **2. Experimental**

### *Materials and methods*

The water samples (100.....500 cm<sup>5</sup>) were collected from upstream and downstream of the Ialomita River, in glass or plastics bottle in according with ISO 13946:2004. The samples are analyzed in maximum 24 hours and, if the analyses demand, must to be conserved with concentrated acid [7].

For all smples are determined the pH using a DREL 2800 / Complete Water Quality Control HACH-LANGE, which containe DR 2800 Spectrofotometer, Digital Titrator, Multi-parameter for the determining of pH, conductivity, temperature, salinity an dissolved oxygen. For the determining of these indicators are used the standardized methods in according with SR ISO 10523:1997 for pH, SR EN 27888:1997 for conductivity, EN ISO 9963-1:2002 for salinity.

The turbidity of surface water was analyzed with Turb-550 apparatus and the used method is in according with SR EN ISO 7027:2001.

The ions from water samples were analyzed with Portable Ion Chromatograph PIA 1000 (for anions  $\text{NO}_3^-$ ,  $\text{SO}_4^{2-}$ ,  $\text{PO}_4^{3-}$  and ions  $\text{NH}_4^+$ ,  $\text{Ca}^{2+}$ ,  $\text{Mg}^{2+}$ ) DR 2800 Spectrofotometer (for cuprum, iron).

The CCO-Cr calculated value of surface water (category III) was analyzed with method present in SR ISO 6060:1996, but also directly by using a ECO 8 apparatus. In Romania the accepted limit value for water from quality class III (O.M. 1146-2003) is 50 mg  $\text{O}_2/\text{L}$ .

The results obtained for upstream and downstream samples from Ialomita River, in consecutive 7 day from May are presented in table 1 and 2.

**Table 1. The results of upstream water samples from Ialomita River**

Indicators	UM	MCL*	Day 1	Day 2	Day 3	Day 4	Day 5	Day 6	Day 7
pH	pH	$\geq 6.5$ $\leq 9.5$	6.35	6.59	6.70	6.79	6.9	7.05	7.15
Temperature	$^{\circ}\text{C}$	-	14.5	15.0	14.2	14.8	13.8	13.1	12.9
Turbidity	NTU	$\leq 10$	9.5	9.7	9.1	9.3	9.7	9.2	9.8
Conductivity at $20^{\circ}\text{C}$	g/cm	2500	457	480	459	478	483	482	480
Ammonium $\text{NH}_4^+$	mg/dm <sup>3</sup>	0.5	0.38	0.36	0.41	0.46	0.44	0.47	0.42
Nitrate ( $\text{NO}_3^-$ )	mg N/dm <sup>3</sup>	50	43.7	41.6	37.4	34.2	31.6	37.8	33.4
Phosphorus ( $\text{PO}_4^{3-}$ )	mg P/L	0.2	0.29	0.22	0.31	0.34	0.28	0.27	0.31
Iron	mg/ L	1.0	1.59	1.78	1.53	1.89	1.45	1.48	1.62
Cuprum	mg/ L	0.02	0.03	0.025	0.028	0.024	0.027	0.028	0.022
Total hardness	Germ. Grade	Min. 5	14.3	14.5	13.4	13.9	13.4	13.4	13.9
CCO-Cr	mg/L	50	57.6	53.2	61.9	67.8	59.0	51.8	54.7

\*Maximum Contaminant Level conforms to Romanian legislation.

**Table 2. The results of downstream water samples from Ialomita River**

Indicators	UM	MCL*	Day 1	Day 2	Day 3	Day 4	Day 5	Day 6	Day 7
pH	pH	$\geq 6.5$ $\leq 9.5$	7.05	7.31	7.29	7.45	7.60	8.01	7.65
Temperature	$^{\circ}\text{C}$	-	14.5	15.2	14.5	14.8	13.9	13.1	12.9
Turbidity	NTU	$\leq 10$	10.4	10.2	9.9	9.5	10.2	10.4	10.3
Conductivity at $20^{\circ}\text{C}$	g/cm	2500	467	481	463	473	492	491	498
Ammonium $\text{NH}_4^+$	mg/dm <sup>3</sup>	0.5	0.43	0.44	0.45	0.48	0.46	0.49	0.47
Nitrate ( $\text{NO}_3^-$ )	mgN/dm <sup>3</sup>	50	46.9	44.3	40.9	38.5	37.4	41.8	39.8
Phosphorus ( $\text{PO}_4^{3-}$ )	mg P/L	0.2	0.38	0.39	0.37	0.36	0.37	0.39	0.35
Iron	mg/ L	1.0	2.49	2.31	2.46	2.27	2.15	2.34	2.43
Cuprum	mg/ L	0.02	0.039	0.032	0.034	0.032	0.031	0.038	0.035
Total hardness	Germ. Grade	Min. 5	13.9	14.6	14.3	14.6	14.5	14.5	14.4
CCO-Cr	mg/L	50	79.4	86.2	82.3	84.7	81.2	80.3	84.2

\*Maximum Contaminant Level conforms to Romanian legislation.

### 3. Results and discussion

The water pollution represents an alteration of physical, chemical, organoleptic and biological quality of this which is produced directly or indirectly of human activity; therefore, these waters become wrongs for the using of them in the aims purpose [3].

It is known fact that in accordance with maximum admitted values of polluted substances mentioned in standards, is possible to realize a classification of waters on categories[7]:

- I category waters – potable waters;
- II category waters – used for industrial processes, agreement etc.
- III category waters – used for industrial alimentation, irrigation etc.

Also, the pollutants are classified about your persistence in water: biodegradable – they can be metabolized and neutralized by aquatic flora and fauna; non-biodegradable – the pollutants are maintained in water a long time and they contain from heavy metals salts, surfactants, pesticides, radioactive and oil substances; thermic pollutants [3].

Ialomita River, in according with results presented in table 1 and 2 has founded in III category waters class. The limited values for this surface water are very high and this fact due of human activities. The results presented in tables 1 and 2 shown the next aspects:

- the water course present a great organic load (57...67.8 mg/L for upstream water and 79.....86.2 mg/L for downstream water); the human activities influence the CCO obtained results.
- the anions  $\text{PO}_4^{3-}$  and  $\text{NO}_3^-$  present similarly concentrations in the both location of the river and exceed the critical values of the III class in considerate period from May, with an relative uniform distribution;
- the heavy metal, iron and cuprum, founded in river, in the both location, lead at conclusion that the surface water present a contamination with these metals;

#### **4. Conclusions**

The measured values were moment values and characterize the singular contamination level, relative at period and chosen location of investigation campaign. The results of investigation represent a report on present pollution level of Ialomita River.

The investigation were effectuated on a short period of time (7 days from May) but founded pollutants, which present the great values comparative with MCL, represent an alteration potential of surface water quality by negative influences on autoepuration processes of river due of the decrease of biological activities.

In generally, it is remarked, in the both of location, the great concentration of anions  $\text{PO}_4^{3-}$  and  $\text{NO}_3^-$  and heavy metals, iron and cuprum which lead at inadequate condition for developing of aquatic life.

#### **References**

- [1] Boumphrez, R., Tinslez, D., Forrow, D., Moxon, R., *The evaluation of whole effluent in UK. Workshop OSPAR (Convention from Oslo and Paris for Sea Environment Protection)*, 2003, Lelystad, Olanda
- [2] USEPA 1999. *Technical document for the water quality based on toxic control*. Washington DC: Water Office EPA /505/2-90-001
- [3] Danet, F.A., *Environmental Pollution Monitoring: Pollution, Analysis, Legislation, Quality Assurance and Managing*, Leonardo da Vinci Project, no. RO/02/B/F/PP – 141004, Bucuresti, 2005
- [4] Cofino, W.P., *Quality assurance in environmental analysis. Techniques in Environmental Analysis*, Amsterdam Elsevier 1993
- [5] Bala, C., Magearu, V., *Biosensors. Applications and perspectives*, Ars Docendi Publishing House, Bucuresti, 2003
- [6] Volmer, B., Heller, H., *Environmental UV Radiation*, Ulm Fischer Publishing House, Stuttgart, 2000
- [7] Weber, W.J., *Physicochemical Processes for Water Quality Control*, Wiley-Interscience, Jhon Wiley & Sons, Inc., 1972
- [8] Francia, F., Palazzo, G., Cordone, L., *Biophysical Journal*, 85, 2003, 2760-2768

## **C. MATHEMATICS - INFORMATICS SECTION**

## ABOUT SOME INTEGRALS

ANDREI VERNESCU<sup>1</sup>

<sup>1</sup>Valahia University Târgoviște, Faculty of Sciences and Arts, 18-22 Unirii Bvdl., Târgoviște, Romania

**Abstract:** In this note we survey some results concerning the integrals  $I_p = \int_0^{\pi/2} \sin^p x \, dx$ , where  $p \in [0, \infty)$  ( $p$  being not obviously an integer), namely the possibility to express it in terms of  $B$  and  $\Gamma$  functions.

**Keywords:** The Walli's formula, beta and gamma functions MSC: 26-A-42; 33-B-15; 40-A-20

1. We consider the definite integrals:

$$I_p = \int_0^{\pi/2} \sin^p x \, dx \quad (p \geq 0 \text{ being a real number}) \quad (1)$$

These integrals are connected to the summation of the series  $\sum_{n=1}^{\infty} \frac{\Omega_n}{n^p}$ , where  $\Omega_n = \frac{1 \cdot 3 \cdot 5 \cdot \dots \cdot (2n-1)}{2 \cdot 4 \cdot 6 \cdot \dots \cdot 2n}$  and  $p > 0$ ;

The aim of this note is to show how are obtained the formulas for compute these integrals.

The case I:  $p \in \mathbb{N} = \{0, 1, 2, \dots\}$ . The integrals of this case are the simplest and the most used ones. By a direct calculation, we have  $I_0 = \pi/2$  and  $I_1 = 1$ . Using an integration by parts we obtain the recurrence relation:

$$I_k = \frac{k-1}{k} I_{k-2} \quad (k \geq 2). \quad (2)$$

So, by iteration:

$$\begin{cases} I_{2n} = \frac{1 \cdot 3 \cdot \dots \cdot (2n-1)}{2 \cdot 4 \cdot \dots \cdot 2n} \cdot \frac{\pi}{2} \\ I_{2n+1} = \frac{2 \cdot 4 \cdot \dots \cdot 2n}{3 \cdot 5 \cdot \dots \cdot (2n+1)} \end{cases} \quad (3)$$

These formulas are used to prove the Walli's formula. Indeed, using the theorem of strict positivity for the integrals, (see [3]) it follows that  $I_p > 0$  and  $I_{2n+2} < I_{2n+1} < I_{2n}$  and so  $\frac{I_{2n+2}}{I_{2n}} < \frac{I_{2n+1}}{I_{2n}} < 1$  or, by, the recurrence formula:

$$\frac{2n+1}{2n+2} < \frac{I_{2n+1}}{I_{2n}} < 1,$$

and so  $\lim_{n \rightarrow \infty} \frac{I_{2n+1}}{I_{2n}} = 1$ .

According to (3), we obtain the Walli's formula:

$$\lim_{n \rightarrow \infty} \frac{2 \cdot 2 \cdot 4 \cdot 4 \cdot 6 \cdot 6 \cdot \dots \cdot 2n \cdot 2n}{1 \cdot 3 \cdot 5 \cdot 7 \cdot \dots \cdot (2n-1) \cdot (2n+1)} = \frac{\pi}{2}$$

(for all the details, see [4]).

An interesting evaluation of the integrals (1) is given by an inequality of A. Lupaş (see [6]):

$$\sqrt{\frac{\pi}{2(p+1)}} < \int_0^{\pi/2} \sin^p x \, dx < \sqrt{\frac{\pi}{2p}} \quad (p \in \mathbb{N}^*)$$

The case II:  $p \in (0, \infty)$ , where  $p$  is not an integer<sup>1</sup>. In this case it is necessary to use the Euler's functions  $B$  and  $\Gamma$ :

$$B(p, q) = \int_0^1 x^{p-1} (1-x)^{q-1} \, dx; \quad p, q \in (0, \infty);$$

$$\Gamma(p) = \int_0^1 t^{p-1} e^{-t} \, dt; \quad p \in (0, \infty)$$

For the beginning we consider an auxiliary result:

**1.1. Theorem.** We have:

$$\int_0^{\pi/2} \sin^p x \cos^q x \, dx = \frac{1}{2} B\left(\frac{p+1}{2}, \frac{q+1}{2}\right). \quad (4)$$

**Proof:** We have

$$\begin{aligned} \int_0^{\pi/2} \sin^p x \cos^q x \, dx &= \int_0^{\pi/2} \sin^{p-1} x \cos^{q-1} x (\sin x \cos x) \, dx = \\ &= \int_0^{\pi/2} (\sin^2 x)^{\frac{p-1}{2}} (\cos^2 x)^{\frac{q-1}{2}} (\sin x \cos x) \, dx = \int_0^{\pi/2} (\sin^2 x)^{\frac{p-1}{2}} (1 - \sin^2 x)^{\frac{q-1}{2}} \, dx = \\ &= \int_0^1 t^{\frac{p-1}{2}} (1-t)^{\frac{q-1}{2}} \frac{dt}{2} = \frac{1}{2} \int_0^1 t^{\frac{p+1}{2}-1} (1-t)^{\frac{q+1}{2}-1} \, dt = \frac{1}{2} B\left(\frac{p+1}{2}, \frac{q+1}{2}\right). \end{aligned}$$

Top of Form

Bottom of Form

(We have used the change of variable  $t = \sin^2 x$ ).

Taking  $q = 0$ , we obtain the following

**1.2. Corollary.**

$$I_p = \frac{1}{2} B\left(\frac{p+1}{2}, \frac{1}{2}\right). \quad (5)$$

**1.3. Theorem.** We have the equality:

$$I_p = 2^{p-1} B\left(\frac{p+1}{2}, \frac{p+1}{2}\right). \quad (6)$$

**Proof.** Because of the previous corollary, the equality (6) is equivalent to:

$$\frac{1}{2} B\left(\frac{p+1}{2}, \frac{1}{2}\right) = 2^{p-1} B\left(\frac{p+1}{2}, \frac{p+1}{2}\right)$$

To prove this last formula it is necessary to use the formulas:

$$B(p, q) = \frac{\Gamma(p)\Gamma(q)}{\Gamma(p+q)};$$

$$\Gamma(2p) = \frac{1}{\sqrt{\pi}} 2^{2p-1} \Gamma(p) \Gamma\left(p + \frac{1}{2}\right).$$

<sup>1</sup> The case  $p = 0$  has been eliminated, being involved in the case I.

**1.4. Theorem.** We have the equality:

$$I_p = 2^{p-1} \frac{\Gamma\left(\frac{p+1}{2}\right)}{\Gamma(p+1)}. \quad (7)$$

**Proof.** It follows from (6) and (a).

2. In the case  $p \in \mathbb{N}$ ,  $p \geq 2$ , it is possible to find again the elementary formulas (3) starting from the formula (7) ?

The answer is affirmative and we will establish it separately, in the case of  $p$  odd and in the case of  $p$  even.

The **case I:**  $p = 2k + 1$ . In this case, from (7), we have:

$$I_p = I_{2k+1} = \frac{2^{2k} \Gamma^2(k+1)}{\Gamma(2k+2)} = \frac{2^{2k} (k!)^2}{(2k+1)!} = \frac{1}{\Omega_k} \cdot \frac{1}{2k+1},$$

where we have used the notation  $\Omega_k = \frac{1 \cdot 3 \cdot 5 \cdot \dots \cdot (2k-1)}{2 \cdot 4 \cdot 6 \cdot \dots \cdot 2k}$  (the last equality from the previous chain had needed a little calculation).

The **case II:**  $p = 2k$ . We use the formulas:

(a)  $\Gamma(m+1) = m!$  (used in case I);

(b)  $\Gamma(2p) = \frac{1}{\sqrt{\pi}} \cdot 2^{2p-1} \Gamma(p) \Gamma\left(p + \frac{1}{2}\right)$  (used in the proof of the theorem 3);

(c)  $\Gamma\left(m + \frac{1}{2}\right) = \frac{(2m-1)!! \Gamma\left(\frac{1}{2}\right)}{2^m}$  ;

(d)  $\Gamma\left(\frac{1}{2}\right) = \sqrt{\pi}$ .

We obtain:

$$\begin{aligned} I_p = I_{2k} &= \frac{2^{2k-1} \Gamma^2\left(\frac{2k+1}{2}\right)}{\Gamma(2k+1)} = \frac{2^{2k-1} \Gamma^2\left(k + \frac{1}{2}\right)}{\Gamma\left(2\left(k + \frac{1}{2}\right)\right)} \stackrel{(b)}{=} \\ &= \frac{2^{2k-1} \Gamma^2\left(k + \frac{1}{2}\right)}{\frac{1}{\sqrt{\pi}} 2^{2k} \Gamma\left(k + \frac{1}{2}\right) \Gamma(k+1)} = \frac{\sqrt{\pi}}{2} \cdot \frac{(2k-1)!! \sqrt{\pi}}{2^k k!} = \Omega_k \frac{\pi}{2}. \quad \in \end{aligned}$$

**Remark.** The antiderivative  $\int \sin^p x \, dx$  can be expressed by a finite number of elementary functions only if  $p \in \mathbb{N}$  (see [7]).

I thank Professor C. P. Niculescu for some interesting remarks concerning the formulas of this work.

## References

- [1] Abramowitz, M., Stegun, I., *Handbook of Mathematical Functions*, National Bureau of Standards, 1964, USA
- [2] Bateman, H., Erdélyi, A., *Higher Transcendental Functions*, McGraw-Hill, Book Company, New York, Toronto, 1953, London
- [3] Boboc, N., Colojoară, I., *Elements of Mathematical Analysis*, Handbook for the 12Th Form, Didactical and Pedagogical Publishing House, Bucharest, several editions 1980-2001.



- [4] Iacob, C., *A course of higher mathematics*, Technical Publishing House, 1957, Bucharest,
- [5] Janke, E., Emde, F., Lösch, F., *Tafeln Höherer Funktionen*, B. G. Teubner Verlagsgesellschaft, 1960, Stuttgart,
- [6] Lupaş, A., *Problem 17.544*, *Gaz. Math.*, 12, 533, 1978
- [7] Niculescu, C. P., Vernescu, A., *The Problem 233*, *Gaz. Math.*, A Series 1, 47, 2007
- [8] Rîjik, I.M., Gradstein, I.S., *Tables of Integrals, sums, series and products*, Technical Publishing House, 1955, Bucharest.

## A SCHURER-POPOVICIU TYPE OPERATOR

INGRID OANCEA<sup>1</sup>

<sup>1</sup>Valahia University Târgoviște, Faculty of Sciences and Arts, 18-22 Unirii Bdv., Târgoviște, Romania

**Abstract:** Starting from Schurer operators we construct a Popoviciu type operator and we give a convergence theorem.

### Preliminaries

**Definition:** A sequence of polynomials  $(b_n)_{n \in \mathbb{N}}$  is said to be polynomial sequence of binomial type if it satisfies the following conditions:

1.  $\text{grad}(b_n) = n, (\forall) n \in \mathbb{N}$
2.  $b_n(x+y) = \sum_{k=0}^n \binom{n}{k} b_k(x) b_{n-k}(y), (\forall) x, y \in \mathbb{R}$

**Definition:** If  $\Pi$  is the commutative algebra of polynomials with coefficients real numbers then an operator  $T: \Pi \rightarrow \Pi$  which commutes with all shift operators  $E^a: \Pi \rightarrow \Pi, E^a p(x) = p(x+a)$  is called shift-invariant operator.

**Definition:** A shift-invariant operator  $Q$  is called delta-operator if  $Qx$  is a nonzero constant.

**Definition:** A polynomial sequence  $b = (b_n)_{n \geq 0}$  is called the sequence of basic polynomials for the delta-operator  $Q$  if for any  $x \in \mathbb{R}$  and  $n \in \mathbb{N}$  we have:

1.  $b_0(x) = 1$
  2.  $b_n(0) = 0$
  3.  $(Qb_n)(x) = nb_{n-1}(x).$
- (see [4]).

**Theorem (First Expansion Theorem):** If  $T$  is a shift invariant operator, and  $Q$  a delta operator having the basic set  $b = (b_n)_{n \geq 0}$  then

$$T = \sum_{k \geq 0} \frac{a_k}{k!} Q^k \quad (1)$$

**Theorem:** There exists an isomorphism between the ring of formal power series in the variable  $t$  over the same field and the ring of shift-invariant operators, which carries

$$f(t) = \sum_{k \geq 0} \frac{a_k}{k!} t^k \text{ into } T = \sum_{k \geq 0} \frac{a_k}{k!} Q^k$$

where  $Q$  is a delta operator.

**Corollary:** Let  $Q$  be a delta operator with basic polynomials  $b = (b_n)_{n \geq 0}$  and  $\phi(t)$  is the formal power series that corresponds to  $Q$ . Then

$$\sum_{n \geq 0} \frac{b_n(x)}{n!} t^n = e^{x\phi^{-1}(t)}. \quad (2)$$

$\phi$  is called generating function for basic polynomials  $(b_n)_{n \geq 0}$ .

**Remark:** A formal power series  $\phi(t)$  is invertible if and only if  $\phi(0) = 0$  and  $\phi'(t) \neq 0$  and its inverse has the form

$$\varphi(t) = \sum_{k \geq 1} c_k t^k$$

Let  $(b_n)_{n \geq 0}$  be a sequence of basic polynomials for a delta-operator  $Q$  such that  $b_n(1) \neq 0$  for any  $n \in \mathbb{N}$ .

In [6] T. Popoviciu constructed the operators  $T_n^Q f: C([0,1]) \rightarrow C([0,1])$

$$(T_n^Q f)(x) = \frac{1}{b_n(1)} \sum_{k=0}^n \binom{n}{k} b_k(x) b_{n-k}(1-x) f\left(\frac{k}{n}\right)$$

where  $x \in [0,1]$  and  $n \in \mathbb{N}$ .

In [7] P. Sablonniere uses the generating function for bynomial sequence  $(b_n)_{n \geq 0}$  to determine the values of  $T_n^Q f$  on test functions  $e_j(x) = x^j, j = 0, 1, 2$ :

$$(T_n^Q e_0)(x) = e_0(x) \quad (3)$$

$$(T_n^Q e_1)(x) = e_1(x) \quad (4)$$

$$(T_n^Q e_2)(x) = x^2 + x(1-x)\rho_n \quad (5)$$

where

$$\rho_n = \frac{1}{n} + \frac{n-1}{n} \frac{r_{n-2}(1)}{b_n(1)} \quad (6)$$

the sequence  $(r_n(x))_{n \geq 0}$  being generated by

$$\varphi'' e^{x\varphi(z)} = \sum_{n \geq 0} r_n(x) \frac{z^n}{n!} \quad (7)$$

If  $c_1 > 0$  and  $c_n \geq 0$  for  $n \geq 2$  then the Popoviciu operators are positives.

### Main result

For  $p \in N_0$  the Bernstein-Schurer operator are defined as:  $B_{n,p}: C([0, 1+p]) \rightarrow C([0, 1])$

$$(B_{n,p} f)(x) = \sum_{k=0}^{n+p} \binom{n+p}{k} x^k (1-x)^{n+p-k} f\left(\frac{k}{n}\right) \quad (8)$$

We construct the operators  $B_{n,p}^Q: C([0, 1+p]) \rightarrow C([0, 1])$ ,

$$(B_{n,p}^Q f)(x) = \frac{1}{b_{n+p}(1)} \sum_{k=0}^{n+p} \binom{n+p}{k} b_k(x) b_{n+p-k}(1-x) f\left(\frac{k}{n}\right) \quad (9)$$

For the test functions  $e_j(x) = x^j, j = 0, 1, 2$ , using (3), (4) and (5), we obtain:

$$\begin{aligned} (B_{n,p}^Q e_0)(x) &= \frac{1}{b_{n+p}(1)} \sum_{k=0}^{n+p} \binom{n+p}{k} b_k(x) b_{n+p-k}(1-x) = \\ &= \frac{1}{b_{n+p}(1)} b_{n+p}(x+1-x) = 1 = e_0(x) \end{aligned}$$

and

$$\begin{aligned} (B_{n,p}^Q e_1)(x) &= \frac{1}{b_{n+p}(1)} \sum_{k=0}^{n+p} \binom{n+p}{k} b_k(x) b_{n+p-k}(1-x) \frac{k}{n} = \\ &= \frac{1}{b_{n+p}(1)} \sum_{k=0}^{n+p} \binom{n+p}{k} b_k(x) b_{n+p-k}(1-x) \frac{k}{n+p} \frac{n+p}{n} = \\ &= \frac{n+p}{n} (T_{n+p}^Q e_1)(x) = \frac{n+p}{n} e_1(x) \end{aligned}$$

and

$$\begin{aligned} (B_{n,p}^Q e_2)(x) &= \frac{1}{b_{n+p}(1)} \sum_{k=0}^{n+p} \binom{n+p}{k} b_k(x) b_{n+p-k}(1-x) \left(\frac{k}{n}\right)^2 = \\ &= \frac{1}{b_{n+p}(1)} \sum_{k=0}^{n+p} \binom{n+p}{k} b_k(x) b_{n+p-k}(1-x) \left(\frac{k}{n+p}\right)^2 \left(\frac{n+p}{n}\right)^2 = \\ &= \left(\frac{n+p}{n}\right)^2 (T_{n+p}^Q e_2)(x) = \left(\frac{n+p}{n}\right)^2 (x^2 + x(1-x)\rho_{n+p}) \end{aligned}$$

where  $\rho_{n+p}$  is described by (6) and (7).

**Theorem:** If Bernstein-Schurer operators  $B_{n,p}^Q, n \in \mathbb{N}$  and  $p \in \mathbb{N}_0$  are positives then the following relations hold true:

1.  $(B_{n,p}^Q e_0)(x) = 1$
2.  $(B_{n,p}^Q e_1)(x) = \frac{n+p}{n} e_1(x)$
3.  $(B_{n,p}^Q e_2)(x) = \left(\frac{n+p}{n}\right)^2 (x^2 + x(1-x)\rho_{n+p})$  where  $\rho_{n+p}$  is given by (6) and (7).
4.  $\lim_{n \rightarrow \infty} (B_{n,p}^Q f)(x) = f(x)$  uniformly on  $[0, 1+p]$  for every continuous function  $f \in C([0, 1+p])$  if and only if  $\lim_{n \rightarrow \infty} \frac{r_{n+p-1}(1)}{B_{n+p}(1)} = 0$ .

We have

$$\lim_{n \rightarrow \infty} (B_{n,p}^Q e_0)(x) = 1$$

$$\lim_{n \rightarrow \infty} (B_{n,p}^Q e_1)(x) = \lim_{n \rightarrow \infty} \left(x + \frac{p}{n}x\right) = x$$

$$\lim_{n \rightarrow \infty} (B_{n,p}^Q e_2)(x) =$$

$$= \lim_{n \rightarrow \infty} \left(\frac{n+p}{n}\right)^2 \left(x^2 + x(1-x) \left(\frac{1}{n+p} + \frac{n+p-1}{n+p} \frac{r_{n+p-1}(1)}{B_{n+p}(1)}\right)\right) = x^2$$

uniformly on  $[0, 1+p]$  and using the Bohman Korovkin theorem the last relation is proved.

## References

- [1] Agratini, O., *Approximation by linear operators (Romanian)*, Presa Universitara Clujeana, Cluj-Napoca, 2000
- [2] Bohman, H., *On approximation of continuous and analytic functions*, Ark. Mat., 2 43-56, 1952
- [3] Korovkin, P.P., *On convergence of linear operators in the space of continuous functions (Russian)*, Dokl. Akad. Nauk. SSSR (N.S.), 90, 961-964, 1953
- [4] S. M. Roman, G. C. Rota, *The Umbral Calculus*, Advances in Mathematics 27(2), 95-188, 1978
- [5] Stancu, D.D., Coman, Gh., Agratini, O., Trimbitas, R., *Numerical Analysis and Approximation Theory*, Vol.I (Romanian), Presa Universitara Clujeana, Cluj-Napoca, 2001
- [6] Popoviciu, T., *Remarques sur les polynômes binomiaux*, Mathematica 6, 8-10, 1932
- [7] Sablonniere, P., *Positive Bernstein-Sheffer operators*, J. Approx. Theory 83 330-341, 1995

## ABOUT DIFFERENTIAL STOCHASTIC AND INTERGRAL CALCULATION ITÔ

DOINA CONSTANȚA MIHAI<sup>1</sup>

<sup>1</sup>Valahia University Târgoviște, Faculty of Sciences and Arts, 18-22 Unirii Bdv., Târgoviște,  
Romania

**Abstract:** This study presents the integration trough parts formula, specific to the differential stochastic Itô, deducted from Itô's formula for stochastic differential, one-dimensional case. There are being solved some Itô integrals by the integration trough parts formula.

**1. Introduction:** Let be  $B_1$ , one-dimensional Brownian motion  $g: R^2 \rightarrow R$ ,  $g(t, x) = tx$ , a deterministic function and the stochastic process  $Y_t = g(t, B_t)$ . Our goal is to calculate the stochastic differential Itô,  $dY_t$ .

Appling Itô's formula, [12], for differential stochastic differential we obtain:

$$dY_t = B_t dt + t dB_t, \quad (1)$$

Relation that can be also written as:

$$d(tB_t) = B_t dt + t dB_t \quad (1')$$

or  $tB_t = \int_0^t B_s ds + \int_0^t s dB_s$ , or  $\int_0^t s dB_s = tB_t - \int_0^t B_s ds$ , formula that suggest us the next integration trough parts:

**2. Theorem (integration trough parts formula):** If  $f: [0, t] \rightarrow R$  is a deterministic integrable function, then the integral in Itô's way may be calculated like this:

$$\int_0^t f(s) dB_s = f(t)B_t - f(0)B_0 - \int_0^t B_s df(s) \quad (2)$$

$$\int_0^t f(s) dB_s = f(t)B_t \Big|_0^t - \int_0^t B_s df(s)$$

*Demonstration:* Let be  $g: R^2 \rightarrow R$ ,  $g(t, x) = f(t)x$ ,  $Y_t = g(t, B_t)$ , by Itô's formula, [12], the stochastic differential of  $Y_t$  process is:

$$dY_t = g'_t dt + g'_x dB_t + \frac{1}{2} g''_{xx} (dB_t)^2 = f'(t)B_t dt + f(t)dB_t$$

From which we deduct:

$$d(f(t)B_t) = B_t df(t) + f(t)dB_t$$

And from which we deduct (2)

*Corollary:* If  $X_t, Y_t$  are two integral stochastic Itô processes, then the next integration trough parts formula take place:  $\bar{Y}_t = g(t, X_t, Y_t) = X_t Y_t$ , applying the formula for Itô systems [12], (10), we obtain the stochastic differential for the process  $\bar{Y}_t$ :

$$\int_0^t X_s dY_s = X_t Y_t - X_0 Y_0 - \int_0^t Y_s dX_s - \int_0^t dX_s \cdot dY_s \quad (3)$$

*Demonstration:* Let be  $g: R^3 \rightarrow R$ ,  $g(t, x, y) = xy$ , a deterministic function  $X_t, Y_t$  two Itô integral stochastic processes and  $\bar{Y}_t$ :

$$d\bar{Y}_t = g'_t dt + g'_x dX_t + g'_y dY_t + \frac{1}{2} \left[ g''_{x^2} dX_t \cdot dX_t + 2g''_{xy} dX_t dY_t + g''_{y^2} dY_t dY_t \right]$$

Replacing the partial derivatives and by the formula

$$X_t Y_t - X_0 Y_0 = \int_0^t Y_s dX_s + \int_0^t X_s dY_s + \int_0^t dX_s \cdot dY_s$$

Equivalent with (3)

**3. Applications:** Using stochastic calculation, demonstrate that:

$$\int_0^t B_s^n dB_s = \frac{1}{n+1} B_s^{n+1} \Big|_0^t - \frac{n}{2} \int_0^t B_s^{n-1} ds \quad (4)$$

where  $B_1$  is a one-dimensional Brownian motion.

*Demonstration:* Applying the integration trough parts formula (3) to the stochastic processes  $X_t = (B_t)^n$ ,  $Y_t = B_t$ :

$$I_n = \int_0^t (B_s)^n dB_s = (B_s)^{n+1} \Big|_0^t - \int_0^t B_s d(B_s)^n - \int_0^t dB_s \cdot d(B_s)^n$$

To calculate the integral we first apply:

$$dB_s \cdot d(B_s)^n = dB_s \cdot \left( n(B_s)^{n-1} dB_s + \frac{1}{2} n(n-1)(B_s)^{n-2} ds \right) = n(B_s)^{n-1} ds$$

But keeping attention to the following laws [12] of differential calculation

$$dB_t \cdot dB_t = ds, \quad dB_t \cdot dt = dt \cdot dB_t = 0$$

And the power-function of Brownian motion:

$$d(B_t)^n = n(B_t)^{n-1} dB_t + \frac{1}{2} n(n-1)(B_t)^{n-2} ds$$

And replacing the result we obtain:

$$I_n = (B_s)^{n+1} \Big|_0^t - nI_n - \frac{n(n+1)}{2} \int_0^t (B_s)^{n-1} ds,$$

Equivalent with (4)

For  $n=2$  trough (4) we obtain

$$\int_0^t (B_s)^2 dB_s = \frac{1}{3} (B_s)^3 \Big|_0^t - \int_0^t B_s ds \quad (5)$$

And for  $n=3$

$$\int_0^t (B_s)^3 dB_s = \frac{1}{4} (B_s)^4 \Big|_0^t - \frac{3}{2} \int_0^t B_s ds \quad (6)$$

**4. Conclusions.** The integration trough parts formula had been demonstrated using differential Itô calculation. The corollary allows us to apply this formula for integral calculation of stochastic processes. Solved applications may become the integration law of integral stochastic processes Itô.

## References

- [1] Ciucu, G., Craiu, V., *Teoria estimăției și verificarea ipotezelor statistice*, Editura Didactică și Pedagogică, București, 1968.
- [2] Ciucu, G., Tudor, C., *Probabilități și procese stocastice*, Editura Academiei Române, București, 1979.
- [3] Cuculescu, I., *Teoria Probabilităților*, Editura All, București, 1998.
- [4] Dincă, F., Teodosiu, C., *Introduction to the theory of random processes*, Editura Academiei Române, București, 2000.
- [5] Doob, J. L., *Stochastic Processes*, Jhon Wiles & Stone, Inc., New York, N. Y., 1955.
- [6] Gihman, I. I. and Skorokhod A. A., *Stochastic Differential Equations*, Springer–Verlag, Berlin, 1972.
- [7] Iosifescu, M., Mihoc, Gh., Theodorescu, R., *Teoria probabilităților și statistică matematică*, Editura Tehnică, București, 1966.
- [8] Itô, K., *Lectures on Stochastic Processes (mimeographed notes)* Tata Institute of Fundamental Research, Bombay, India, 1961.
- [9] Itô, K., *Stochastic Integral*, Proc. Imp. Acad., Tokyo, 20, 519 – 524, 1944.
- [10] Itô K., *On Stochastic Differential Equations*, Mem. Amer. Math. Soc. 4, 1951.
- [11] Mihai, D. C. *Teză de Doctorat*, Universitatea Transilvania din Brașov, 2006.
- [12] Mihai, D. C. *About the Roules of Itô Stochastic Differential Calculus, Applications*, Proceeding, 4<sup>th</sup> Conferences on Nonlinear Analysis and Applied Mathematics, Târgoviște, 2006.
- [13] Øksendal, B., *Stochastic Differential Equations*, Springer-Verland, 1985.
- [14] Orman, G. V., *Some Problems of Stochastic Calculus and Applications*, Proceeding, 17<sup>th</sup> Scientific Session on Mathematics and its Applicaions, Brașov, 2003, p. 29-55.

## USING FINITE DIFFERENCE METHOD TO PARALLEL ALGORITHMS DESIGN

DUMITRU FANACHE<sup>1</sup>

<sup>1</sup>*Valahia University Târgoviște, Faculty of Sciences and Arts, Department of Mathematics,  
18-22 Unirii Bdv., Târgoviște, Romania, email : [d\\_fanache@yahoo.com](mailto:d_fanache@yahoo.com)*

**Abstract.** *The paperwork pursues the task/channel theoretical model of parallelizing an algorithm, which is based on a direct method of solving partial derivative equations – the finite differences method.*

*After identifying the primitive tasks and communication ways between them we will then choose an agglomeration which represents the best compromise between communication minimization and maximization processors usage.*

*The mode in which the ghost points are used is presented for memorization of the values received from other processes. Right after the values have been memorized in these points, all the elements can be actualized with the same code section.*

*We will examine the possibility of growing the ghost points and supplementary value dispatching, thus reducing the frequency of communications for enlarging the calculus power per processor. The optimal number of ghost points depends on the latency, the bandwidth and time necessary for calculating the value of an element of the matrix. In the end an optimization of the C/MPI program is tried by using threads in the execution of some cycles, given under standardized form.*

**Keywords:** *the finite differences method, the Poisson equation, the Jacobi method, isoefficiency, scalability, thread.*

### I. Introduction

The chosen mathematical model, although famous one, is only the pretext for bringing into the discussion a series of qualitative aspects in the domain of parallel algorithms projecting techniques.

A *task* in task/channel model[1] becomes a *process* in the transferring messages model [4]. The existence of an interconnecting network intermediates the existence of a communication channel between each pair of processes; thus, each process can communicate with each other process. We set out the possibility of experimental determination of *channel/bandwidth* and *latency* for a given network[5].

The approximate solving of limits problems, for differential equations with partial derivatives (PDE) has extended in 3 main directions: *the method of finite differences*, *the method of finite element* and *the method of the border element*.

In the method of finite differences, the differential equation system or the partial effectual derivatives for any point of the analysis domain becomes a effectual equation system only for certain points of the domain, points which define the discretization network domain. The principal disadvantage of this method is the utilization of a *rectangular network* of discretization of the analysis domain.

### II. Analysis of the sequential algorithm

The mathematical model on which the algorithm stands comes from studying problems from domains such as: electricity, magnetism, gravitation, the uniform distributing or electrical



distributing status in an uniform and, inevitably problems in fluids flow. The *Poisson* equation is a particular case of PDE, elliptic type, on a sub aggregate of bidimensional space :

$$\frac{\partial^2 u}{\partial x^2} + \frac{\partial^2 u}{\partial y^2} = f(x, y) \quad (1)$$

The metode of finite differences aproximates the solution of a PDE through the division of the variables (for many times in time and space) in discreet intervals. Let's assume that  $f$  is a continual function which has a derivative in every point. A resonable aproximation of  $f(x)$  is:

$$f'(x) \approx \frac{f(x+h/2) - f(x-h/2)}{h} \quad (2)$$

By the abatement of  $h$  we can reduce the aproximation errors.

Using (2) we appraise  $f''(x) = f'(f'(x))$ .

$$\begin{aligned} f''(x) &\approx \frac{\frac{f(x+h/2-h/2) - f(x+h/2-h/2)}{h} - \frac{f(x-h/2+h/2) - f(x-h/2-h/2)}{h}}{h} \\ &\approx \frac{f(x+h) - f(x) - (f(x) - f(x-h))}{h^2} \approx \frac{f(x+h) - 2f(x) + f(x-h)}{h^2} \end{aligned} \quad (3)$$

Will consider the parallelization of the program which determins the uniform distribution of heat in a thin rectangular plate, model given by (1) by the notations  $\frac{\partial^2 u}{\partial x^2} = u_{xx}$  and  $\frac{\partial^2 u}{\partial y^2} = u_{yy}$  takes the form:

$$u_{xx} + u_{yy} = f(x, y) \quad 0 \leq x \leq a, 0 \leq y \leq b \quad (4)$$

by boundary conditions:

$$\begin{aligned} u(x, 0) &= G_1(x) \text{ and } u(x, b) = G_2(x) \quad 0 \leq x \leq a \\ u(0, y) &= G_3(y) \text{ and } u(a, y) = G_4(y) \quad 0 \leq y \leq b \end{aligned} \quad (5)$$

If the functions  $G_1$ ,  $G_2$ ,  $G_3$  and  $G_4$  are continual on the borders and the function  $f$  is continual in the inside of the rectangular, then the problem has an unique solution [7].

Each point of the grid  $(x_i, t_j)$  represents the value of the solution in a particular location  $(x, y)$  of the rectangular. We will repeatedly update the values of every interior grid point until the values converge. We define  $h = a/n$  and  $k = b/m$ , then we deduce:

$$\begin{aligned} u_{xx}(x_i, y_j) &\approx \frac{u(x_i+h, y_j) - 2u(x_i, y_j) + u(x_i-h, y_j)}{h^2} \approx \frac{u_{i+1,j} - 2u_{i,j} + u_{i-1,j}}{h^2} \\ u_{yy}(x_i, y_j) &\approx \frac{u(x_i, y_j+k) - 2u(x_i, y_j) + u(x_i, y_j-k)}{k^2} \approx \frac{u_{i,j+1} - 2u_{i,j} + u_{i,j-1}}{k^2} \end{aligned} \quad (6)$$

Replacing (6) in (4):

$$\frac{u_{i+1,j} - 2u_{i,j} + u_{i-1,j}}{h^2} + \frac{u_{i,j+1} - 2u_{i,j} + u_{i,j-1}}{k^2} = f(x_i, y_j) \Rightarrow$$

$$h^2 k^2 f(x_i, y_j) = k^2(u_{i+1,j} - 2u_{i,j} + u_{i-1,j}) + h^2(u_{i,j+1} - 2u_{i,j} + u_{i,j-1}) \Rightarrow$$

$$2u_{i,j}(k^2 + h^2) = k^2(u_{i+1,j} + u_{i-1,j}) + h^2(u_{i,j+1} + u_{i,j-1}) - h^2 k^2 f(x_i, y_j)$$

Assume  $\lambda = k/h$ , we obtain:

$$u_{i,j} = \frac{\lambda^2(u_{i+1,j} + u_{i-1,j}) + u_{i,j+1} + u_{i,j-1} - k^2 f_{i,j}}{2(1 + \lambda^2)} \quad (7)$$

We simplify (4)+(5) for private case:

$$\begin{cases} a = b \\ u(x, 0) = u(x, a) = 100, & 0 \leq x \leq a \\ u(0, y) = 100, u(a, y) = 0, & 0 \leq y \leq a \end{cases} \quad (8)$$

If the points are uniform distribution then  $h = k$  and  $\lambda = 1$ . If the board is isolated doesn't exist worm between the boards, only at the edges. It results that  $f_{ij} = 0$ .

Hence our finite difference approximation to the solution of the linear second-order PDE reduces to:

$$u_{i,j} = \frac{u_{i+1,j} + u_{i-1,j} + u_{i,j+1} + u_{i,j-1}}{4} \quad (9)$$

Leaving with the initial estimations for all values can calculate iterative the new estimations departing from previous estimations until the values converge. The which method are based on the estimations from the  $i$  iteration to calculate the new estimations of  $i + 1$  iteration is known like Jacobi method. In the C implementation of the **Figure 1** we distinguish 3 stages, and for  $N = 10$  we obtain the results from **Table 1**. The 3 stages will become 3 functions in the parallel variant of the algorithm.

```
#define N 100
#define EPSILON 0.01
int main()
{double diff; int i, j;
double mean=0.0, u[N][N], w[N][N];
/* initialize grila */
for(i=0; i<N; i++){
u[i][0]=u[i][N-1]=u[0][i]=100.0;
u[N-1][i]=0.0;
mean+=u[i][0]+u[i][N-1]+u[0][i]+u[N-1][i]; }
mean/=(4.0*N);
/*Initializare valori interioare */
for(i=1; i<N-1; i++)
for(j=1; j<N-1; j++) u[i][j]=mean;
/*det solutia distributiei-uniforme*/
for(;;){diff=0.0;
for(i=1; i<N-1; i++){
for(j=1; j<N-1; j++){
w[i][j]=(u[i-1][j]+u[i+1][j]+
u[i][j-1]+u[i][j+1])/4.0;
if(fabs(w[i][j]-u[i][j])>diff)
diff=fabs(w[i][j]-u[i][j]);}
if(diff<EPSILON) break;
for(i=1; i<N-1; i++){
for(j=1; j<N-1; j++) u[i][j]=w[i][j];}
/* scrie solutie */
for(i=0; i<N; i++){ for(j=0; j<N; j++)
printf("%6.2f ", u[i][j]);
putchar('\n');}
return 0; }
```

**Figure 1.** C program solving the steady-state heat distribution problem using the Jacobi method

### III. Design qualitative aspects of parallel algorithm

**III.1. Decomposition date domain.** We can associate a primitive task with the computation of each  $w[i][j]$ . In the Jacobi method the updating step is perfectly parallel. To compute  $w[i][j]$  each task requires the  $u$  values from its neighbors to the north, south, east, and west (**Figure 2**). We want to agglomerate tasks and assign one agglomerated task to each parallel process. *What is the best way to do the agglomeration?*

If every process is responsible for every rectangular region, then computing elements of  $w$  on the interior of the rectangle can be performed using locally available values of  $u$ . Computing elements of  $w$  on the edge of the rectangle requires values held by other process.

We can introduce *ghost points* along every block of the values that were retained by every process. After the values received from other process are retained in ghost points, then a double cycle for allows all the values of  $w$  to be calculated.

If we make a decomposition on *rowwise-block* (Figure 3.a) then every inside process changes messages with other two process. An obvious alternative is the decomposition as a *checkerboard block*, when every inside process changes messages with other four neighbour process.

100.00	100.00	100.00	100.00	100.00	100.00	100.00	100.00	100.00	100.00
100.00	98.61	97.40	96.51	96.05	96.05	96.51	97.40	98.61	100.00
100.00	97.04	94.48	92.62	91.64	91.64	92.62	94.48	97.04	100.00
100.00	95.10	90.88	87.86	86.29	86.29	87.86	90.88	95.10	100.00
100.00	92.47	86.12	81.67	79.40	79.40	81.67	86.12	92.47	100.00
100.00	88.67	79.49	73.33	70.29	70.29	73.33	79.49	88.67	100.00
100.00	82.72	69.87	61.91	58.17	58.17	61.91	69.87	82.72	100.00
100.00	72.37	55.39	46.28	42.35	42.35	46.28	55.39	72.37	100.00
100.00	51.35	33.06	25.48	22.61	22.61	25.48	33.06	51.35	100.00
100.00	0.00	0.00	0.00	0.00	0.00	0.00	0.00	0.00	100.00

Table 1. Results obtains on grid 10×10 of Jacobi method

**III.2. Isoefficiency analysis.** Let's suppose that we have a grating architecture. While the calculating time for one element of the grating is constant the complexity for the calculation of the sequential algorithm is  $\Theta(n^2)$  per iteration.

Let's consider the decomposition on the *rowwise-block*. Every of the  $p$  process manages a submesh of size approximately  $(n/p) \times n$ . During every iteration, every interior process must send  $n$  values to each of its neighbors and receives  $n$  values from every of them, leading to a communication complexity of  $\Theta(n)$ . The communication overhead of each iteration of the parallel algorithm is  $\Theta(np)$ .

	$u[i+1][j]$	
$u[i][j-1]$	$w[i][j]$	$u[i][j+1]$
	$u[i-1][j]$	

Figure 2. The value of  $w[i][j]$  depends upon values  $u[i+1][j]$ ,  $u[i-1][j]$ ,  $u[i][j-1]$  and  $u[i][j+1]$

The isoefficiency function [3] for the algorithm based on the decomposition on the *rowwise-block* is:

$$n^2 \geq Cnp \Rightarrow n \geq Cp.$$

Because  $M(n) = n^2$ , the function of scalability is:

$$M(Cp)/p = C^2 p^2 / p = C^2 p \quad (10)$$

This means that the parallel system doesn't have a high scalability.

Let's consider now the decomposition as a chess table. Every of the  $p$  process subordinate a part of the grating of the  $(n/\sqrt{p}) \times (n/\sqrt{p})$  size. During every iteration every inside process has to send  $n/\sqrt{p}$  values at every of his neighbours and receives  $n/\sqrt{p}$  values from these ones, the

complexity of communication being of  $(\Theta n/\sqrt{p})$ . The overhead owed to communication of iteration of the parallel algorithm is  $\Theta(n/\sqrt{p})$ .

The isoefficiency function for the algorithm based on a checkerboard block decomposition is:

$$n^2 \geq Cn\sqrt{p} \Rightarrow n \geq C\sqrt{p}$$

Evaluating the scalability function:

$$M(C\sqrt{p})/p = C^2 p/p = C^2 \quad (11)$$

We deduct that the parallel system is the high scalability.

**III.3. Implementation Details.** The bordering of two-dimensional blocks with ghost points refers to message transfer operations which impose supplementary steps of copying. The virtual points for the upper and lower part of the lines are in contiguous locations of memory, but the ghost points for the columns on the right and on the left are not. As long as the elements are not in contiguous locations of memory, we cannot receive a direct message in a multitude of ghost points. In exchange, it is necessary to receive messages in a temporary buffer and then we copy the values in the ghost points.

Similar, a temporary buffer must be used when we assemble values sent to the neighbour processes oriented on the column of ghost points.

In **Figure 5** we see the structure of the C/MPI program. After declaring the variables, next are the subprogram prototypes which implement the 3 steps mentioned in its sequential version.

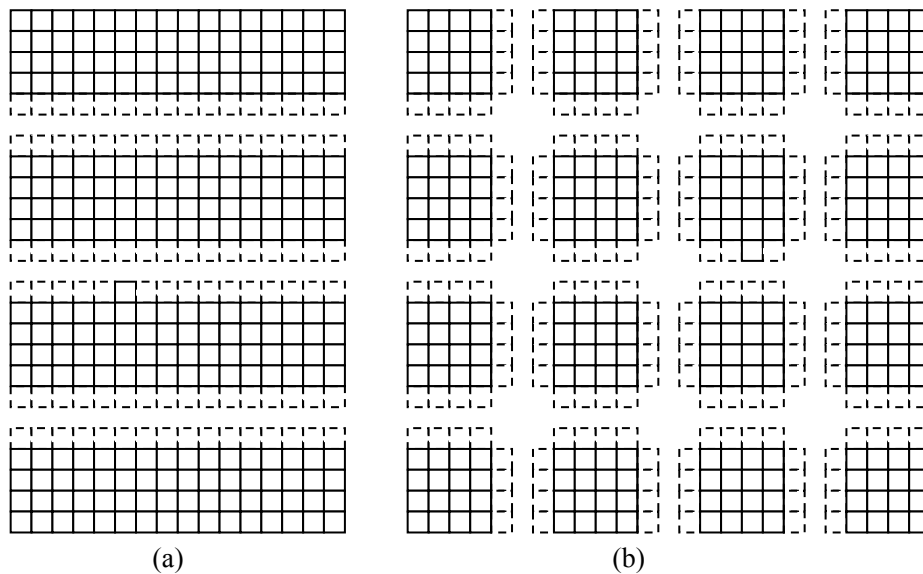


**Figure 3.** Possible data decomposition for solving the two-dimensional steady-state temperature distribution problem. (a) A 16x16 grid is mapped at 4 processors using a decomposition on rowwise-blocks. Each process manages an  $(n/p) \times n$  region. Ghost points appear as cells edged by dashed lines. (b) A grid of type 16x16 mapped on 16 processes in a checkerboard block decomposition. Each process manages a region of size  $(n/\sqrt{p}) \times (n/\sqrt{p})$ . The ghost points are the cells edged by dashed lines.

The memory space allocated to every process it is realized dynamic with `alocale_2d` function (**Figure 4**). The calling parameters of the function `parallel_distribution` have the next semnification:  $p$ -number of processes disponibles on cluster,  $id$ -the process identifier,  $u$  and  $w$  the bidymensional tables representing the current temperatures and the actual temperatures.

```
void alocare_2d (int r, int c, double ***a)
{double *storage;int i;
 storage =
(double *) malloc (r * c * sizeof(double));
*a = (double **) malloc (r * sizeof(double *));
for (i = 0; i < r; i++)
    (*a)[i] = &storage[i * c];}
```

**Figure 4.** Allocation spaces a processes in parallel version of algorithm

```
#include <mpi.h>
#include<stdio.h>
#define BLOCK_LOW(id,p,n)      ((id)*(n)/(p))
#define BLOCK_HIGH(id,p,n)    (BLOCK_LOW((id)+1,p,n)-1)
#define BLOCK_SIZE(id,p,n)    \
    (BLOCK_HIGH(id,p,n)-BLOCK_LOW(id,p,n)+1)
int main (int argc, char *argv[])
{double **u,**w; /* temperatura precedenta/curenta */
 int      my_rows, /* liniile controlate de proces */
          p,id,its; /* numarul proceselor, rangul procesului, nr iteratii */
double elapsed; /* timp de executie */
 void initializare_grila (int, int, int *, double ***,double ***);
 int parallel_distribution (int, int, int, double **, double **);
 void print_solution (int, int, double **);
 MPI_Init (&argc, &argv);elapsed = -MPI_Wtime();
 MPI_Comm_size (MPI_COMM_WORLD, &p);
 MPI_Comm_rank (MPI_COMM_WORLD, &id);
 omp_set_num_threads (atoi(argv[1]));
 initializare_grila (p, id, &my_rows, &u, &w);
 its = parallel_distribution (p, id, my_rows, u, w);elapsed += MPI_Wtime();
 print_solution (p, id, u);
 if (!id) {printf ("Converge dupa %d iteratii\n", its);
          printf ("Timp de executie = %8.6f\n", elapsed);}
 MPI_Finalize();}
```

**Figure 5.** General structure of MPI program

We remark the fact that function `initializare_grila` has the parameters  $p$  and  $id$  and the line distribution at processes is realized by macro `BLOCK_SIZE` which has the same parameters  $id, p, n$ -the dimension of the domain date. A part of this function is represented in **Figure 6**.

```
void initializare_grila(int p, int id, int *my_rows,double ***u, double ***w)
{int      i, j;double mean;
 if (p == 1) *my_rows = BLOCK_SIZE(id,p,N);
 else if ((id == 0) || (id == p-1))*my_rows = BLOCK_SIZE(id,p,N) + 1;
 else *my_rows = BLOCK_SIZE(id,p,N) + 2;
 alocare_2d (*my_rows, N, u);alocare_2d (*my_rows, N, w);
 . . . . .
 /* conditiile la limita, etc */}
```

**Figure 6.** Partitioning date domain on rowwise-block corresponding  $id$  of processes

#### IV. Optimization in parallel algorithm

The ability of the shared-memory model to support incremental parallelization is one of its greatest advantage over the message-passing model(**Figure 7**).

We have chosen a rowwise-block decomposition of the two-dimensional matrix representing the finite difference mesh. Our first step is to profile the parallel program's on one and four processors

of cluster on which to test the model. The results are summarized in **Table 2**. The vast majority of time is spent inside function `parallel_distribution`.

**IV.1. Parallelizing function `parallel_distribution`.** Except for two early initializations and a return statement, function `parallel_distribution` consists of a for loop. There are many reasons we cannot execute the loop in parallel: it is not canonical form[3], it contains a break statement, it contains calls to MPI functions. The most significant reason, however, is that there are data dependences between iterations. Each iteration relies on values computed in the previous iteration. So we need to look for parallelism inside an iteration of the outer for loop.

Our focus shifts to the first for loop indexed by `i`. This is the loop that iterates through the rows of this process's share of the matrix, computing elements of `w` from elements of `u`. These assignment statements are independent of each other and may execute simultaneously.

Function	1CPU	4CPU
<code>initializare_grila</code>	0.01%	0.03%
<code>parallel_distribution</code>	98.48%	93.49%
<code>print_solution</code>	1.51%	6.48%

**Table 2.** Result of profiling a C/MPI program implementing the Jacobi method. The target architecture is a cluster with four dual-processors.

However, when the absolute value of `w[i][j]` is greater than the current value of `diff`, it is necessary to actualize the variable `diff`. If we need more threads which refer to the shared variable `diff`, it is necessary to obtain the instruction `if` in the interior of a *critical section*, but this could decrease the parallel acceleration. In a change, we could introduce a new private variable called `tdiff`. Each thread can initialize the copy of `tdiff` with zero before the cycle for indexed after `i` and compare each value of `w[i][j]` which it calculates with `tdiff`.

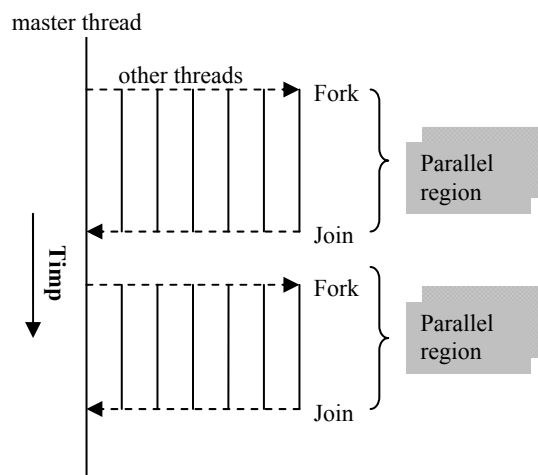


**Figure 7.** The shared-memory model is characterized by fork/join parallelism, in which parallelism comes and goes. At the beginning of execution only a single thread is active. The master thread executes the serial portions of the program. It forks additional threads to help it execute parallel portions of the program. These threads are deactivated when serial execution resumes.

While all threads assign values to different elements of `w` and different copies of `tdiff`, we can use the option `for` of the directive `pragma` to indicate that the cycle for indexed after `i` can be made parallel.

The second cycle `for` indexed after `i` copies the elements of `w` in those that correspond to `u`. We put an option `for` of the directive `pragma` before this cycle to specificate to the compiler that we have a parallel construction. After the second cycle `for` indexed after `i` we will create a critical section in which each thread compares his value of `tdiff` with the value of the shared variable `diff`, and actualizes the value of `diff` to `tdiff` when `tdiff` is big.

We observe that creating the private variable `tdiff` we are allowed to build a solution in which each thread enters in a critical section once for each iteration of the Jacobi method. If all the threads would have referred `diff` in the initial pair of imbricated cycles, each thread should enter in a critical section for `i x j` times for each iteration of the Jacobi method. We use “{”, “}” to create a code block which delimitates two options `for` and an option `critical` of the directive `pragma` as well as the initialization instruction of the private variable `tdiff`. At the start of this bloc of the code we insert a directive `pragma parallel`. The modified version of the function `parallel_distribution` is in **Figure 8**. In the main function is added the instruction:

```
omp_set_num_threads(atoi(argv[1]));
```

in this way the user can specify the number of the active threads on each MPI process from the command line[6].

**IV.2. Benchmarking.** We will analyze the performances of the MPI program and of the hybrid program MPI/OpenMP on a cluster that contains four nodes of dual-processors. At first we execute only the C program that uses only MPI. In the program benchmarking MPI/OpenMP, we create only a MPI process on each cluster node. We observe that the hybrid program is systematically faster than the initial program C/MPI executed on the same number on processors (**Figure 9**). This is owed on the fact that the operation/communication statement of the hybrid program is superior. *The number of the mesh point updated per element of communicated is twice as high per node for the hybrid program.* The lower communication overhead leads to a higher speedup. On eight CPU the hybrid program is 19% faster than the parallel program based only on MPI.

```
int parallel_distribution(int p, int id, int my_rows, double **u, double **w)
{double diff, global_diff, tdiff;
 int    its=0, i,j;
 MPI_Status status;
 for(;;){
  if(id>0)MPI_Send(u[1],N,MPI_DOUBLE,id-1,0,MPI_COMM_WORLD);
  if(id<p-1){
   MPI_Send(u[my_rows-2],N,MPI_DOUBLE,id+1,0,MPI_COMM_WORLD);
   MPI_Recv(u[my_rows-1],N,MPI_DOUBLE,id+1,0,MPI_COMM_WORLD,&status);}
  if(id>0) MPI_Recv(u[0],N,MPI_DOUBLE,id-1,0,MPI_COMM_WORLD,&status);
  diff=0.0;
#pragma omp parallel private (i,j, tdiff)
  {tdiff=0.0;
#pragma omp for
   for(i=1;i<my_rows-1;i++)
    for(j=1;j<N-1;j++){
     w[i][j]=(u[i-1][j]+u[i+1][j]+u[i][j-1]+u[i][j+1])/4.0;
     if(fabs(w[i][j]-u[i][j])>diff)diff=fabs(w[i][j]-u[i][j]);
    }
#pragma omp for nowait
   for(i=1;i<my_rows-1;i++)
    for(j=1;j<N-1;j++) u[i][j]=w[i][j];
#pragma omp critical
   if(tdiff>diff)diff=tdiff;
  }
  MPI_Allreduce(&diff,&global_diff,1,MPI_DOUBLE,MPI_MAX, MPI_COMM_WORLD);
  if(global_diff<=EPSILON)break;
  its++; }
```

```
return its;}
```

**Figure 8.** Function `parallel_distribution` after OpenMP pragmas have been inserted.

## Conclusions

Being given the great popularity of the C language and the possibilities of work with the mechanism of dynamic allocation of the memory, it can be chosen as a evolving environment for the parallel algorithms of programation C and library MPI. For a increase performance, it has been used the OpenMP library. The first step of the transformation is profiling the original parallel program to discover the functions consuming the most CPU cycles. Often, relatively few function need to be the focus of the parallelization effort. An other motivation is that the existent computer networks are exploited almost 10% of the power of calculating put up for use, but the creation of a parallel virtual machine is simple.

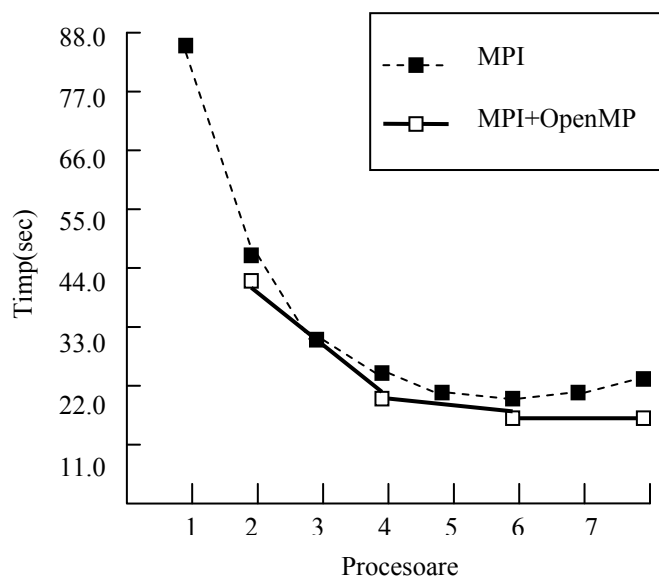


**Figure 9.** The result of benchmarking programs MPI and of course MPI+OpenMP which uses the Jacobi method for the resolution of the Poisson equation on a scale  $200 \times 200$ . The time is expressed in seconds. The architecture is a cluster which contains four dual-processor nodes [3].

## References

- [1] Foster, I., *Designing and Building Parallel Programs: Concepts and Tools for Software Engineering*, Reading, MA: Addison-Wesley, 1995
- [2] Wilkinson, B., and Michael, A., *Parallel Programming: Techniques and Applications Using Networked Workstations and Parallel Computers*, Upper Saddle River, NJ: Prentice-Hall, 1999
- [3] Quinn J. M., *Parallel programming in C with MPI and OpenMP*, McGraw-Hill, New York, 2004
- [4] Pacheco, S. Peter, *Parallel programming with MPI*, Morgan Kaufman Publishers, Inc, San Francisco, California. An Imprint of Elsevier, 2002
- [5] Dumitrescu, B., *Calcul paralel*. Universitatea "Politehnica" București, suport de curs format electronic, 2005
- [6] Dongarra, J.J., Duff, I.S., Sorenson, D.C. and H.A. van der Vorst. *Solving Linear Systems on Vector and Shared Memory Computers*. Philadelphia: SIAM Press, 1991
- [7] Smith, G.D., *Numerical Solution of partial Differential Equations: Finite Difference Methods*, Oxford:Oxford University Press, 1985



## A THEORETICAL CONSTRUCT FOR PARALLEL COMPUTATION

DUMITRU FANACHE<sup>1</sup>

<sup>1</sup>Valahia University Târgoviște, Faculty of Sciences and Arts, Department of Mathematics,  
18-22 Unirii Bdv., Târgoviște, Romania, email : [d\\_fanache@yahoo.com](mailto:d_fanache@yahoo.com)

**Abstract.** Many times the parallelization of an algorithm is made starting from its sequential version. The optimization of the execution is being made by the experience and the intuition of the programmer. Concerning unitary design of parallel algorithms, it is presented a methodology which assures the maximization of calculation per processor and the minimization of communications between processors.

**Keywords:** partitioning, communication, agglomeration, mapping.

### 1. Introduction

Ian Foster proposed a procedure in four steps for the design of parallel algorithms[1] applicable with success for a big variety of problems. The four design steps are called: *partitioning*, *communication*, *agglomeration* and *mapping*.

The model task/channel (**Figure 1**) is a theoretic construction which puts in valor the specified stages. It represents a parallel calculation of a bulk of tasks which can, eventually, interact with each other bulk of tasks or with peripheral I/O with the help of direct message transmission through communication channels. Because no objective can't be touched without compromising the other, a good design must realize an equilibrium between the proposed steps.

A task can send values of local data of other tasks through ports. Contrary, a task can receive values from other tasks through entry ports. A channel is a tail of messages which connect a task through the exit port with another task through entry port. Data values are coming in the entry port in the same succession with those which are placed in the exit port.

On other hand, in the task/channel model the reception is an synchronous operation, how long the transmission is an asynchronous operation.

### 2. Stages in the design of parallel algorithms

**2.1 Partitioning.** In the design on a parallel algorithm, we will experiment many types of possible parallelism. Partitioning is the process of calculations and data division into smaller partitions. A good partitioning shares the process of calculation and data in many other smaller partitions. In other words, we can board each from partitioning modes: data's or calcul's. **Decomposition of domain** is the projecting approach of the parallel algorithm in which you first divide the datas in partitions and then we determine how to associate the calcul with datas previously partitioned.([9]).

**The functional decomposition** is a complementary strategy in wich at first we divide the calculus process and then associate the datas with individual calculs.([7]). Frequently, the functional decompositions produce arrays of tasks which obtain directly the *pipeline* type concurrency. No matter what decomposition we choose, we will name each of the partitions as *primitive tasks*(elementary). Our objective is to identify as many primitive tasks as possible, because the number of primitive tasks is a superior margin which we can exploit in the designing process.

**2.2 Establishing communications.** After we have identified primitive tasks, the next step is to determine the communication ways between them. Parallel algorithms have 2 ways of communicating: *local* and *global*. We name communication between tasks the overhead part of the parallel algorithm, because it represents someway the execution of sequential algorithm but without

the need of communications. The minimization of the overhead is an important objective in designing parallel algorithm.

**2.3 The agglomeration** is the process of grouping smaller tasks into larger tasks so that the performance is improved or the programming is simplified. Sometimes the number of tasks grouped this way can be greater than the number of processors on which the the parallel algorithm can be executed. One of the agglomeration's objectives is the overhead's minimization due to communications. If we agglomerate the primitive tasks that communicate with each other, then the communication is completely eliminated, because values controlled by the primitive tasks are now in the bigger task's memory(consolidated). We call this action **localization's increase** of the parallel algorithm.

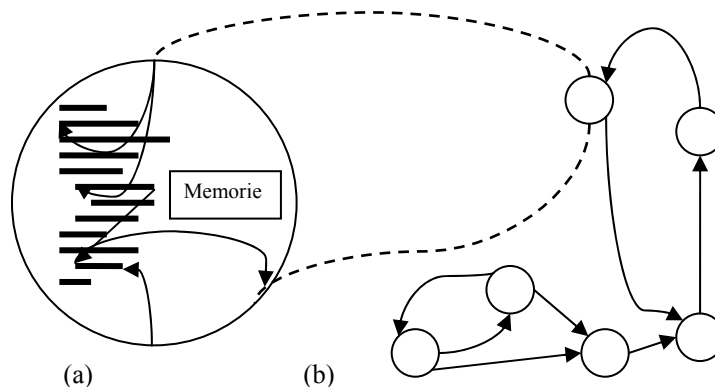


**Figure 1.** A task/channel programming model. (a) A task consists of a program, local memory and a bunch of ports I/O. (b) A parallel calculation model can be visualized as a orientated graph in wich the nodes represent the tasks and the orientated edges represents the communication channels.

Dispatching less, the longer messages will take less time than dispatching more short messages with the same total length, because there is a initial cost of the message(**latency**) produced each time a message is send, and this time is independent from the message length.

Other objectives of agglomeration are: maintenance the scalability of the parallel projection, reducing the software's projection costs. This way, if we parallelize a sequential program, an agglomeration permits us to give a larger utilization to the existent sequential code, reducing the time and expenses to developing the parallel program.

**2.4. Mapping** is the process of association tasks to processors. If we execute the program on a multi-tasking centralized processor, the operating system is automatically mapping the processes to the processors. We define the processor utilization as the medium sistem's (sic) time of the processor's which are active and executing necessary tasks for solving the problem. The processor utilization is maximized when the calcul (sic) is balanced, permitting all processors to start and finish the execution at the same time.(otherwise, the processor utilization decreases when one or more processors are standing by while the rest of the processors are permanently occupied).

Because the mapping strategy depends on previous strategies concerning parallel algorithm, it is important to keep increased attention during the designing process.

### 3. Application to solving partial derivated equations

**3.1 Utterance and problem modelation.** Let's apply the steps described in section 2 for simple problem[5]: “ *A thin conductor made out of a uniform material surrounded by an isolating layer so that temperature changes along the conductor are a result of heat transfer at it's ends and conduction along it's lenght. The conductor's length is 1. Both ends of the conductor are in a dock full of ice at 0 degrees Celsius, while the initial temperature at  $x$  from the end of the conductor is  $100\sin(\pi x)$* ”.

An equation with partial derivatives modelates the temperature in any point of the conductor at any time. The method of finite differences is a way to solve the partials derivated equation on a computer [7, 9]. **Figure 2** shows a approximation with finite differences of the problem of the cold conductor. Each polygonal line represents the distribution in time of the temperature in several points. “The Curves” slide down as the time rises.

**3.2.The separation of the date domain.** In reality, the distribution of the temperature has to be a regulated curve. The method of the finite differences, calculates almost the solution of the equation with partial derivatives memorizing the temperatures in a bidimensional matrix(**Figure 3**).

Each line contains the distribution in time of the leaders temperature in several points. The leader is divided in  $n$  sections of  $h$  in length, thus each line has  $n+1$  elements. The rise of  $n$  reduces the approximation errors. The time from 0 to  $T$  is divided in  $m$  discrete entities of  $k$  in length, thus the matrix contains  $m+1$  lines. The initial distribution of temperature long side the length of the conductor is represented thru points in the bottom lines. The values are known. The temperatures at the end of the conductor are represented thru the left border and the right of the grill. These values are also known. Let it be  $u_{i,j}$  the temperature of the conductor in point  $i$  at the moment  $j$ . In the method of the finite differences, as long as we go forward in time, using the values at the moment  $j$  the algorithm can calculate the value at the moment  $j+1$  using the formula (where  $r = k/h^2$ ) which expresses the equation in diffusion:

$$u_{i,j+1} = ru_{i-1,j} + (1-2r)u_{i,j} + ru_{i+1,j}$$

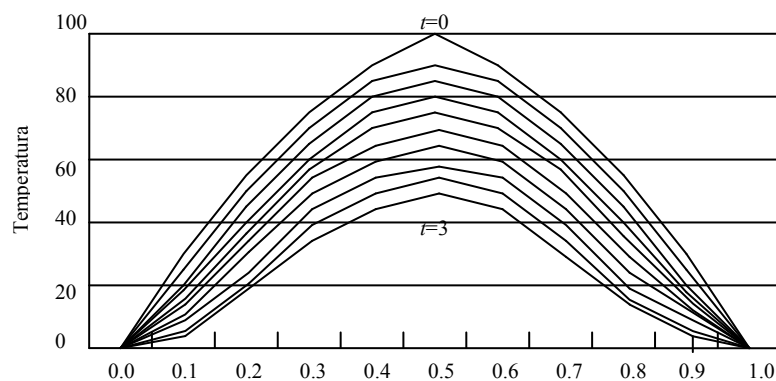


**Figure. 2** The evolution of the chilling of the conductor in time. The method of the finite differences finds the temperature in a fixed number of points in the conductor at several gaps of time. The decreasing of the size of the paces in space and time can lead to bigger occurrence of the solutions.

**3.3. Communications, agglomeration and mapping.** At first, we associate an elementary task with every point of the grid. This makes a bidimensional decomposition of the data base. After we identified the tasks, is necessary to determine the communication ways between them. It results that the task which calculates  $u_{i,j+1}$  needs the values for  $u_{i-1,j}$ ,  $u_{i,j}$  and  $u_{i+1,j}$ , in general each task may have three entrance ways and three exit ways(**Figure 4.a**). The tasks on the border have less ways.

Regularly if there are enough available processors, it's impossible to calculate each task shown in **Figure 4 (a)**, because the tasks which calculates the conducts temperature at an ulterior moment depend on the results made by the tasks which calculates the temperature at the previous moment. Let's concentrate all tasks associate with every point in the conduct, which means that the tasks in the same column in **Figure 4 (a)**. It results the task/channel chart shown in **Figure 4(b)** which is much less complicated. Now we have a linear chart of tasks, each task communicating only with his neighbours. Each is responsible for the calculating the temperature in a particular point of the chart for every measured moment in time. It results that a good strategy is to create a task per processor, concentrating then the primitive tasks in this manner that the work to be

balanced and the communications minimized. Associating a continue part of the conduct with every task (**Figure 4(c)**) we keep the communication between tasks with the approached neighbours and we eliminate useless communications for that dates from the interior of an only task.

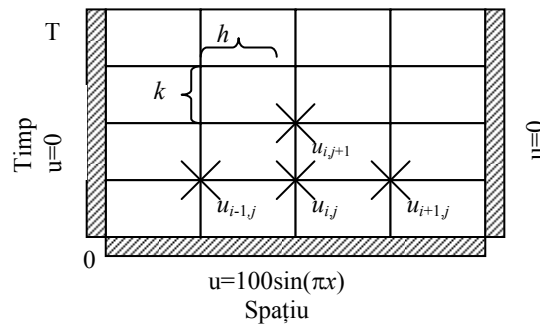


**Figure 3.** The data structure used in approximating with finite differences of the cooling problem of the conduct. Each point  $u_{i,j}$  represents an element of the matrix which contains the temperature on the position  $i$  on the draw bar at moment  $j$ . At the each end of the conduct the temperature is always 0, the temperature in  $x$  point is  $\sin(\pi x)$ .

**3.4 Benchmarking.** The conductor is divided in  $n$  portions of length  $h$ . Let  $\chi$  is the symbol that represents the time for calculating  $u_{i,j+1}$ , being  $u_{i-1,j}$ ,  $u_{i,j}$  and  $u_{i+1,j}$ . Using a single processor for actualization of  $n-1$  interior values of the conductor need the time  $(n-1)\chi$ . Because the algorithm has  $m$  time steps, the total execution time of the sequential algorithm is  $m(n-1)\chi$ .

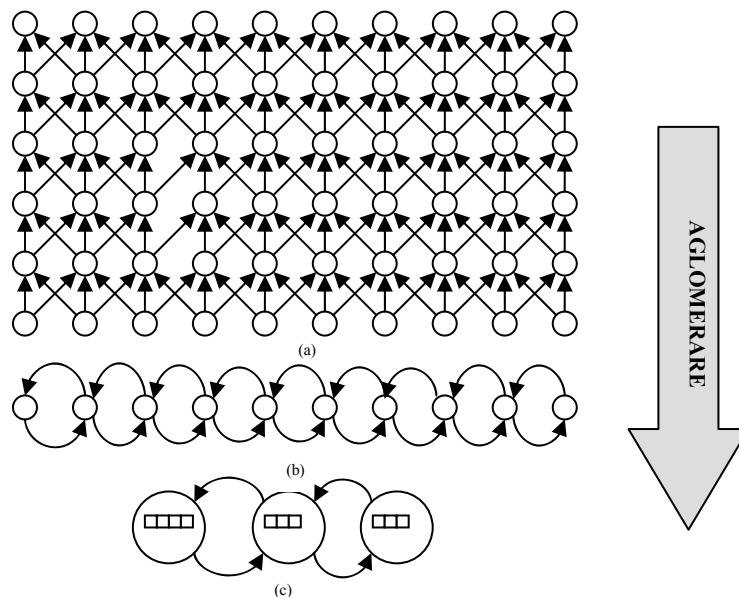


**Figure 4.** The graf task/channel for the parallel solutions of a problem with limited values.. (a) First of all decomposing of the domain associates a task with each temperature that can be calculated; (b) . After the first step of the agglomeration, a single task represents now the temperature's calcul of a single element  $i$  for all the time moments; (c) After the second agglomeration step, a task is responsible for for the calculation, in every time moments, of the temperatures for a continuous conductor's group established.

Now let's calculate the execution time estimated for the parallel algorithm. Being  $p$  the number of processors which are executing the algorithm. If each processor is responsible for a piece

of draw bar's elements size alike, the necessary time for the calculation for each iteration is  $\chi \lceil (n-1)/p \rceil + 2\lambda$ . Anyway, the parallel algorithm involves the communication that are not in the sequential algorithm and we must calculate this time too. Generally, each processor must send its values to 2 of its neighbour processors and it receives 2 values from them. If  $\lambda$  represents the necessary time for a processor to send (receive) a value to (from) another processor, then communications necessary for raising the parallel execution time for each iteration is  $2\lambda$ . In the task/channel model, a task may send only a message at a certain time, but may receive a message at the same time while he is sending a message. So, the task requires a time interval of  $2\lambda$  to send values to 2 of its neighbours but necessarily it receives, 2 values from its neighbours at the same time.

Combining the calculating time to the communication time, we conclude that the general parallel execution time per iteration is  $\chi \lceil (n-1)/p \rceil + 2\lambda$ , and we estimate that the parallel execution parallel time for m iterations of the algorithm is  $m[\chi \lceil (n-1)/p \rceil + 2\lambda]$ .

#### **4. Conclusions**

Task/channel model is similar message-passing programming model. A task in the task/channel model becomes a process in the message-passing model. The existence of the interconnection network means there is an implicit channel between every pair of processes; that is, every process can communicate with every other process.

#### **References**

- [1]. Foster, I., *Designing and Building Parallel Programs: Concepts and Tools for Software Engineering*, Reading, MA: Addison-Wesley, 1995
- [2] Carriero, N., and Gelerntner, D., *How to Write Parallel Programs: A First Course*. Cambridge, MA: The MIT Press, 1990
- [3] Valiant, L. G., *A bridging model for parallel computation*, Communication of the ACM 37(4):54-64, 1994
- [4] Garey, M. R., and Jonson, D. S., *Computers and Intractability: A Guide to the Theory of NP-Completeness*, San Francisco: W.H. Freeman, 1979
- [5] Quinn J. M., *Parallel programming in C with MPI and OpenMP*, McGraw-Hill, New York, 2004
- [6] Grigoraş, D., *Calcul paralel*, Editura Libris Agora, Cluj-Napoca, 2002
- [7] Fanache, D., *The Jacobi method of solving linear equation systems on a parallel calcul system*, Analele Univ. "Valahia", Târgovişte, iunie, 2005
- [8] Fanache, d., *Transformarea schemelor de program secvenţiale în unele paralele prin utilizarea reţelelor FIFO*, Sesiunea de comunicări Ştiinţifice a Facultăţii de Ştiinţe, Univ. "Valahia", Târgovişte, iunie 2005
- [9] Fanache, D., *The Complexity of Parallel Version of Floyd's Algorithm*, The Fourth Conference on Nonlinear Analysis and Applied Mathematics, Târgovişte, 8th-9th Dec, 2006